

Synthesis and Reactivities of Iron Complexes
Bearing a Tetradentate PNNP Ligand

Tomohiro Takeshita

February 2019

Synthesis and Reactivities of Iron Complexes
Bearing a Tetradentate PNNP Ligand

Tomohiro Takeshita
(Doctoral Program in Chemistry)

Submitted to the Graduate School of
Pure and Applied Sciences
In Partial Fulfillment of the Requirements
For the Degree of Doctor of Philosophy in
Science

at the
University of Tsukuba

Contents

Chapter 1	Synthesis and Properties of PNNP-Iron Complexes
Chapter 2	Metal-Ligand Cooperation of the PNNP-Iron System
Chapter 3	Selective Synthesis of Hydrosiloxanes via Dehydronegative Coupling of Silanols with Hydrosilanes Catalyzed by PNNP-Iron Complexes
Chapter 4	Synthesis and Properties of Chloro(Silyl)Iron Complexes via Oxidative Addition Reaction of Si–Cl Bond
List of publications	
Acknowledgements	

General Introduction

In 1827, Zeise's salt ($K[PtCl_3(C_2H_4)] \cdot H_2O$) was reported as a first structurally well-characterized organometallic compound.¹ Since then, organometallic chemistry have continued remarkable development, and six Nobel prizes have been awarded in this field so far.² In the history of organometallic chemistry, various structures, physical properties, and diverse reactivity have been unveiled along with the development of various analytic methods. It is also to be noted that the prominent milestones have been made by the discovery of ligands in this field. In addition, the development of novel supporting ligand systems had also made a significant contribution to the development of organometallic chemistry. One of good examples is the development of Suzuki-Miyaura cross-coupling reaction of aryl halides ($Ar-X$) or alkyl halides with boronic acids,^{2,3} which is useful for C–C bond forming reactions. In the pioneering period, the substrate scope is only limited to reactive $Ar-I$, $Ar-Br$.^{3a} After a while, the use of 1,1'-bis(diphenylphosphino)ferrocene (dppf), which is a bidentate phosphine ligand, opened up the way for the transformation of alkyl halides.^{3b} Furthermore, it was also revealed that strong σ -donating phosphine or *N*-heterocyclic carbene ligands effectively facilitate the reaction of less reactive $Ar-Cl$.^{2g} Likewise, the metal catalysts for the cross-coupling reaction have been expanded to the use of not only Pd but also Ni and Fe as cheap and versatile candidates by utilizing a series of ligands.^{2g}

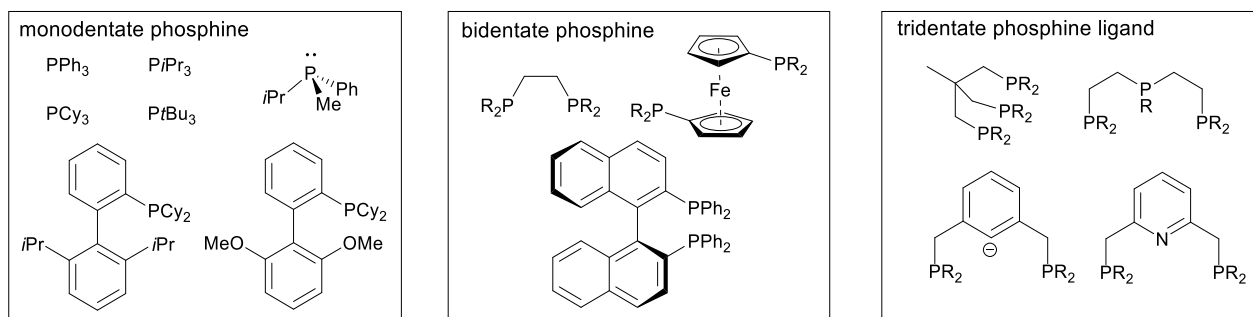


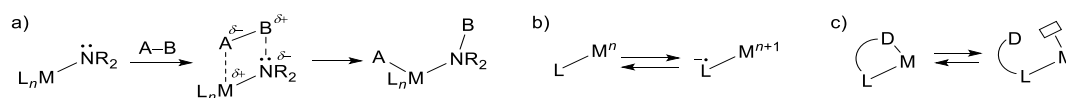
Figure. 1 Phosphorus ligand

As seen in the development of cross-coupling reactions mentioned above, phosphine ligands play an important role among the ligands because they constitute a series of ligands with a range of electronic and steric properties by changing the substituents on the P atom.⁴ As a result, phosphine ligands are nowadays utilized in various synthetic reactions.⁴ In this context, several polydentate ligands have been developed in an attempt to further

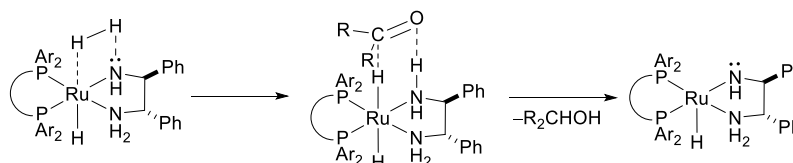
design the electronic and steric properties of the ligands (Fig. 1).⁴ By using these chelate-type ligands, site-, chemo-, and enantio-selectivity can be easily controlled in many reactions.

Metal-Ligand Cooperation

Recently, “metal-ligand cooperation (MLC)” have drawn an increasing attention as a new function of ligands (Scheme 1).^{5a-c} The concept initially only includes the redox active feature of the ligands, which sometimes acts as an electron reservoir during the reaction. So far, intensive studies have revealed that the diverse functions of MLC could bring many breakthroughs in the organometallic chemistry. As a result, the concept of “MLC” is nowadays expanded to include a) bifunctional activity,^{5a-c} b) redox activity,^{5b,c} and c) hemilability.^{5d}



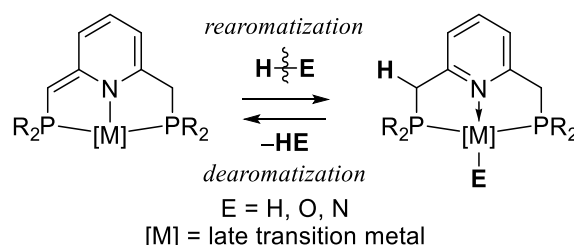
Scheme 1. metal–ligand cooperation a) bifunctional activity, b) redox activity and c) hemilability



Scheme 2. Noyori-Ikariya hydrogenative reaction.

As a representative example of the MLC-supported substrate activation, Noyori, Ikariya and co-workers discovered that Ru complexes bearing amido ligand(s) could cleave a hydrogen–hydrogen bond via heterolysis and catalyze hydrogenation of carbonyl compounds. Furthermore, they applied the reaction system to hydrogenation of carbonyl compounds via hydrogen transfer reaction mechanism (Scheme 2).^{2x,6} Similarly, MLC using metal–oxygen, metal–sulfide and metal–cyclopentadienone were also reported, and not only hydrogenation but also hydroborylation, hydrosilation etc. were achieved with high efficiency.⁶ Recently, another representative example of MLC was reported by Milstein and co-workers. They discovered the MLC associated with aromatization /dearomatization using PNP pincer complexes (Scheme 3).⁷ In the systems, the lutidines or 2-picolines backbone having CH₂ groups at the *ortho*-position of a central pyridine unit was deprotonated by a base, resulting in the dearomatization of the pyridine unit. Since the deprotonation and reprotonation are reversible, the combination of metal and lutidines or

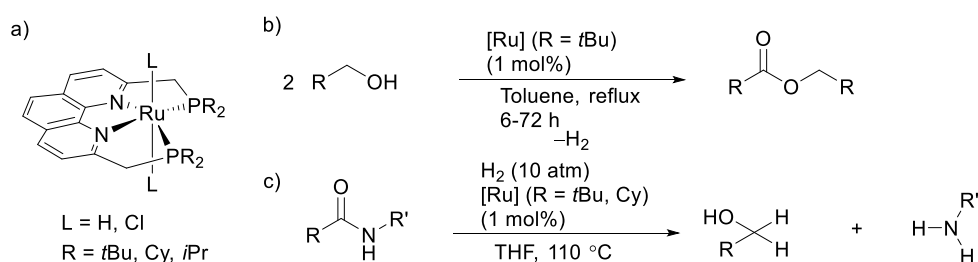
picolines backbone can exhibit the function of MLC. By using this system, the Milstein's group has demonstrated various bond cleavage including H–H,⁸ O–H,⁹ and N–H¹⁰ bond cleavage reactions, catalytic hydrogenations,¹¹ and others.¹² Through these studies, various tridentate pincer systems have been developed.



Scheme 3. metal–ligand cooperation by dearomatization/rearomatization.

Tetradentate-PNNP-Pincer Ligands

In an attempt to precisely design the reaction sphere of metal complexes in more details, a PNNP-Ph (2,9-bis((diphenylphosphino)methyl)-1,10-phenanthroline) ligand^{13a} was developed. The concept of MLC involving aromatization/dearomatization process was then further expanded to the PNNP system by Milstein and co-worker using Ru as a metal center (Scheme 4-a). However, the utility of PNNP-Ru complexes was only limited to hydrogenation and hydrogen transfer reactions (Scheme 4-b, c).^{13b-d} The major reason is assumed that the soft Lewis basic phosphine side-arm, strongly bind with a Ru center, and thus construct a rigid meridional tetradentate coordination. As a result, it is difficult to form a reactive coordinatively unsaturated species by phosphine-side-arm-dissociation during the reaction. Based on these facts, the author focused on the use of Fe as a metal center, due to its smaller binding energy compared with that of Ru. The author expected that the hemilability of the PNNP ligand is invoked in the PNNP-Fe complexes and thus could expand the chemistry of the PNNP ligand system into the further stage.

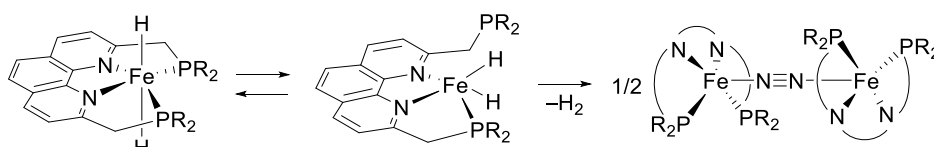


Scheme 4. a) PNNP-Ru complexes, b) esterification by dehydrogenation of alcohols, and c) dehydrogenation of amides using PNNP-Ru complexes

Other features to use iron as a metal center are the low toxicity, high abundance and cheap price. Owing to these reasons, the development of a novel iron complex as an environmentally-benign catalyst precursor is one of the biggest concerns in the recent organometallic chemistry. On the other hand, it is known that Fe can adopt a wide oxidation state ranging from -2 to $+5$ (rarely to $+8$), with various spin states (high spin, medium spin and low spin states).¹⁴ Furthermore, the spin state easily changes via spin-crossover due to its small ligand field.¹⁴ Due to this changeable electronic state of iron, the reactivity of iron complexes sometimes changes dramatically, and thus the application of iron complexes as catalysts is extremely challenging. In this context, the author expected that the utilization of PNNP-R ligand shows the great advantages in the chemistry of iron complex: Thus, the strong electron-donating ability of PNNP-R help it to act as a high-field ligand that effectively stabilizes iron complexes with a low-spin state. As a result, PNNP-R-supported iron complexes are expected to behave as a stable diamagnetic species and are potentially useful as inexpensive and nontoxic surrogates for precious-metal catalysts.

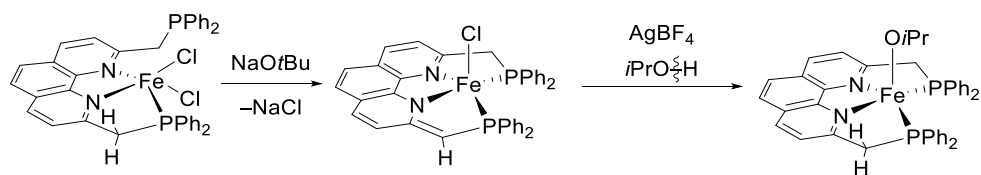
Overview of this thesis:

In chapter 1, synthesis of a series of iron complexes with PNNP-R ligands ($R = \text{Ph}$ and Cy) are described (Scheme 5). It was revealed that PNNP-R-iron dihalide complexes $[\text{FeCl}_2(\text{PNNP-R})]$ reacted with 2 equiv of NaBEt_3H to form dinuclear iron(0) complex bridged by dinitrogen ligand $[\text{Fe}(\text{PNNP-R})(\mu\text{-N}_2)]_2$. As a result of the detailed mechanistic study, the formation of a dihydride intermediate $[\text{Fe}(\text{H})_2(\text{PNNP-Cy})]$ was evidenced. Thus, it was revealed that the reaction of the iron dihalide proceeds via successive hydrogenation and reductive elimination of H_2 , which proceeds associated with the dissociation of iron–phosphine bond. The result strongly supported the hemilabile behavior of the PNNP-R.



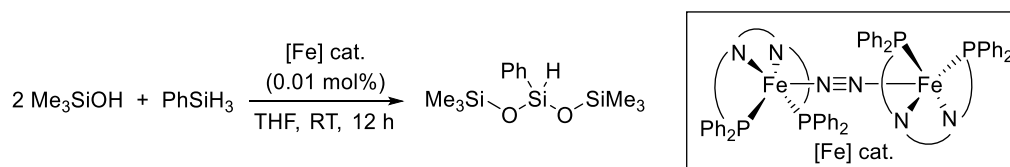
Scheme 5. Reductive elimination of H_2 via iron phosphine bond dissociation.

In chapter 2, the author discusses a MLC character of the PNNP-iron complexes (Scheme 6). Deprotonation of a methylene moiety in PNNP-Ph-iron(II) dichloride $[\text{FeCl}_2(\text{PNNP})]$ underwent upon treatment with NaOtBu to afford the corresponding iron(II) complex where a partially dearomatized PNNP ligand coordinates to the iron(II) center in a tetradentate manner. The resulting complex further reacted with $i\text{PrOH}$ in the presence of AgOTf , resulting in the formation of dicationic complex $[\text{Fe}(\text{PNNP-Ph})]^{2+}$ via successive rearomatization of the pyridine ring and ligand disproportionation.



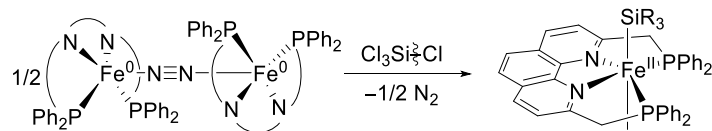
Scheme 6. The MLC process of PNNP-Ph iron complex. Dearomatization reaction deprotonation by NaOtBu and rearomatization reaction via O–H cleavage.

In chapter 3, the catalytic activity of the PNNP-R-Fe complexes was discussed. $[\{\text{Fe}(\text{PNNP-R})\}_2(\mu\text{-N}_2)]$ catalyzed dehydrogenative coupling of silanols with silanes to selectively form various hydrosiloxanes, which are important building blocks for the synthesis of a range of siloxane compounds. The system exhibited the highest catalytic efficiency among the previously reported transition-metal-catalyzed systems (Scheme 7).

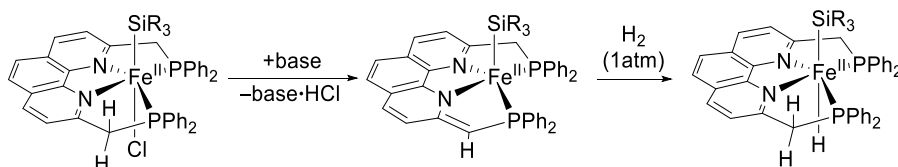


Scheme 7. Catalytic syntheses of hydrottrisiloxanes via dehydrogenative coupling of silanols with hydrosilanes by a PNNP-Ph iron complex.

In chapter 4, the author describes the reactivity of iron(0) complex toward the activation of strong chemical bonds. It was revealed that the inactive Si–Cl bond of chlorosilanes reacts with iron(0) complexes via oxidative addition, resulting in the formation of iron silyl(chloro)complexes (Scheme 8). The mechanistic study supported the occurrence of the Si–Cl bond cleavage via radical pathway. The partial hydrogenation of iron silyl(chloro)complex successfully underwent to form iron silyl(hydrido)complex, which is facilitated by the MLC (Scheme 9).



Scheme 8. The cleavage reaction of Si–Cl bond by PNNP iron(0) complex.



Scheme 9. Selective substitution reaction of Fe–Cl bond to Fe–H bond via MLC process. Dearomatization reaction of silyl(chloro)iron complex to form dearomatized complex and rearomatization reaction of dearomatized complex by hydrogen.

References

1. a) W. C. Zeise and O. K. Dan, *Vidensk. Selskabs. Forh* **1825**, 13. b) W. C. Zeise, *Pogg. Ann. Phys.* **1827**, 9, 632.
2. a) E. C. Constable and C. E. Housecroft, *Chem. Soc. Rev.* **2013**, 42, 1429. b) J. J. Boor, Jr., *Ziegler-Natta Catalysts and Polymerization*; Academic Press: New York, **1979**. c) T. J. Colacot, *Chem. Rev.* **2003**, 103, 3101. d) R. L. Davis, J. Stiller, T. Naicker, H. Jiang and K. A. Jørgensen, *Angew. Chem. Int. Ed.* **2014**, 53, 7406. e) R. Noyori and S. Hashiguchi, *Acc. Chem. Res.* **1997**, 30, 2, 97. f) G. C. Vougioukalakis and R. H. Grubbs, *Chem. Rev.* 110, 3, 1746. g) C. C. C. J. Seechurn, M. O. Kitching, T. J. Colacot and V. Snieckus, *Angew. Chem. Int. Ed.* **2012**, 51, 5062.
3. a) N. Miyaura and A. Suzuki, *J. Chem. Soc., Chem. Commun.* **1979**, 866. b) T. Hayashi, M. Konishi, Y. Kobori, M. Kumada, T. Higuchi and Ken Hirotsu, *J. Am. Chem. Soc.* **1984**, 106, 158. c) J. P. Wolfe, R. A. Singer, B. H. Yang and S. L. Buchwald, *J. Am. Chem. Soc.* **1999**, 121, 9550.
4. a) P. C. J. Kamer and P. W. N. M. van Leeuwen, *Phosphorus(III) Ligands in Homogeneous Catalysis: Design and Synthesis*, Wiley West Sussex, UK, **2012**. b) C. A. Tolman, *Chem. Rev.* **1977**, 77, 313.
5. a) J. R. Khusnutdinova, D. Milstein, *Angew. Chem. Int. Ed.* **2015**, 54, 12236. b) J. I. van der Vlugt, *Eur. J. Inorg. Chem.* **2012**, 363. c) P. J. Chirik and K. Wieghardt, *Science*, **2010** 327, 794. d) V. T. Annibale and D. Song, *RSC Adv.* **2013**, 3, 11432. e) D. G. A. Verhoeven and M. E. Moret, *Dalton Trans.* **2016**, 45, 15762.
6. a) S. Hashiguchi, A. Fujii, J. Takehara, T. Ikariya and R. Noyori, *J. Am. Chem. Soc.* **1995**, 117, 7562. b) A. Fujii, S. Hashiguchi, N. Uematsu, T. Ikariya and R. Noyori, *J. Am. Chem. Soc.* **1996**, 118, 2521. c) R. Noyori, T. Ohkuma and M. Kitamura, *J. Am. Chem. Soc.* **1987**, 109, 5856.
7. J. Zhang, G. Leitus, Y. Ben-David and D. Milstein, *J. Am. Chem. Soc.* **2005**, 127, 10840.

8. a) B. Bichler, C. Holzhacker, B. Stöger, M. Puchberger, L. F. Veiros and K. Kirchner, *Organometallics* **2013**, *32*, 4114. b) T. P. Gonçalves and K.-W. Huang, *J. Am. Chem. Soc.* **2017**, *139*, 13442.
9. a) S. W. Kohl, L. Weiner, L. Schwartzburd, L. Konstantinovski, L. J. W. Shimon, Y. Ben-David, M. A. Iron and D. Milstein, *Science* **2009**, *324*, 74. b) M. Montag, J. Zhang and D. Milstein, *J. Am. Chem. Soc.* **2012**, *134*, 10325.
10. a) E. Khaskin, M. A. Iron, L. J. W. Shimon, J. Zhang and D. Milstein, *J. Am. Chem. Soc.* **2010**, *132*, 8542. b) Y.-H. Chang, Y. Nakajima, H. Tanaka, K. Yoshizawa and F. Ozawa, *J. Am. Chem. Soc.* **2016**, *138*, 6985.
11. a) J. Zhang, G. Leituss, Y. Ben-David and D. Milstein, *Angew. Chem. Int. Ed.* **2006**, *45*, 1113. b) N. Gorgas, B. Stöger, L. F. Veiros, E. Pittenauer, G. Allmaier and K. Kirchner, *Organometallics* **2014**, *33*, 6905. c) T. Zell, Y. Ben-David and D. Milstein, *Angew. Chem. Int. Ed.* **2014**, *53*, 4685. d) R. Langer, G. Leituss, Y. Ben-David and D. Milstein, *Angew. Chem. Int. Ed.* **2011**, *50*, 2120. e) J. A. Luque-Urrutia and A. Poater, *Inorg. Chem.* **2017**, *56*, 14383. f) E. Balaraman, C. Gunanathan, J. Zhang, L. J. W. Shimon and D. Milstein, *Nat. Chem.* **2011**, *3*, 609.
12. a) C. Gunanathan, Y. Ben-David and D. Milstein, *Science* **2007**, *317*, 790. b) E. Balaraman, E. Khaskin, G. Leituss and D. Milstein, *Nat. Chem.* **2013**, *5*, 122. c) P. Hu, E. Fogler, Y. Diskin-Posner, M. A. Iron and D. Milstein, *Nat. Commun.* **2015**, *6*, 6859. d) M. Feller, E. Ben-Ari, Y. Diskin-Posner, R. Carmieli, L. Weiner and D. Milstein, *J. Am. Chem. Soc.* **2015**, *137*, 4634. e) Y.-H. Chang, K. Takeuchi, M. Wakioka and F. Ozawa, *Organometallics* **2015**, *34*, 1957. f) S. R. M. M. de Aguiar, Ö. Öztöpcü, B. Stöger, K. Mereiter, L. F. Veiros, E. Pittenauer, G. Allmaier and K. Kirchner, *Dalton Trans.* **2014**, *43*, 14669. g) A. Nerush, M. Vogt, U. Gellrich, G. Leituss, Y. Ben-David and D. Milstein, *J. Am. Chem. Soc.* **2016**, *138*, 6985.
13. a) R. Zissel, *Tetrahedron Lett.* **1989**, *30*, 463. b) R. Langer, I. Fuchs, M. Vogt, E. Balaraman, Y. Diskin-Posner, L. J. W. Shimon, Y. Ben-David and D. Milstein, *Chem. Eur. J.* **2013**, *19*, 3407. c) T. Miura, M. Naruto, K. Toda, T. Shimomura and S. Saito, *Sci. Rep.* **2017**, *7*, 1586. d) S. Saito, N. Ryoji, T. Miura, M. Naruto, K. Iida, Y. Takada, K. Toda, S. Nimura, S. Agrawal and S. Lee, *US Pat.* 0107151A1, **2016**.
14. a) B. Plietker, *Iron Catalysis in Organic Chemistry*, Wiley-VCH: Weinheim, Germany, **2008**. b) I. Bauer and H.-J. Knölker, *Chem. Rev.* **2015**, *115*, 3170. c) C. Bolm, J. Legros, J. Le Pailh and L. Zani, *Chem. Rev.* **2004**, *104*, 6217. d) A. Fürstner, *ACS Cent. Sci.* **2016**, *2*, 778.

Chapter 1

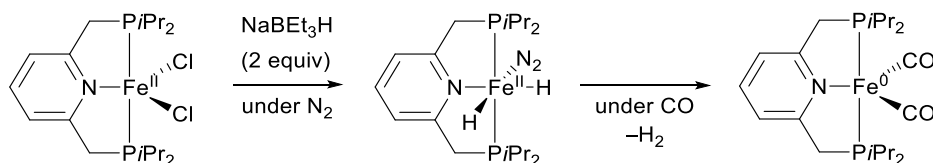
Synthesis and Properties of PNNP-Iron Complexes

Abstract

A well-defined iron complex system was established using PNNP-R (R = Ph and Cy) as a strong σ -donating ligand with a rigid meridional tetradentate structure. Treatment of PNNP-R with iron dihalide provided $[\text{FeCl}_2(\text{PNNP-Ph})]$ (**1a**) and $[\text{FeBr}_2(\text{PNNP-Cy})]$ (**1b**). The reaction of **1a** with 2 equiv of NaBEt_3H quickly provided nitrogen bridged dinuclear iron(0) complex $[\{\text{Fe}(\text{PNNP-Ph})\}_2(\mu\text{-N}_2)]$ (**2a**). In contrast, the reaction of **1b** with 2 equiv of NaBEt_3H initially afforded $[\text{Fe}(\text{H})_2(\text{PNNP-R})]$ (**4b**), which slowly changed to $[\{\text{Fe}(\text{PNNP-Cy})\}_2(\mu\text{-N}_2)]$ (**2b**) with hydrogen elimination. According to these results, it was concluded that the reduction of **1a** and **1b** proceeded via successive formation of dihydride intermediates **4a** and **4b** and H_2 reductive elimination, which strongly support the hemilabile behavior of PNNP-R. Complex **2a** smoothly underwent ligand exchange to form $[\text{Fe}(\text{CO})(\text{PNNP-Ph})]$ (**5a**) and $[\text{Fe}(\text{H-SiPhH}_2)(\text{PNNP-Ph})]$ (**6a**).

Introduction

Unsaturated low-valent iron complexes (e.g. iron(0) and iron(I) complexes) are known to show unique reactivity as seen in the reactions catalyzed by metalloenzymes, such as nitrogenase, which is composed of iron-sulfide clusters.¹ Iron(0) complexes as common low-valent iron complexes are generally synthesized by iron dihalide complex with Na or KC_8 as reducing agents.² The alternative pathway to synthesize iron(0) complexes is the reduction of iron dihalide complexes with hydride reagents such as LiAlH_4 , NaBEt_3H and R_3SiH .³ The reaction proceeds via formation of the corresponding hydride complex and dehydrogenation by reductive elimination reaction, successively. The reaction sometimes provides the dihydride complex intermediate, since the low-valent iron(0) complexes are sometimes less stable unless they are supported by π -acidic ligands such as CO, which strongly coordinated with the iron(0) center due to their strong π -acidity.⁴ For example, Chirik reported that the reaction of $[\text{Fe}(\text{II})\text{Cl}_2\text{PNP}^{\text{iPr}}]$ (PNP^{iPr} = bis(diisopropylphosphino)pyridine) with 2 equiv of NaBEt_3H resulted in the formation of $[\text{Fe}(\text{II})\text{H}_2\text{PNP}^{\text{iPr}}]$.⁵ The reductive elimination of $[\text{Fe}(\text{II})\text{H}_2\text{PNP}^{\text{iPr}}]$ underwent under CO atmosphere to provide $[\text{Fe}(\text{0})(\text{CO})_2\text{PNP}^{\text{iPr}}]$. The resulting complex is enough stabilized by CO, and thus the resulting iron(0) complexes exhibit suppressed reactivity unless CO elimination was performed by heating or irradiation to form the reactive coordinatively unsaturated iron(0) species (Scheme 1-1).



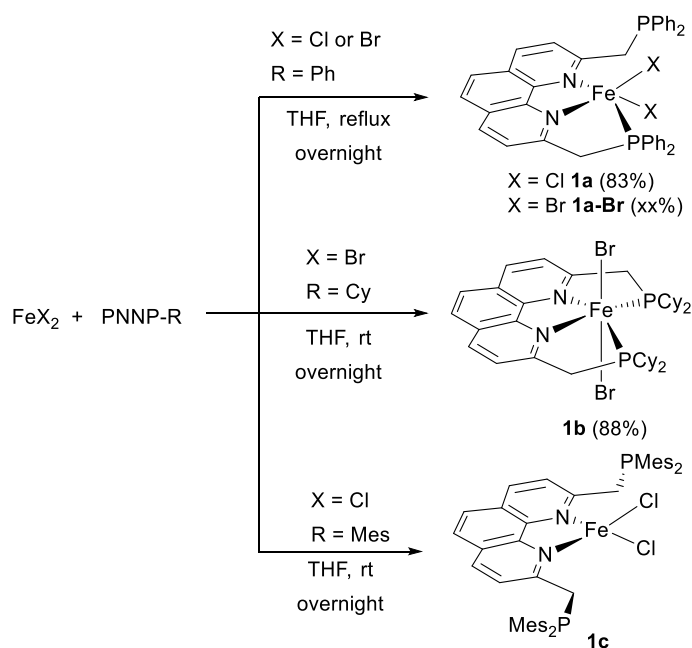
Scheme 1-1. The reaction of $[\text{Fe}(\text{II})\text{Cl}_2\text{PNP}^{\text{iPr}}]$ with NaBEt_3H .

Based on these observations, the author focused on the PNNP-R ligand.⁵ The π -acidic phenanthroline backbone of the PNNP-R are known to act as a redox active ligand, and thus could moderately stabilize iron(0) center. As a result, the author expected that the synthesis of iron(0) complexes without CO ligands, which could easily afford reactive coordinatively unsaturated iron(0) species with the electron rich iron(0) center. In this chapter, various PNNP-R-supported-iron(0) complexes, which are active towards ligand exchange, were synthesized and

structurally characterized.

Results and discussion

PNNP-R (R = Ph, Cy, Mes) ligands were synthesized according to the modified procedure of the previously reported literature method, in which neocuproine was used as a starting compound is initially lithiated and then treated with the corresponding phosphine chlorides.⁶



Scheme 1-2. The synthesis of **1a**, **1a-Br**, **1b**, and **1c**.

Complexation of an iron metal source with a PNNP-R ligand was performed by mixing FeX_2 (X = Cl and Br) and PNNP-Ph ligand in THF at 60 °C (Scheme 1-2). After overnight refluxing, PNNP-Ph-supported iron dichloride $[\text{FeCl}_2(\text{PNNP-Ph})]$ (**1a**) was obtained as a red solid (82% yield). In contrast, the reaction of PNNP-Cy or PNNP-Mes with FeCl_2 resulted in the formation of a complicated mixture (Scheme 1-2). From the mixture, $[\text{FeCl}_2(\text{PNNP-Mes})]$ (**1c**) was isolated after the recrystallization from the Et_2O /Hexane solution, and identified by a single crystal X-ray diffraction study (*vide infra*). According to the previous report,⁶ the reaction of FeBr_2 with PNNP-Cy was performed in THF to selectively provide $[\text{FeBr}_2(\text{PNNP-Cy})]$ (**1b**) in 88% yield (Scheme 1-2). The prepared complexes **1a-c** exhibited the paramagnetic broad signals in the ^1H NMR spectra in CD_2Cl_2 . The single-

crystal X-ray diffraction studies of **1a-Cl** and **1a-Br** indicated that both of the complexes possess the iron center coordinated with two halide ions, two nitrogen atoms of the phenanthroline moiety, and one phosphine side-arm. The other phosphine-side-arm was found to be free from the iron metal. The bond angles around the iron in **1a** were $149.90(3)^\circ$ (N2-Fe1-P1) and 119.94° (average of N1-Fe1-Cl1 , N1-Fe1-Cl2 and Cl1-Fe1-Cl2). Thus, it was indicated that **1a** exhibited a distorted trigonal-bipyramidal structure ($\tau = 0.50$).⁷ Similarly, complex **1a-Br** exhibited the distorted trigonal-bipyramidal structure, with the τ value of 0.50. In contrast, **1b** supported by PNNP-Cy, which has stronger electron donating cyclohexyl phosphino groups, was found to form a ‘closed’ hexacoordinate octahedral structure. Complex **1c** incorporating bulky mesityl groups on the phosphorus atom was found to adopt a distorted tetrahedral geometry, in which the iron center was coordinated with two chloride ions and two nitrogen atoms of the phenanthroline moiety. The bond lengths around the iron center in **1a**, **1b** and **1c** were in the normal range of those of iron(II) complexes with a high spin state.

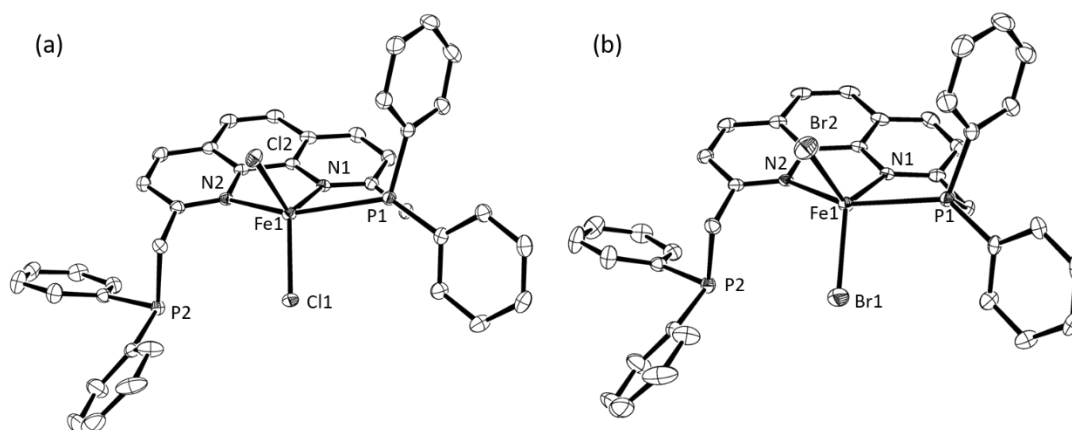


Figure 1-1. Molecular structures of **1a-Cl** (a) and **1a-Br** (b). Hydrogen atoms are omitted for clarity.

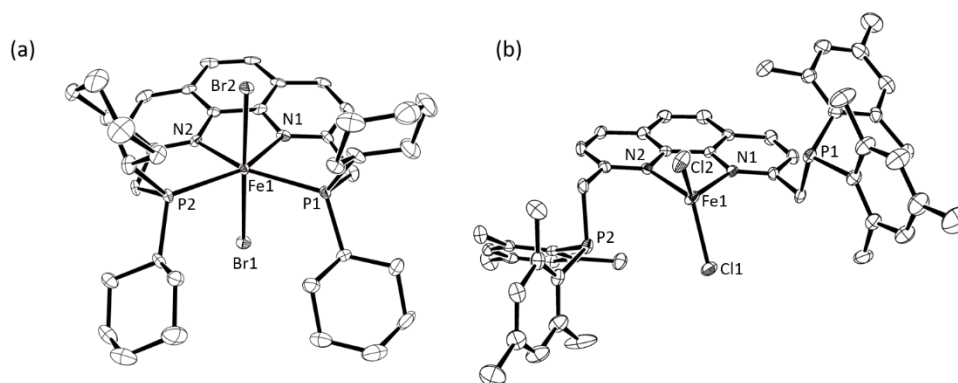
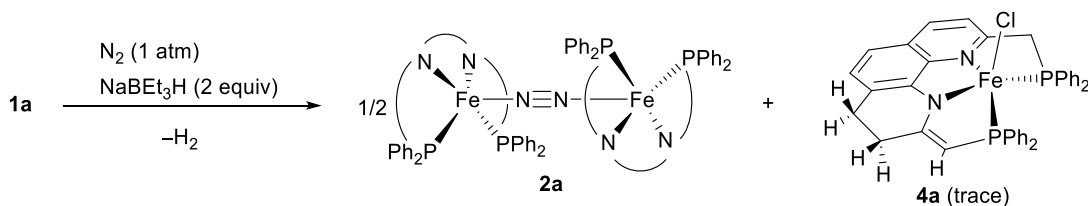


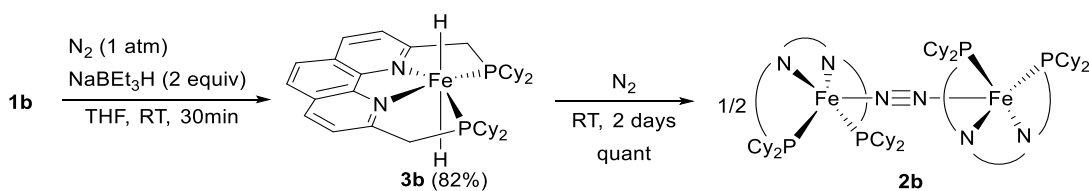
Figure 1-2. Molecular structures of **1b** (a) and **1c** (b). Hydrogen atoms are omitted for clarity.

Several iron(II) complexes were reported as being convertible into catalytically active iron(0) species by treatment with a suitable reducing agent; e.g. by the use of a mild hydride reagent.³ In the reaction of bipyridine-supported iron complexes, the evolution of H₂ gas was detected, and thus strongly supporting the formation of intermediary dihydride species. However, the hydride reduction process of iron(II) complexes are not well-defined yet.^{3b-e} Motivated by these facts, the author aimed at demonstrating the reduction pathway of iron(II) complexes in an attempt to isolate an active iron(0) species by utilizing a rigid PNNP-R ligand. Treatment of **1a** with NaBEt₃H (2 equiv) under an Ar atmosphere resulted in the formation of a complicated mixture. On the other hand, when the reaction was performed under a N₂ atmosphere, iron(0) dinitrogen complex [$\{\text{Fe}(\text{PNNP-Ph})\}_2(\mu\text{-N}_2)$] (**2a**) was obtained as a major product, accompanied by **4a** as a trace by-product (Scheme 1-3). **4a** possesses the asymmetric PNNP-Ph' ligand with one dearomatized pyridine backbone. Milstein also reported hydride reduction of Ru analogous complex [Ru(H)₂(PNNP-*t*Bu)], resulting in the formation of structurally similar asymmetric Ru complex [Ru(H)(PNNP-*t*Bu')] as a sole product, which was generated via H atom shift of the dihydride intermediate [Ru(H)₂(PNNP-*t*Bu)].^{6b}

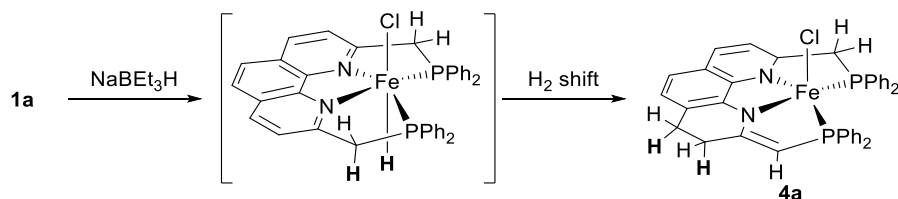
The reaction of **1b** with NaBEt₃H resulted in the formation of a dihydride complex [Fe(H)₂(PNNP-Cy)] (**3b**) in 82% yield (Scheme 1-4). Complex **3b** was gradually converted into **2b**, which was obtained as a mixture containing several unidentified compounds. Therefore, **2a** is likely formed via intermediary dihydride complex **3b**, which underwent H₂ reductive elimination.



Scheme 1-3. The reaction of **1a** with NaBEt₃H.

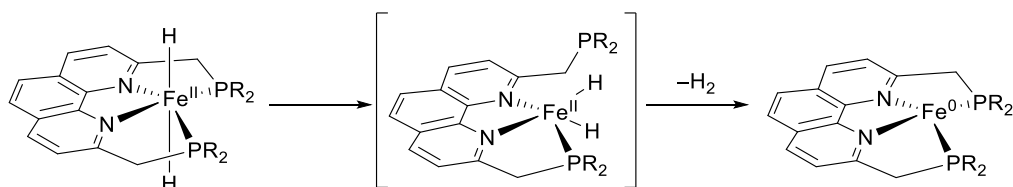


Scheme 1-4. The reaction of **1b** with NaBEt₃H.



Scheme 1-5. H₂ shift reaction to provide **4a**.

Notably, two hydride ligands in **3b**, which located in *trans* positions, underwent reductive elimination reaction. Therefore, the occurrence of phosphine side-arm dissociation is strongly suggested in this step. This is also supported by the reluctant step-wise reduction of **1b** via **3b**, which has the more donating PNNP-Cy ligand than the PNNP-Ph ligand. It is likely that the hemilabile behavior of PNNP-R ligands is the characteristic properties in the Fe system, which exhibit lower bonding energy than the corresponding **4d** and **5d** analogues. This could be a reason for the facile formation of Fe(0) complexes **2a** and **2b** in our system (Scheme 1-6).



Scheme 1-6. Reductive elimination reaction of [Fe(H)₂(PNNP-R)] facilitated by the hemilabile behavior.

Complexes **2a** and **2b** readily decomposed under 1 atm of N₂ atmosphere even in the solid state because of the facile liberation of the N₂ ligand. Thus, it was difficult to isolate **2a** and **2b**, and they were prepared *in situ* and identified by NMR spectroscopic analysis.

Fortunately, when the THF/hexane solution of the reaction mixture was cooled to -40 °C, single deep-red crystals of **2a** or **2b** were obtained and quickly subjected to a single crystal X-ray analysis under a cold N₂ stream, which supports the N₂-bridged dinuclear Fe structure of **2a** and **2b** (vide infra).

Since **2a** and **2b** are supported by the electron-donating PNNP-R ligand, they are expected to possess a highly electron-rich iron(0) center. However, the ν_{N2} was not detected either by infrared and raman spectroscopy. To evaluate the π-back-bonding ability between the iron(0) and PNNP-Ph moiety, the iron(0) carbonyl complex [Fe(CO)(PNNP-Ph)] (**5a**) was synthesized by the ligand exchange of **2a** with CO. Reaction of **2a** with CO (1 atm) immediately proceeded at room temperature to form **5a** quantitatively (Scheme 1-7). **5a** exhibits a strong ν_{CO} band

at a rather lower field of 1866 cm^{-1} than structurally similar iron(0) complexes bearing a bipyridine or a phosphinomethyl(bipyridine) ligand.^{4,8}

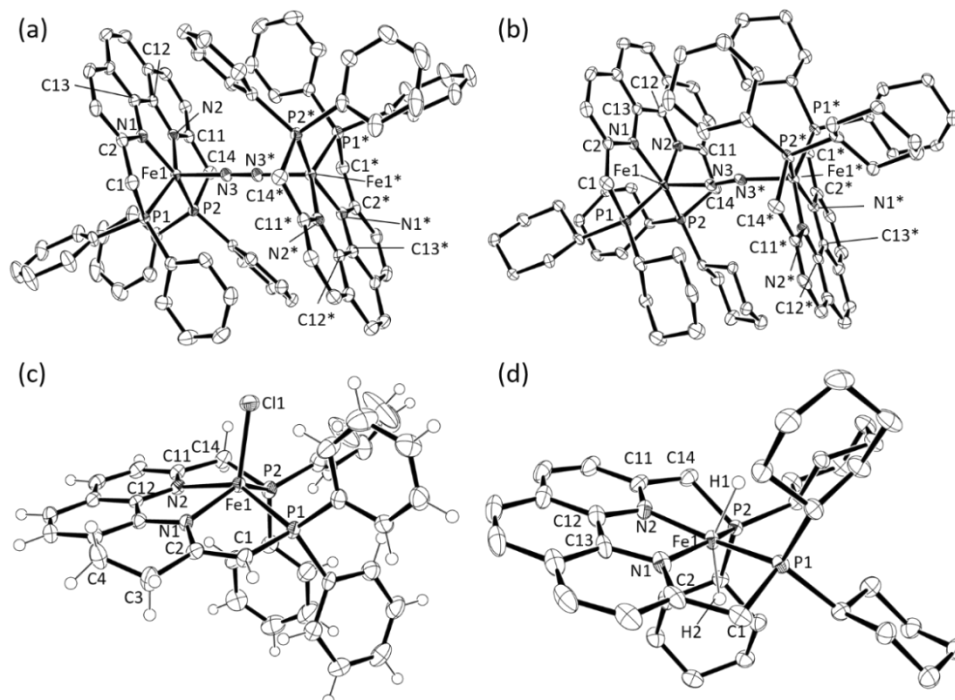
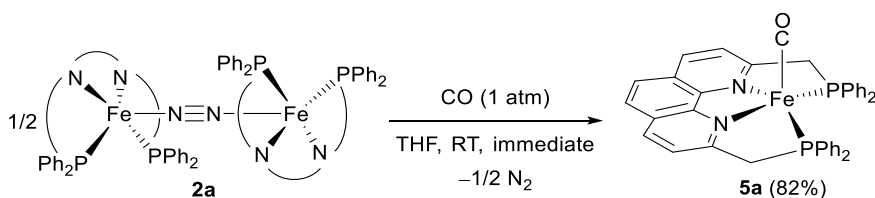


Figure 1-3. Molecular structures of **2a** (a), **2b** (b), **4a** (c), and **3b** (d). Hydrogen atoms are omitted for clarity excepted Fe–H (H1 and H2) in **3b** and **4a**.



Scheme 1-7. The synthesis of **5a**.

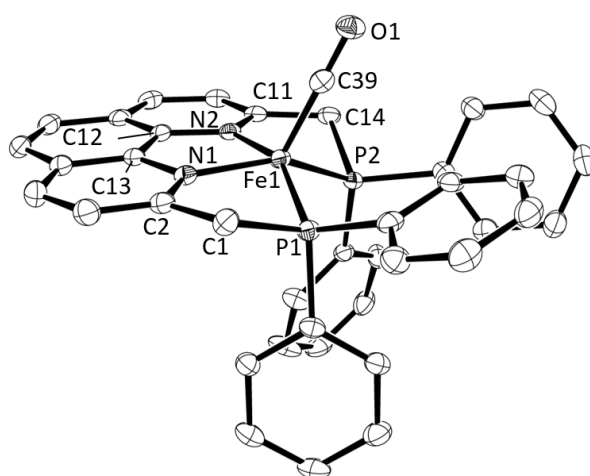
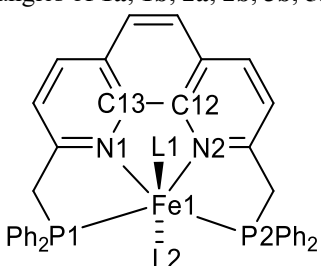


Figure 1-4. Molecular structure of **5a**. Hydrogen atoms are omitted for clarity.

Complexes **2a**, **2b**, and **5a** adopted a square-pyramidal geometry [$\tau = 0.099$ (**2a**), 0.143 (**2b**), and 0.143 (**4a**)],⁷ in which the N₂ or CO ligands were located at the axial position. The core structure around the Fe atom was comparable to those of previously reported iron(0) analogous complexes (Figure 1-2).⁹ The bond lengths of N–N bonds in **2a** and **2b** of 1.135(4) and 1.134(6) Å are in the range of normal N–N triple bond lengths. The phenanthroline ligands were reported to act as redox-active ligands and exhibit shortened C11–C12 and elongated N–C11/C12 bond lengths in their reduced form.⁹ Indeed, the C11–C12 bonds in **2a**, **2b**, and **5a** (1.390–1.396 Å) were slightly shorter than those in Fe(II) complexes **1a** and **1b** (1.41–1.44 Å), whereas N–C11/C12 bonds were slightly longer in **2a**, **2b**, and **5a** (1.382–1.391 Å) than in **1a** and **1b** (1.354–1.367 Å) (Table 1). Thus, the occurrence of the electron transfer from the Fe(0) atom to the PNNP-R ligand was indicated in **2a**, **2b**, and **5a**.

Table 1 Selected bond lengths and angles of **1a**, **1b**, **2a**, **2b**, **3b**, **5a**, and **6a**



Complex	C12–C13	N2–C12	N1–C13
1a	1.438(2)	1.364(2)	1.360(2)
1b	1.426(9)	1.354(8)	1.367(8)
2a	1.392(4)	1.382(3)	1.387(3)
2b	1.390 (av.)	1.387 (av.)	1.384(av.)
3b	1.379(5)	1.382(4)	1.377(4)
5a	1.390(4)	1.375(4)	1.384(4)
6a	1.407(5)	1.387(4)	1.381(4)

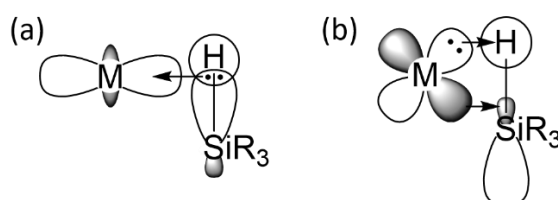
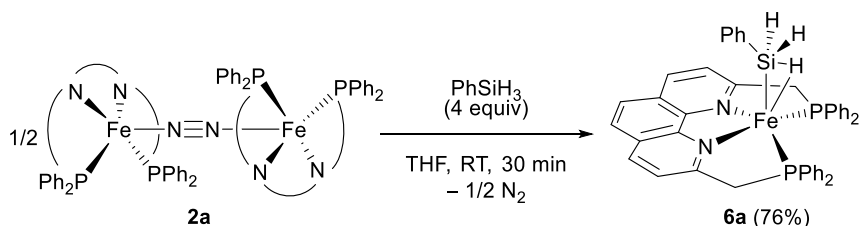


Figure 1-5. The fragment of silane complex. (a) σ donation from the occupied Si–H donated to metal center (b) π back-donation from the metal center to empty Si–H on orbital.

Interestingly, **2a** also underwent the ligand exchange with PhSiH_3 to form the $\text{Fe}(0)$ silane complex **6a** as the sole product in 76% yield (Scheme 1-8). Hydrosilanes are known to form the corresponding silane complexes, which are recognized as a precursor towards the oxidative addition reaction of hydrosilanes.¹⁰ The silane complexes are generally stabilized by two interactions. One is the σ donation from occupied Si–H bond to the metal center and the other is π back-donation from the metal center to empty σ^* orbital of the Si–H bond (Figure 1-5). As discussed above, complexes **2a** and **5a** were stabilized by π back-donation from the iron(0) center to N_2 or CO , it was therefore assumed that the Si–H bond in **6a** also underwent π -back-donation from the iron(0) metal to some extent. In the ^1H NMR spectrum, the agostic Si–H signal was observed in a high-field region, $\delta = -8.06$ ppm as a triplet ($^2J_{\text{PH}} = 36.8$ Hz) and SiH_2 protons are equivalently observed at $\delta = 4.75$ ppm as a singlet signal. The silyl signal was observed at $\delta = 12.2$ ppm in the $^{29}\text{Si}\{^1\text{H}\}$ NMR spectrum. The CH_2 moieties in the PNNP-Ph ligand exhibits diastereotopic two doublet signals at $\delta = 4.26$ and 3.81 ppm with the geminal coupling of 63.8 Hz.



Scheme 1-8. Synthesis of **6a**.

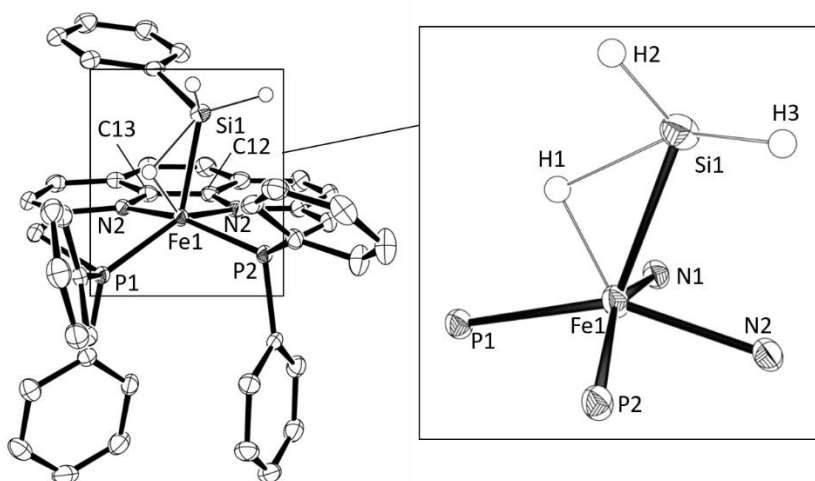


Figure 1-6. ORTEP diagram of **6a** with 50% probability ellipsoids. Selected bond lengths (Å) and bond angles (°): Fe1–N1 1.928(2), Fe1–N2 1.917(2), Fe1–P1 2.2032(9), Fe1–P2 2.1629(9), Fe1–Si1 2.2926(10), Fe1–H1 1.51(4), Si1–H1 1.71(3), Si1–H2 1.47(4), Si1–H3 1.31(3), N1–Fe1–N2 81.71(10), P1–Fe1–P2 103.75(3), N1–Fe1–Si1 99.70(8), N2–Fe1–Si1 87.28(8), P1–C14–Si1 125.71(4), P2–C14–Si1 95.38(4).

X-ray diffraction studies revealed a highly distorted squarepyramidal structure of **6a** ($\tau = 0.11$) (Figure 1-6). The agnostic proton H1, which was determined by difference Fourier synthesis, located at the bridging position between the Si and the Fe atoms. The Si1–H1 bond length was slightly elongated (1.711 Å) compared to normal Si–H single bonds. In addition, the P1–Fe1–Si1 angle was 125.71(4), which was significantly larger than P2–Fe1–Si1 angle of 95.38(4). Thus, the agostic coordination mode of the Si1–H1 moiety was also evidenced.¹⁰ The C11–C12 and N–C11/C12 bond lengths exhibit similar values to those in **2a**, **2b**, and **5a**, again indicating the electron transfer from the Fe(0) centre to the PNNP-Ph ligand in **6a**.

Conclusion

In summary, the PNNP-R ligands with strong σ -donating ability successfully enabled us to isolate various iron complexes as stable low-spin species. Notably, efficient hydride reduction of iron(II) complexes to reactive iron(0) complexes **2a** and **2b** was demonstrated to support the formation of dihydrido complexes **3a** and **3b** as intermediates. It was also confirmed that **3b** underwent the reductive elimination reaction of H₂, which possibly initiated with the dissociation of the phosphine side-arm of the PNNP-Cy ligand. Thus, the hemilabile behavior of the PNNP-R ligands was suggested. In addition, the nitrogen coordinated to the iron(0) metal in **2a** and **2b** was replaced by various ligands such as CO and hydrosilane to give the corresponding iron(0) complexes **5a** and **6a**. The agnostic Si–H bond in **6a** was confirmed by both NMR and X-ray structural analysis, which support the efficient activation of Si–H bond by π back-donation from the Fe(0) center.

Experimental section

General considerations

All experiments were performed under a nitrogen atmosphere using Schlenk techniques or a glove box unless otherwise noted. n-Hexane, tetrahydrofuran, toluene and dichloromethane were purified by a solvent purification system (MBraun SPS-800 or a Glass Contour Ultimate Solvent System). C₆D₆ was dried over sodium benzophenone

ketyl and distilled. CD_2Cl_2 was dried over CaH_2 and distilled. Neocuproine was recrystallized by C_6H_6 from neocuproine hemihydrate. All other reagents were purchased from commercial suppliers and used without further purification unless otherwise noted. ^1H , $^{13}\text{C}\{^1\text{H}\}$, $^{29}\text{Si}\{^1\text{H}\}$, and $^{31}\text{P}\{^1\text{H}\}$ NMR spectra (^1H , 600 MHz; ^{13}C , 150 MHz; ^{29}Si , 119 MHz; ^{31}P , 243 MHz) were recorded on a Bruker AVANCE III HD 600 spectrometer. Chemical shifts are reported in δ (ppm) and referenced to the residual solvent signals for ^1H and ^{13}C , 1,4-bis(trimethylsilyl)benzene for ^{29}Si , and 85% H_3PO_4 as an external standard for ^{31}P . The highresolution ESI mass spectra were obtained on a Bruker microTOF II. Column chromatography was performed with silica gel (Kanto Chemical CO., INC. Silica gel 60 N, 100–210 μm).

Synthesis of 2,9-bis((diphenylphosphino)methyl)-1,10 phenanthroline (PNNP-Ph)

PNNP-Ph was prepared according to the modified procedure of the reported method.^{6a} To a THF solution of Neocuproine (0.500 mg, 2.4 mmol), was added a THF solution of LDA (1 M in THF, 14.4 mL, 9.84 mmol) at $-30\text{ }^\circ\text{C}$. PPh_2Cl (1.05 g, 4.81 mmol) was added to the solution at $0\text{ }^\circ\text{C}$ and the solution was slowly warmed to room temperature and stirred overnight. The solution was quenched with H_2O (0.5 mL) and stirred for 1 h. After removal of solvent *in vacuo*, the residue was dissolved in CH_2Cl_2 (10 mL) and washed with H_2O (5 mL). The organic layer was corrected, dried over Na_2SO_4 and filtered. After evaporation, the residue was dissolved in CH_2Cl_2 (10 mL) and subjected to silica gel column chromatography (THF/hexane = 1/1). Crystallization of the obtained orange solid from $\text{CH}_2\text{Cl}_2/\text{Et}_2\text{O}$ (1:50 v/v) afforded PNNP-Ph as a white crystalline solid (1.24 g, 82.4 %). ^1H NMR (600 MHz, C_6D_6): δ 7.67 (t, 8H, $J = 16.2\text{ Hz}$, PPh-*H*), 7.40 (d, 2H, $J = 8.16\text{ Hz}$, Phen-*H*), 7.14–7.11 (m, 10H, Ar-*H*), 7.07 (d, 2H, $J = 8.16\text{ Hz}$, Phen-*H*), 7.04 (t, 4H, $J = 7.85\text{ Hz}$, PPh-*H*), 4.00 (s, 4H, PCH_2) ppm. $^{13}\text{C}\{^1\text{H}\}$ NMR (150 MHz, C_6D_6): δ 159.05 (d, $^2J_{\text{P}} = 8.7\text{ Hz}$), 146.6, 139.7, 135.7, 133.7 ($^1J_{\text{P}} = 18.7\text{ Hz}$), 128.8, 128.7, 128.7, 128.2, 125.6, 123.3, 123.2, 40.4 ($^1J_{\text{P}} = 17.9\text{ Hz}$) ppm. $^{31}\text{P}\{^1\text{H}\}$ NMR (243 MHz, C_6D_6): δ –10.2 ppm.

Synthesis of 2,9-bis((dicyclohexylphosphino)methyl)-1,10 phenanthroline (PNNP-Cy)

PNNP-Cy (1.31 g, 2.18 mmol, 78.0 %) was prepared following the same procedure of PNNP-Ph using Neocuproine (0.600 g, 2.8 mmol), LDA (1 M in THF, 11.5 ml, 11.5 mmol) and PClCy_2 (1.34 g, 5.8 mmol). ^1H NMR (600 MHz, C_6D_6): δ 7.62 (d, 2H, $J = 8.22$, Phen-*H*), 7.57 (d, 2H, $J = 8.28$, Phen-*H*), 7.26 (s, 2H, Phen-*H*), 3.44 (s, 4H, PCH_2), 1.94-1.92 (m, 8H, Cy-*H*), 1.80-1.70 (m, 12H, Cy-*H*), 1.62-1.61 (m, 4H, Cy-*H*), 1.46 (qt, 4H, $J = 12.30$, 7.23, Cy-*H*), 1.33-1.16 (m, 16H, Cy-*H*) ppm. $^{13}\text{C}\{^1\text{H}\}$ NMR (150 MHz, C_6D_6): δ 161.7 (d, $^2J_{\text{P}} = 9.9$ Hz), 146.5, 135.7, 127.1, 125.5, 123.5 (d, $^3J_{\text{P}} = 7.3$), 34.2 (d, $^1J_{\text{P}} = 16.2$ Hz), 33.8 (d, $^1J_{\text{P}} = 23.1$ Hz), 30.5 (d, $^2J_{\text{P}} = 14.3$ Hz), 29.6 (d, $^3J_{\text{P}} = 9.1$ Hz), 27.8 (d, $^2J_{\text{P}} = 17.6$ Hz), 27.7, 27.0 ppm. $^{31}\text{P}\{^1\text{H}\}$ NMR (243 MHz, C_6D_6): δ 2.6 ppm.

Synthesis of bromodimesitylphosphine (PBrMes_2)

2,4,6-Trimethylbromobenzene 0.200 g (1.01 mmol) was dissolved in 20 ml of THF was slowly added to the THF solution (10 ml) of magnesium 0.035 (1.50 mmol) and catalytic amount of iodine at 50 °C. The preparation of 2,4,6-trimethylphenyl magnesium bromide was tracked by ^1H NMR and TLC. After 5 hours at 50 °C, the solution was cooled to room temperature. PBr_3 0.130 g (0.48 mmol) in 30 ml THF solution, which was prepared another Schlenk tube, was cooled to -78 °C and slowly transferred the 2,4,6-Trimethylphenyl magnesium bromide solution by cannular and stirred from -78 °C to room temperature overnight. Removal of the solvent *in vacuo*, 50 ml of hexane were added and the solution was passed through celite. Concentrate of the solvent to 2 ml, the solution was stood on -40 °C and the colorless crystals of PClMes_2 were obtained. ^1H NMR (600 MHz, C_6D_6): δ 6.59 (d, $J = 3.06$ Hz, 4H), 2.38 ($^4J_{\text{P}}$, $J = 2.40$ Hz, 12H), 2.00 (s, 6H) ppm. $^{13}\text{C}\{^1\text{H}\}$ NMR (150 MHz, C_6D_6): δ 197.8 (d, $^1J_{\text{P}} = 13.4$ Hz), 190.7, 153.3, 120.3, 74.8 (d, $^3J_{\text{P}} = 1.4$ Hz), 62.0 ppm. $^{31}\text{P}\{^1\text{H}\}$ NMR (243 MHz, C_6D_6): δ 74.9 ppm.

Synthesis of 2,9-bis((dimesitylphosphino)methyl)-1,10 phenanthroline (PNNP-Mes)

PNNP-Cy (1.31 g, 2.18 mmol, 78.0 %) was prepared following the same procedure of PNNP-Ph using Neocuproine (0.600 g, 2.8 mmol), LDA (1 M in THF, 11.5 ml, 11.5 mmol) and PBrMes_2 (1.34 g, 5.8 mmol). ^1H NMR (600 MHz, C_6D_6): δ 7.40 (d, $J = 8.16$, 2H), 6.74 (dd, $J = 8.1$, 1.23, 2H), 6.62 (d, $J = 2.28$, 2H), 4.43 (s, 4H), 2.22 (s, 12H), 2.04 (s, 6H) ppm. $^{13}\text{C}\{^1\text{H}\}$ NMR (150 MHz, C_6D_6): δ 161.7 (d, $^2J_{\text{P}} = 9.9$ Hz), 146.5, 135.7, 127.1, 125.5, 123.5 (d, $^3J_{\text{P}} = 7.3$), 34.2

(d, $^1J_P = 16.2$ Hz), 33.8 (d, $^1J_P = 23.1$ Hz), 30.5 (d, $^2J_P = 14.3$ Hz), 29.6 (d, $^3J_P = 9.1$ Hz), 27.8 (d, $^2J_P = 17.6$ Hz), 27.7, 27.0 ppm. $^{31}\text{P}\{^1\text{H}\}$ NMR (243 MHz, C_6D_6): δ 2.6 ppm.

Synthesis of $[\text{FeCl}_2(\text{PNNP-Ph})]$ (**1a**)

A Schlenk tube equipped with a Teflon valve was charged with a THF solution (10 mL) of PNNP-Ph (0.200 g, 0.34 mmol) and FeCl_2 (0.045 g, 0.35 mmol). The solution was stirred at 60 °C overnight. Cooling to room temperature, the red solids were filtered and evaporated. The residue was extracted with CH_2Cl_2 to obtain red solution and dried *in vacuo* to give **1a** as a red solid (0.201 g, 82.3%). Single crystal of **1a** was obtained from a cold $\text{CH}_2\text{Cl}_2/\text{Et}_2\text{O}$ solution. ^1H NMR (600 MHz, CD_2Cl_2): δ 51.42 (br), 24.81 (br), 15.53 (br), 11.11 (br), 7.32 (s), 4.96 (br), 2.67 (br), -8.89 (br).

Anal. Calcd for $\text{C}_{38}\text{H}_{30}\text{Cl}_2\text{FeN}_2\text{P}_2$: C 64.89; H 4.30; N 3.98%. Found: C 64.91; H 4.48; N 4.07%.

Synthesis of $[\text{FeBr}_2(\text{PNNP-Ph})]$ (**1a-Br**)

A Schlenk tube equipped with a Teflon valve was charged with a THF solution (10 mL) of PNNP-Ph (0.100 g, 0.17 mmol) and FeBr_2 (0.038 g, 0.18 mmol). The solution was stirred at 60 °C overnight. Cooling to room temperature, the red solids were filtered and evaporated. The residue was extracted with CH_2Cl_2 to obtain blue solution and dried *in vacuo* to give **1a-Br** as a red solid (0.201 g, 82.3%). Single crystal of **1a** was obtained from a cold $\text{CH}_2\text{Cl}_2/\text{Et}_2\text{O}$ solution. ^1H NMR (600 MHz, CD_2Cl_2): δ 51.42 (br), 24.81 (br), 15.53 (br), 11.11 (br), 7.32 (s), 4.96 (br), 2.67 (br), -8.89 (br).

Synthesis of $[\text{FeBr}_2(\text{PNNP-Cy})]$ (**1b**)^{6d}

Complex **1b** was synthesized by modified procedure of the previous report.^{6d} A Schlenk tube equipped with a Teflon valve was charged with a THF solution (10 mL) of PNNP-Cy (0.500 g, 0.83 mmol) and FeBr_2 (0.180 g, 0.84 mmol). The solution was stirred at room temperature overnight. Removal of the volatiles, and the residue was washed with toluene (10 ml \times 3) and dried. The resulting red solids were extracted with THF and filtered. Volatile were removed to give **1b** as a red solid (0.598 g, 88.1%). Single crystal of **1b** was obtained from $\text{CH}_2\text{Cl}_2/\text{Et}_2\text{O}$ solution at room temperature. ^1H NMR (600 MHz, CD_2Cl_2): δ 64.12 (br), 30.81 (br), 26.80 (br), 9.93 (br), 8.72 (br), 7.46 (s), 7.35 (s), 4.91 (br), 1.90-0.82 (m), -12.81 (br) ppm.

Synthesis of [FeCl₂(PNNP-Mes)] (**1c**)

1c was prepared following the same procedure of **1b** using PNNP-Mes (0.500 g, 0.71 mmol), FeCl₂ (0.091 g, 0.72 mmol). Single crystal of **1c** was obtained from CH₂Cl₂/Et₂O solution at room temperature from complex mixture. However, **1c** couldn't be isolated from the complex mixture.

Synthesis of [Fe(PNNP-Ph)]₂(μ-N₂) (**2a**) with (**4a**)

1a (0.5 mg, 7.1 μmol) was suspended in C₆D₆ (0.4 mL) and NaBEt₃H (1 M in THF, 86 μl, 86 μmol) was added. The resulting deep red solution was filtered and measured ¹H and ³¹P NMR spectra to confirm the quantitative formation of **2a** as a sole product. Alternatively, preparation of a single crystal of **2a** is as follows. To a THF suspension (5 mL) of **1a** (0.030 g, 43 μmol), was added NaBEt₃H (1 M in THF, 86 μl, 86 μmol) under N₂ atmosphere. The solution was stirred at room temperature for 30 minutes and filtered. After adding hexane (5 ml), the solution was kept at -40 °C for 2 days to give **2a** and **4b** as deep red crystals, which easily decompose at room temperature. ¹H NMR (600 MHz, C₆D₆): δ 7.51 (d, 2H, *J* = 6.72 Hz, Phen-*H*), 7.37 (d, 2H, *J* = 6.28 Hz, Phen-*H*), 7.23 (s, 2H, Phen-*H*), 6.94 (t, 2H, *J* = 6.78 Hz, PPh-*H*), 6.61-6.66 (m, 8H, PPh-*H*), 6.57 (t, 2H, *J* = 13.7 Hz, PPh-*H*), 6.41-6.38 (br, 8H, PPh-*H*), 4.27 (d, 2H, *J* = 15.61 Hz, PCH₂), 4.16 (d, 2H, *J* = 14.58 Hz, PCH₂) ppm. ³¹P{¹H} NMR (243 MHz, C₆D₆): δ 93.0 ppm. ¹³C NMR spectrum of **2a** was obscured due to the significant overlap with NaBEt₃H/THF signals.

Synthesis of [Fe(PNNP-Cy)]₂(μ-N₂) (**2b**)

2b was prepared following the same procedure of **2a**. ¹H NMR (600 MHz, C₆D₆): δ 7.61 (d, 2H, *J* = 6.48 Hz, Phen-*H*), 7.50 (d, 2H, *J* = 5.30 Hz, Phen-*H*), 7.16 (s, 2H, Phen-*H*), 3.68 (d, 2H, *J* = 14.71 Hz, PCH₂), 3.41 (d, 2H, *J* = 15.03 Hz, PCH₂), 1.90-0.31 (44H, PCy-*H*) ppm. ³¹P{¹H} NMR (243 MHz, C₆D₆): δ 94.1 ppm. ¹³C NMR spectrum of **2b** was obscured due to the significant overlap with NaBEt₃H/THF signals.

Synthesis of [Fe(H)₂(PNNP-Cy)] (**3b**)

To C₆H₆ suspension (5 mL) of **1b** (0.030 g, 37 μmol), was added NaBEt₃H (1 M in THF, 74 μl, 74 μmol) under N₂ atmosphere. The solution was stirred at room temperature for 30 minutes and filtered. Removal of the solvent gave **3b** as

a green solid. (0.0201 mg, 31 μ mol, 82.4%). **3b** was crystallized from THF/*n*-hexane in -40 °C for 1 day to form green block crystals. ^1H NMR (600 MHz, C_6D_6): δ 7.36 (s, 2H, Phen-*H*), 7.32 (d, 2H, $J = 7.32$ Hz, Phen-*H*), 7.16 (d, H, $J = 7.31$ Hz, Phen-*H*), 3.63-3.62 (m, 4H, PCH_2), 2.26 (d, 4H, $J = 7.26$ PCH), 1.87-1.64 (m, 24H, PCy-*H*), 1.37-1.16 (m, 16H, PCy-*H*), -8.45 ppm (t, 2H, $^2J_{\text{P}} = 68.9$ Hz, FeH_2) ppm. $^{31}\text{P}\{^1\text{H}\}$ NMR (243 MHz, C_6D_6): δ 93.0 ppm. Complex **3b** easily decompose and its elemental analysis was not available.

Synthesis of $[\text{Fe}(\text{PNNP-Ph})(\text{CO})]$ (**5a**)

In a Schlenk tube, **2a** was in situ generated by the reaction of **1a** (0.050 g, 0.071 mmol) with 2 equiv of NaBEt_3H (1 M in THF, 86 μ l, 86 μ mol). After freeze-thaw-pump cycles ($\times 3$), CO (1 atm) was introduced into the reaction vessel. After stirring at room temperature for 30 minutes, all the volatiles were evaporated. The residue was dissolved in C_6H_6 (5 mL) and filtered with an alumina pad. After evaporation, **5a** was obtained as a deep green solid (0.038 g, 82.2%). Single crystals of **5a** was obtained from cold THF/hexane solution. ^1H NMR (600 MHz, C_6D_6): δ 7.60-7.51 (m, 8H, PPh-*H*), 7.15-7.12 (m, 10H, Phen-*H* + PPh-*H*), 6.84 (d, 2H, $J = 6.84$ Hz, Phen-*H*), 6.78-6.76 (m, 4H, PPh-*H*), 6.65 (t, 2H, $J = 7.02$ Hz, Phen-*H*), 6.49 (t, $J = 7.62$ Hz, PPh-*H*), 4.32 (d, 2H, $J = 14.58$ Hz, PCH_2), 4.08-4.03 (m, 2H, PCH_2) ppm. $^{13}\text{C}\{^1\text{H}\}$ NMR (150 MHz, C_6D_6): δ 216.3, 156.4, 139.3, 139.0, 132.7, 130.8, 130.5, 129.2, 125.8, 117.5, 112.1, 46.5 ppm. $^{31}\text{P}\{^1\text{H}\}$ NMR (243 MHz, C_6D_6): δ 108.6 ppm. IR (ATR) ν_{CO} 1866 cm^{-1} . Anal. Calcd for $\text{C}_{39}\text{H}_{30}\text{FeN}_2\text{OP}_2$: C 70.92; H 4.58; N 4.24%. Found: C 70.99; H 4.69; N 4.07%

Synthesis of $[\text{Fe}(\eta^2\text{-HSiH}_2\text{Ph})(\text{PNNP-Ph})]$ (**6a**)

To a THF suspension of **1a** (0.030 g, 43 μ mol) (3 mL), was added NaBEt_3H (1 M in THF, 86 μ l, 86 μ mol) at room temperature. The mixture was stirred for 30 minutes, added phenylsilane (18.4 mg, 171 μ mol), and further stirred for 30 minutes at the temperature. The solution was concentrated to dryness under vacuum, and the resulting solid was washed by hexane (1 mL \times 3) and dried. The resulting compound was extracted with C_6H_6 and filtered. After evaporation, **6a** was obtained as a black solid (0.024 g, 76 %). **6a** was crystallized from cold $\text{Et}_2\text{O}/n$ -hexane to form block crystals. ^1H NMR (600 MHz, C_6D_6): δ 7.54 (br, 4H, PPh-*H*), 7.20 (s, 2H, Phen-*H*), 7.13-7.05 (m, 8H, Ar-*H*), 6.93 (d, 2H, $J = 7.26$ Hz,

Phen-*H*), 6.83 (t, 1H, $J = 7.26$, SiPh), 6.71-6.69 (m, 6H, Ar-*H*), 6.61 (t, $J = 7.32$ Hz, 2H), 6.51-6.49 (m, 6H), 4.75 (s, 2H, SiH₂), 4.26 (d, 2H, $J = 15.84$ Hz, PCH₂), 3.81 (dt, 2H, $J = 16.5, 5.28$ Hz, PCH₂), -8.06 ppm (t, 1H, $J = 36.8$ Hz, agostic-*H*). ¹³C{¹H} NMR (150 MHz, C₆D₆): δ 155.9, 140.8, 140.6, 133.1, 132.9, 132.8, 131.3, 131.2, 129.5, 128.3, 126.7, 126.0, 118.8, 114.6, 47.1 ppm. ³¹P{¹H} NMR (243 MHz, C₆D₆): δ 106.22 ppm. ²⁹Si{¹H} NMR (119 MHz, C₆D₆): δ 12.2 ppm. Complex **5a** easily decompose via PhSiH₃ dissociation even at -35 °C and elementary analysis is not available.

Single crystal X-ray diffraction studies.

The single crystal X-ray diffraction measurements of **1a**, **1a-Br**, **1b**, **1c**, **2a**, **2b**, **3b**, **4a**, **5a**, and **6a** was performed under a cold nitrogen stream on a Rigaku XtaLAB P200 diffractometer with a Pilatus 200K detector using multi-layer mirror monochromated Mo K α radiation. The determination of crystal systems and unit cell parameters and data processing were performed with the *CrystalClear* program package. The data sets were corrected for Lorentz and polarization effects and absorption. The structure was solved by direct methods using SIR2014 program,¹¹ and refined by full-matrix least squares calculations on F² for all reflections (SHELXL-2014/7),¹² using Yadokari-XG 2009.¹³

Table S1 Crystallographic data of **1a**, **1a-Br**, **1b**, and **1c**.

	1a	1a-Br	1b	1c
Empirical formula	C ₃₈ H ₃₀ Cl ₂ FeN ₂ P ₂	C ₃₈ H ₃₀ Br ₂ FeN ₂ P ₂	C ₃₈ H ₅₄ Br ₂ FeN ₂ P ₂	C ₅₀ H ₅₄ Cl ₂ FeN ₂ P ₂ ·2CH ₂ Cl ₂
Formula weight	703.33	792.25	816.42	1041.49
Temperature/K	93(2)		93(2)	93(2)
Crystal system	monoclinic	monoclinic	monoclinic	triclinic
Space group	<i>P</i> 2 ₁ / <i>c</i>	<i>P</i> 2 ₁ / <i>c</i>	<i>P</i> 2 ₁ / <i>c</i>	<i>P</i> -1
<i>a</i> / Å	12.0414(19)	12.0261(16)	18.299(5)	12.159(4)
<i>b</i> / Å	20.358(3)	20.692(3)	14.140(4)	14.945(4)
<i>c</i> / Å	14.058(2)	14.078(2)	15.178(5)	15.574(5)
α / °	90	90	90	91.656(7)
β / °	107.348(3)	106.737(3)	107.351(7)	112.751(7)
γ / °	90	60	90	99.027(4)
Volume / Å ³	3289.4(9)	3354.8(8)	374.6(19)	2565.0(14)
<i>Z</i>	4	4	4	2
<i>R</i> ₁ / %	0.029	0.0607	0.0744	0.0943
<i>wR</i> ₂ / %	0.0644	0.1650	0.189	0.2563
GOF	1.028	1.032	1.107	1.050

Table S2 Crystallographic data of **2a**, **2b**, and **3b**

	2a	2b	3b
Empirical formula	C ₃₈ H ₃₀ FeN ₃ P ₂ ·0.5C ₄ H ₈ O	2C ₃₈ H ₅₄ FeN ₃ P ₂ ·C ₆ H ₁₄	C ₄₀ H ₃₄ FeN ₃ OP ₂
Formula weight	690.49	1427.44	658.63
Temperature/ <i>K</i>	93(2)	93(2)	93(2)
Crystal system	triclinic	monoclinic	Ortho
Space group	<i>P</i> -1	<i>P</i> 2/ <i>n</i>	<i>Pna</i> 2 ₁
<i>a</i> / Å	9.785(2)	26.075(4)	15.1645(19)
<i>b</i> / Å	12.336(2)	10.1672(15)	13.1906(19)
<i>c</i> / Å	14.142(3)	28.018(4)	16.823(2)
α / °	92.154(4)	90	90
β / °	103.057(5)	93.366(3)	90
γ / °	101.480 (5)	90	90
Volume / Å ³	1623.5(6)	7415.0(19)	3365.1(8)
<i>Z</i>	2	4	4
<i>R</i> ₁ / %	0.0507	0.0771	0.0338
<i>wR</i> ₂ / %	0.104	0.1849	0.0802
GOF	1.063	1.128	1.022

Table S3 Crystallographic data of **4a**, **5a**, and **6a**

	4a	5a	6a
Empirical formula	C ₃₈ H ₃₁ ClFeN ₂ P ₂ ·3C ₄ H ₈ O	C ₃₉ H ₃₀ FeN ₂ OP ₂	C ₄₄ H ₃₈ FeN ₂ P ₂ Si
Formula weight	885.20	660.44	740.64
Temperature/ <i>K</i>	93(2)	93(2)	93(2)
Crystal system	triclinic	triclinic	triclinic
Space group	<i>P</i> -1	<i>P</i> -1	<i>P</i> -1
<i>a</i> / Å	12.3072(17)	9.8699 (9)	96.735(9)
<i>b</i> / Å	13.6666(19)	10.7795(13)	12.1191(8)
<i>c</i> / Å	14.0043(15)	16.578(2)	17.8980(18)
α / °	78.215(11)	82.081(11)	70.273(16)
β / °	73.196(8)	75.1840(10)	74.867(16)
γ / °	88.020(12)	65.260(8)	67.391(14)
Volume / Å ³	2206.6(5)	1547.7(3)	1802.4(4)
<i>Z</i>	2	2	2
<i>R</i> ₁ / %	0.0891	0.0519	0.0576
<i>wR</i> ₂ / %	0.1744	0.1322	0.1111
GOF	1.082	1.07	1.672

Reference

1. P. V. Rao and R. H. Holm, *Chem. Rev.* **2004**, *104*, 527.
2. a) A. A. Danopoulos, J. A. Wright and W. B. Motherwell, *Chem. Commun.* **2005**, 784. b) R. J. Trovitch, E. Lobkovsky and P. J. Chirik, *Inorg. Chem.* **2006**, *45*, 7252. c) T. Hashimoto, R. Hoshino, T. Hatanaka, Y. Ohki and K. Tatsumi, *Organometallics* **2014**, *33*, 921. d) P. A. Rudd, S. Liu, L. Gagliardi, V. G. Young, Jr. and C. C. Lu, *J. Am. Chem. Soc.* **2011**, *133*, 20724.
3. a) S. C. Bart, E. Lobkovsky and P. J. Chirik, *J. Am. Chem. Soc.* **2004**, *126*, 13794. b) N. Guo, M.-Y. Hu, Y. Feng and S.-F. Zhu, *Org. Chem. Front.* **2015**, *2*, 692. c) Y. Toya, K. Hayasaka and Hiroshi Nakazawa, *Organometallics* **2017**, *36*, 9, 1727. d) Y. Sunada, D. Noda, H. Soejima, H. Tsutsumi and H. Nagashima, *Organometallics* **2015**, *34*, 2896.
4. C. Bolm, J. Legros, J. Le Pailh and L. Zani, *Chem. Rev.* **2004**, *104*, 6217.
5. R. J. Trovitch, E. Lobkovsky and P. J. Chirik, *Inorg. Chem.* **2006**, *45*, 7252.
6. a) R. Ziessel, *Tetrahedron Lett.* **1989**, *30*, 463. b) R. Langer, I. Fuchs, M. Vogt, E. Balaraman, Y. Diskin-Posner, L. J. W. Shimon, Y. Ben-David and D. Milstein, *Chem. Eur. J.* **2013**, *19*, 3407. c) T. Miura, M. Naruto, K. Toda, T. Shimomura and S. Saito, *Sci. Rep.* **2017**, *7*, 1586. d) S. Saito, N. Ryoji, T. Miura, M. Naruto, K. Iida, Y. Takada, K. Toda, S. Nimura, S. Agrawal and S. Lee, *US Pat.* 0107151A1, **2016**.
7. A. W. Addison, T. N. Rao, J. Reedijk, J. van Rijn and G. C. Verschoor, *J. Chem. Soc., Dalton Trans.* **1984**, 1349.
8. a) M. D. Varga, R. Costa, R. Reina, A. Núñez, M. Á. Maestro and J. Mahía, *J. Organomet. Chem.* **2003**, 677, 101. b) T. Zell, P. Milko, K. L. Fillman, Y. Diskin-Posner, T. Bendikov, M. A. Iron, G. Leitun, Y. Ben-David, M. L. Neidig and D. Milstein, *Chem. Eur. J.* **2014**, *20*, 4403.
9. a) M. Wang, J. England, T. Weyhermüller and K. Wieghardt, *Eur. J. Inorg. Chem.* **2015**, 1511. b) M. Wang, T. Weyhermüller and K. Wieghardt, *Eur. J. Inorg. Chem.* **2015**, 3246. c) C. Wolff, A. Gottschlich, J. England, K. Wieghardt, W. Saak, D. Haase and R. Beckhaus, *Inorg. Chem.* **2015**, *54*, 4811.
10. a) N. J. Archer, R. N. Haszeldine and R. V. Parish, *J. Chem. Soc., Dalton Trans.* **1979**, *4*, 695. b) Z. Lin, *Chem. Soc. Rev.* **2002**, *31*, 239. c) C. Hauf, J. E. Barquera-Lozada, P. Meixner, G. Eickerling, S. Altmannshofer, D. Stalke, T. Zell, D. Schmidt, U. Radius and W. Scherer, *Z. Anorg. Allg. Chem.* **2013**, 639, 1996. d) P. Meixner, K. Batke, A. Fischer, D. Schmitz, G. Eickerling, M. Kalter, K. Ruhland, K. Eichele, J. E. Barquera-Lozada, N. P. M. Casati, F. Montisci, P. Macchi and W. Scherer, *J. Phys. Chem. A* **2017**, 121, 7219.
11. M.C. Burla, R. Caliendo, B. Carrozzini, G. L. Casciarano, C. Cuocci, C. Giacovazzo, M. Mallamo, A. Mazzone and G. Polidori, *J. Appl. Cryst.* **2015**, *48*, 306.
12. G. M. Sheldrick, SHELXL-2014/7, University of Göttingen, Göttingen, Germany, **2014**.
13. C. Kabuto, S. Akine, T. Nemoto, E. Kwon, Release of software (Yadokari-XG 2009) for crystal structure analyses. *Nippon Kessho Gakkaishi* **2009**, *51*, 218.

Chapter 2

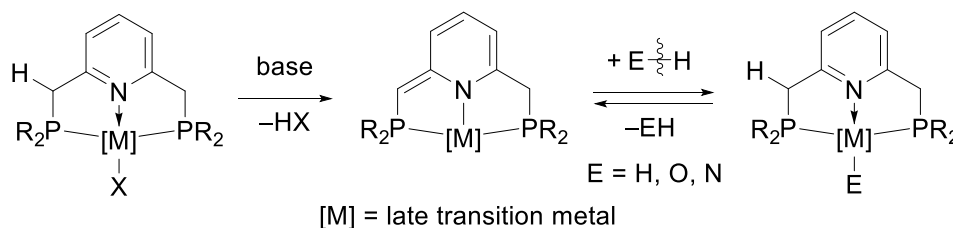
Metal-Ligand Cooperation of the PNNP-Iron System

Abstract

Iron(II) dichloride coordinated with a phenanthroline-based meridional PNNP-Ph ligand $[\text{FeCl}_2(\text{PNNP-Ph})]$ (**1**) underwent deprotonation upon treatment with *t*BuONa to afford the corresponding iron(II) complex **2**, which bears a deprotonated PNNP-Ph ligand with one dearomatized pyridine ring. Single-crystal X-ray diffraction analysis supported the contribution of the charge delocalization both on the ligand and the iron metal in the structure of **2**. Complex **2** further reacted with *t*BuOH in the presence of AgBF_4 in MeCN to form dicationic complex with PNNP-Ph ligand $[\text{Fe}(\text{MeCN})_2(\text{PNNP-Ph})]^{2+}(\text{BF}_4^-)$ (**5**). The result supported the rearomatization of the pyridine ring via O–H bond cleavage.

Introduction

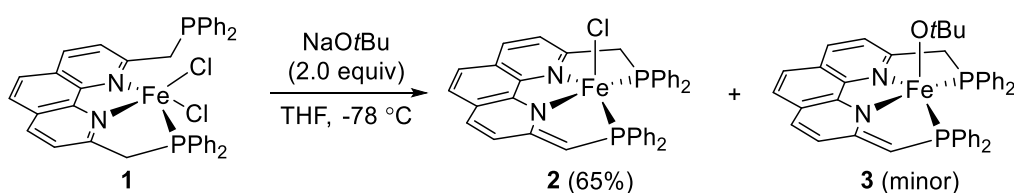
Metal–ligand cooperation (MLC) processes are known as the key step in the activation of various chemical bonds.¹ MLC processes that involve aromatization-dearomatization sequences in acridine- and pyridine-based meridional PNP and PNN pincer ligands² are particularly applicable to various reactions such as H–H,³ O–H,⁴ or N–H⁵ bond cleavage reactions (Scheme 2-1), catalytic hydrogenations,⁶ and others.⁷



Scheme 2-1. Bond cleavage by MLC of a PNP pincer system.

Recently, Milstein^{8a} and Saito^{8b,8c} have independently reported the application of tetradentate PNNP-R ligands as the next generation of rigid meridional ligand systems. The significant progress has been made by Milstein's group; i.e. they successfully demonstrated a new mode of MLC in PNNP-R-Ru complexes, which included the reversible hydrogenation of the conjugated phenanthroline backbone. In this context, the author prepared a series of iron complexes bearing PNNP-R ligands as discussed in chapter 1. It was revealed that the strong donating ability of the PNNP-R ligand efficiently stabilizes iron complexes with a low-spin state. With the prepared diamagnetic PNNP-R-iron complexes in hands, the author next set out to expand the concept of MLC to the PNNP-iron complexes. It is expected that the stabilized low spin iron complex system can be easily handled and analyzed and thus enable us to precisely modulate the iron reaction sphere. In this chapter, novel iron complexes bearing a deprotonated PNNP ligand were synthesized.

Results and discussion



Scheme 2-2. The reaction of **1** with 2 equiv of NaOtBu.

In an attempt to synthesize an iron complex with the dearomatized PNNP-Ph ligand, the deprotonation of **1** did not proceed using organic amines NEt_3 or DBU. Complex **1** reacted with a stronger base NaOtBu at $-78\text{ }^\circ\text{C}$ to afford **2** as a major product (65% using 2 equiv of NaOtBu) and 86% (using 1 equiv of NaOtBu) as well as several by-products including **3** and paramagnetic species (Scheme 2-2, Figure 2-1). It was confirmed that **2** did not react further with NaOtBu . Thus, it is likely that **3** was obtained as a by-product in the formation of **2**.

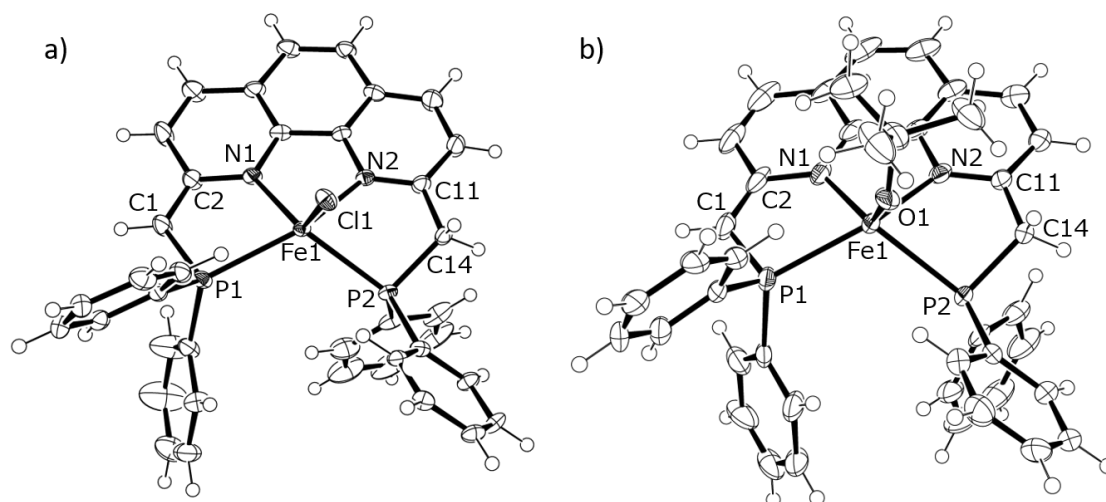
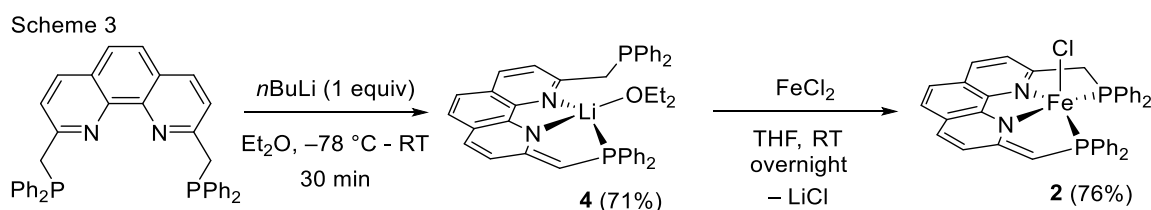


Figure 2-1. Molecular structures of **2** (a) and **3** (b) with 50% probability ellipsoids. Selected bond lengths (\AA) and bond angles ($^\circ$) of **2**: C1–C2 1.380(6), C11–C14 1.501(6), C2–N1 1.387(6), C11–N2 1.324(6), Fe1–N1 2.180(3), Fe1–N2 2.080(3), Fe1–P1 2.5015(14), Fe1–P2 2.5314(15), C1–P1 1.773(5), C14–P2 1.844(5), Fe1–C11 2.2854(14), P1–C1–C2 119.1(4), P2–C14–C11 109.8(3). Selected bond lengths (\AA) and bond angles ($^\circ$) of **3**: C1–C2 1.374(5), C11–C14 1.507(4), C2–N1 1.391(4), C11–N2 1.333(4), Fe1–N1 2.109(3), Fe1–N2 2.186(3), Fe1–P1 2.4927(1), Fe1–P2 2.5073(9), C1–P1 1.756(4), C14–P2 1.850(3), Fe1–O1 1.865(2), P1–C1–C2 117.8(3), P2–C14–C11 109.9(2).

As mentioned above, several by-products were obtained in the reaction. These products exhibited similar solubility towards organic solvents as **2**. Although the reaction product was tried to isolate by recrystallized and purify by column chromatography, separation of **2** from the reaction mixture was unsuccessful. On the other hand, **3** was occasionally obtained as a single crystal during crystallization of the reaction mixture, and its structure was determined by single-crystal diffraction analysis (vide infra).

The author therefore examined the alternative synthetic route to afford complex **2** predominantly. First, selective deprotonation at the benzylic position of PNNP-Ph was performed by the treatment of PNNP-Ph with $n\text{BuLi}$ at $-78\text{ }^\circ\text{C}$, resulting in the formation of dearomatized-PNNP'-coordinated lithium compound **4** in 71% yield (Scheme 2-3, Figure 2-2). The reaction similarly proceeded when $(\text{CH}_3)_3\text{SiCH}_2\text{Li}$ was used, as previously reported.⁹

Complex **4** was fully identified by ^1H and ^{31}P NMR. The distorted square planar structure of **4**, which possesses a coordinated Et_2O molecule, was confirmed by single-crystal X-ray diffraction analysis. Reaction of **4** with FeCl_2 proceeded smoothly in THF at room temperature to give **2** in 76% yield (Scheme 3).



Scheme 2-2. The selective synthesis of **2**.

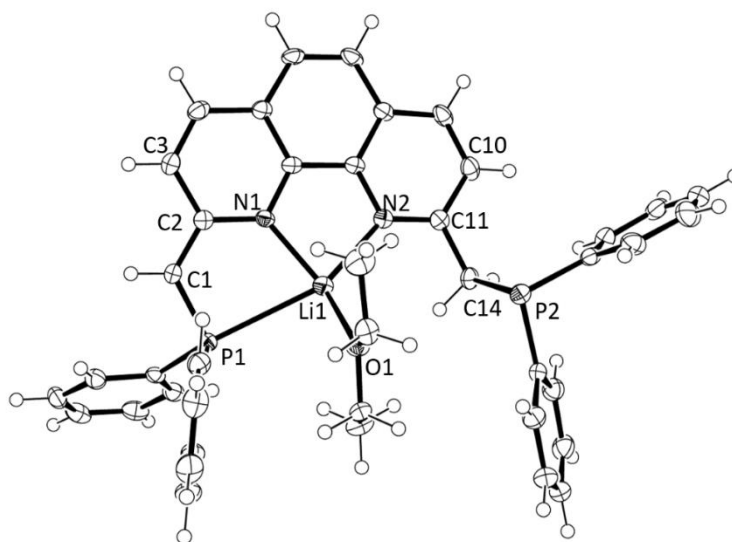


Figure 2-2. Molecular structure of **4** with 50% probability ellipsoids. Selected bond lengths (\AA) and bond angles ($^\circ$): C1–C2 1.380(3), C11–C14 1.501(3), C2–N1 1.333(3), C11–N2 1.383(5), Li1–N1 1.989(4), Li1–N2 2.080(3), Li1–P1 2.884(4), C1–P1 1.775(3), C14–P2 1.865(2), Li1–O1 2.015(4), P1–C1–C2 122.57(2), P2–C14–C11 113.11(2).

In the ^1H NMR spectrum of **2**, the benzylic protons exhibit two doublets (δ 3.80, 3.90 ppm, $^2J_{\text{HH}} = 18\text{ Hz}$). The methine proton is observed at δ 4.34 ppm as a broad singlet. The phenanthroline backbone exhibits six doublets. Thus, the anionic ligand system, which has one dearomatized heterocycle, is supported in **2**. Consistently, the ^{31}P NMR of **2** exhibits two broad signals at δ 42.1 ppm and -18.7 ppm. Since one of the ^{31}P NMR signals appears in the typical region of non-coordinating free phosphine ligands, which correlate with the signals at δ_{H} 3.80 and 3.90, which located in C14, in ^1H - ^{31}P HMBC NMR spectrum, dissociation of the phosphinomethyl-side-arm in **2** is indicated in solution. Variable temperature ^{31}P NMR study revealed that the two phosphorus signals become sharp

singlets at the same chemical shift value at $-20\text{ }^{\circ}\text{C}$. The observation indicates the fluxional behavior of the side-arms in **2**. The observation is sharp contrast from the analogous Ru complex, $[\text{Ru}(\text{H})(\text{PNNP-}i\text{tBu-H})]$, in which both side-arms coordinated to the Ru to exhibit two doublets at ambient temperature.^{8a}

The structures of **2** and **3** were confirmed by X-ray diffraction analysis. Complexes **2** and **3** adopt a square pyramidal molecular geometry, in which the Cl or *O**t*Bu ligands are located at the axial positions. The bond lengths around the iron center of **2** and **3** are in a typical value range for structurally similar iron(II) complexes with a low spin state.^{3a,6c,6e,10} The backbone structures of **2** and **3** are almost identical to that of **4** (Table S1). The C1–C2 bond lengths are 1.380(6) Å (**2**) and 1.374(5) Å (**3**), which are shorter than that of C11–C14 (1.501(6) Å for **2** and 1.507(4) Å for **3**), hence supporting the double bond character of the C1–C2 bond. Associated with this, the C1–C3 (1.454(6) Å for **2** and 1.440(5) Å for **3**) and C2–N1 (1.387(6) Å for **2** and 1.391(4) Å for **3**) are slightly elongated compared with the C10–C11 (1.413(6) Å for **2** and 1.398(4) Å for **3**) and C11–N2 (1.324(6) Å for **2** and 1.333(4) Å for **3**) bonds. Such a structural deviation of the deprotonated PNNP ligand backbone from the normal pyridine ring is also observed in the PNN and PNP systems.^{6e,7e,8a,10,11} The C1–P1 bond lengths are 1.773(5) (**2**) and 1.756(4) (**3**) Å, which are significantly shorter than the C14–P2 single bonds, 1.844(5) (**2**) and 1.850(3) (**3**). The results are consistent with the contribution of charge delocalization in one of the metallacycles, which contains P1, C1, C2, and N2 atoms (Scheme 4).

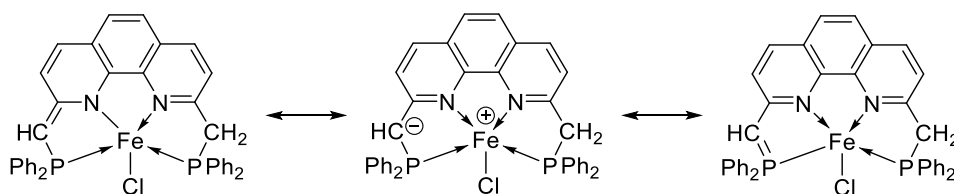
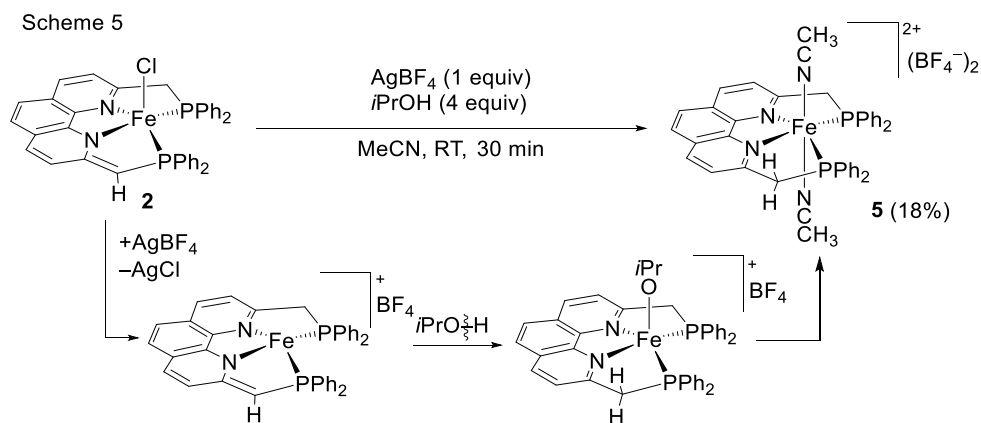


Figure 3. Resonance structure of **1**.

To shed light on the electronic structure of **2**, the DFT calculation was performed. The NAO analysis of **2** and the free PNNP-Ph ligand did not show significant difference between the two compounds. On the other hand, Mayer bond index of the C1–C2 bond slightly increases after the coordination of the iron atom; i.e. the bond index values of C1–C2 are 1.42 (PNNP-Ph) and 1.50 (**2**). On the other hand, the bond index of N1–C2 of PNNP-Ph (1.12)

decreased to 0.96 in **2**. These observations also supported the contribution of the resonance structure of **2** suggested in Scheme 4.



Scheme 2-3. The rearomatized reaction of **2**.

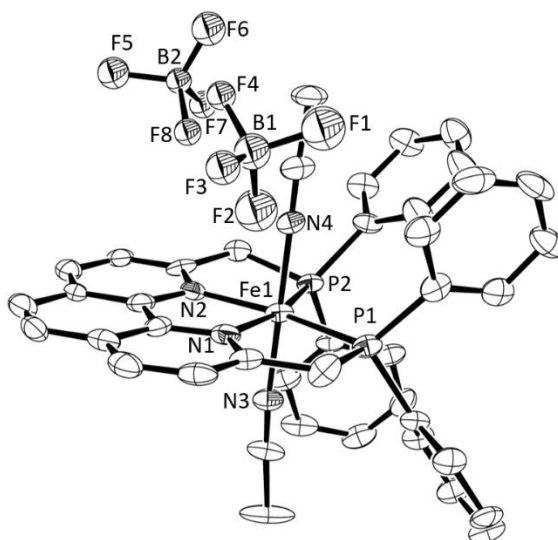


Figure 2-3. Molecular structure of **5** with 50% probability ellipsoids. Selected bond lengths (Å) and bond angles (°): C1–C2 1.380(3), C11–C14 1.501(3), C2–N1 1.333(3), C11–N2 1.383(5), Li1–N1 1.989(4), Li1–N2 2.080(3), Li1–P1 2.884(4), C1–P1 1.775(3), C14–P2 1.865(2), Li1–O1 2.015(4), P1–C1–C2 122.57(2), P2–C14–C11 113.11(2).

Next, the author commenced investigations into the reactivity of **2**. The author found that complex **2** did not react with either H_2O or alcohols. On the other hand, preliminary experiments showed that the reaction of **2** with $i\text{PrOH}$ proceeded in the presence of AgBF_4 as an additive, leading to the formation of complicated reaction mixture containing dicationic complex $[\text{Fe}(\text{CH}_3\text{CN})_2(\text{PNNP-Ph})]^{2+}(\text{BF}_4^-)_2$ (**5**) (18%) as well as insoluble solid compounds (Scheme 5, Figure 2-3). Complex **5** was identified by comparing its NMR spectra of alternatively prepared **5** by the

reaction of **1** with 2 equiv of AgBF₄ in acetonitrile. It is likely that *i*PrO–H bond cleavage proceed by the combination of **2**/AgBF₄ to tentatively form [Fe(O*i*Pr)(PNNP)]⁺(BF₄[−]), which successfully undergoes ligand disproportionation to form **5**.

Conclusion

In summary, the author have synthesized and characterized the iron complexes **2** and **3** bearing a dearomatized PNNP-Ph ligand via deprotonation of the corresponding PNNP-Ph-iron complex. These are, to our knowledge, the first example of a structurally characterized iron complex featuring a deprotonated phenanthroline-based PNNP-Ph ligand. Preliminary reactivity investigation of **2** strongly indicates the bond-cleavage-capability, which could be facilitated by rearomatization of the ligand backbone. Further studies on the reaction details are currently underway and will be reported in due course.

Experimental section

General considerations

All experiments were performed under nitrogen atmosphere using Schlenk techniques or a glove box unless otherwise noted. *n*-Hexane, tetrahydrofuran, benzene and dichloromethane were purified by a solvent purification system (MBraun SPS-800 or Glass Contour Ultimate Solvent System). Dehydrated MeCN was purchased from FUJIFILM Wako Pure Chemical Corporation (Super Dehydrated). C₆D₆ and toluene-*d*₈ were dried over sodium benzophenone ketyl and distilled. CD₂Cl₂ was dried over CaH₂ and distilled. (Trimethylsilyl)methylolithium was crystallized at −40 °C from (Trimethylsilyl)methylolithium solution 1.0 M in pentane. PNNP-Ph and **1** was synthesized by following the procedures of chapter 1. All other reagents were purchased from commercial suppliers and used without further purification unless otherwise noted. ¹H, ¹³C{¹H}, and ³¹P{¹H} NMR spectra (¹H, 600 MHz; ¹³C, 150 MHz; ³¹P, 243 MHz) were recorded on a Bruker AVANCE III HD 600 spectrometer. Chemical shifts are

reported in δ (ppm) and referenced to the residual solvent signals for ^1H and ^{13}C and 85% H_3PO_4 as an external standard for ^{31}P . The high-resolution ESI mass spectra were obtained on a Bruker microTOF II. Infrared (IR) spectra were recorded with a Bruker Alpha-T ATR-FTIR Fourier Transform Infrared Spectrometer.

Synthesis of 4.

Method 1

PNNP-Ph (0.150 g, 0.26 mmol) was dissolved in THF (10 ml) and cooled to -78°C . $n\text{BuLi}$ (1.55 M in THF, 0.18 ml, 0.27 mol) was added to the solution at -78°C , and the solution was warmed to room temperature, stirred overnight, and evaporated *in vacuo*. The resulting solid was dissolved in Et_2O /Hexane solution and stored at -40°C overnight to form red block crystals. Recrystallization was repeated again to give **4** (0.120 g, 0.18 mmol, 71%).

Method 2

PNNP-Ph (0.150 g, 0.26 mmol) was suspended in THF 10 ml. $\text{Me}_3\text{SiCH}_2\text{Li}$ (0.025 g, 2.7 mmol) was added to the suspension, and the mixture was stirred overnight at room temperature and evaporated *in vacuo*. The resulting solid was dissolved in Et_2O /Hexane solution and stored at -40°C overnight to form red block crystals. Recrystallization was repeated again to give **4** (0.133 g, 0.21 mmol, 78%).

^1H NMR (600 MHz, C_6D_6): δ 7.91 (t, $J = 7.29$ Hz, 4H), 7.42-7.38 (m, 5H), 7.17-7.15 (m, 4H), 7.10-7.06 (m, 3H), 6.95-6.93 (m, 6H), 6.86 (dd, $J = 9.10, 1.47$ Hz, 1H), 6.78 (d, $J = 9.12$ Hz, 1H), 6.60 (t, $J = 9.1$ Hz, 2H), 4.52 (d, $J = 6.72$ Hz, 1H), 3.43 (s, 2H), 3.26 (q, $J = 6.98$ Hz, Et_2O), 1.10 (t, $J = 6.99$ Hz, Et_2O) ppm.

$^{13}\text{C}\{^1\text{H}\}$ NMR (150 MHz, C_6D_6): δ 165.9, 152.8, 149.1, 142.7 (d, $^2J_{\text{P}} = 8.0$), 142.3, 137.7, 135.9, 133.1, 132.9, 132.8, 131.7, 129.4, 129.0 (d, $^2J_{\text{P}} = 7.6$), 128.4 (d, $^2J_{\text{P}} = 7.6$), 127.6, 127.3, 125.3 (d, $^2J_{\text{P}} = 9.5$), 121.4, 120.2, 111.1, 73.7 (d, $^1J_{\text{P}} = 27.7$), 65.9, 37.4 (Et_2O), 15.5 (Et_2O) ppm.

$^{31}\text{P}\{^1\text{H}\}$ NMR (243 MHz, C_6D_6): δ -16.1 (quint, $^1J_{\text{Li}} = 21.5$ Hz), -24.0 (quint, $^1J_{\text{Li}} = 29.0$ Hz) ppm. IR (ATR): 3049, 1613, 1578, 1518, 1478, 1433, 1405, 1381, 1325, 1302, 1139, 0193, 999, 852, 819, 739, 696 (cm^{-1}). Either elementary analysis or HRMS was not available due to the instability of **4**.

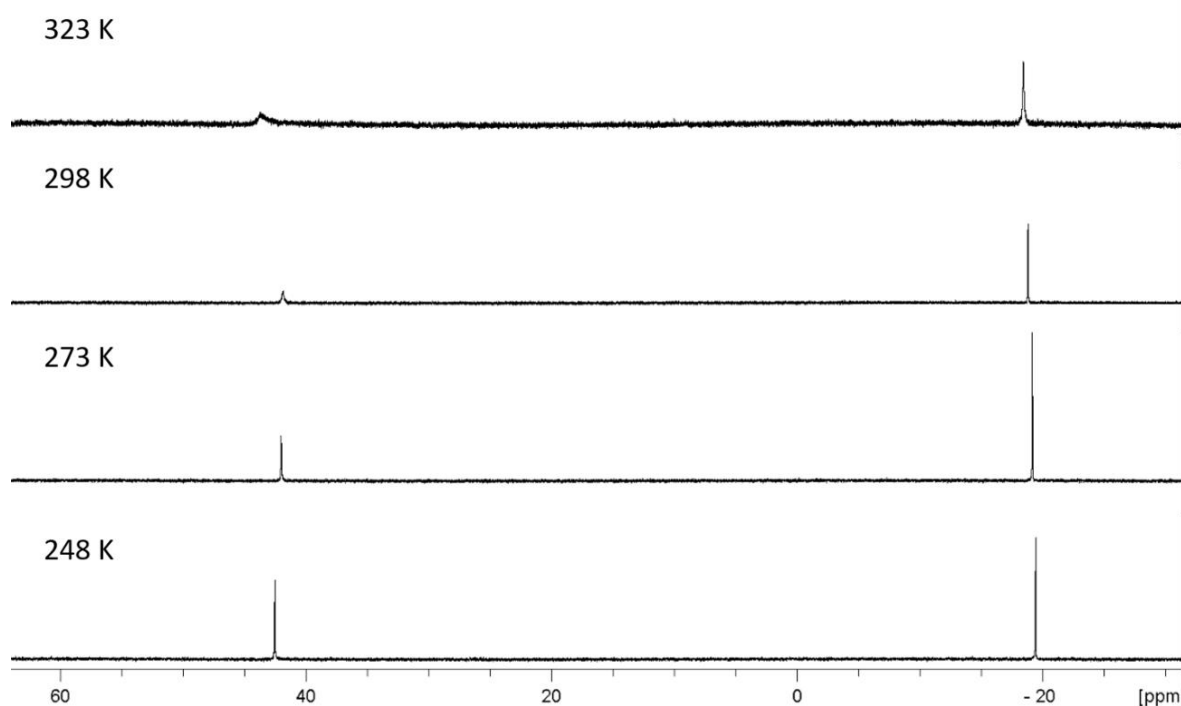
Synthesis of 2.

FeCl_2 (0.010 g, 0.078 mmol) was suspended in THF (5 ml). To the suspension, was added **4** (0.050 g, 0.076 mol) at room temperature, and the solution was stirred overnight and evaporated. The residue was dissolved in C_6H_6 (5 ml) and filtered. The removal of the volatiles *in vacuo* gave **2** as a purple solid (0.038 g, 0.058 g, 76%). A single crystal of **2** was obtained from CH_2Cl_2 /hexane solution at -40°C .

^1H NMR (600 MHz, C_6D_6): δ 7.28 (t, $J = 7.00$ Hz, 2H), 7.17-7.15 (m, 3H), 7.04-7.02 (m, 3H), 6.99-6.91 (m, 5H), 6.89-6.81 (m, 6H), 6.71 (d, $J = 8.16$ Hz, 1H), 6.65 (d, $J = 8.22$ Hz, 1H), 6.52 (t, $J = 7.05$ Hz, 2H), 6.41 (t, $J = 7.47$ Hz, 2H), 6.11 (d, $J = 8.11$ Hz, 1H), 4.33 (s, 1H), 3.90 (d, $J = 14.8$ Hz, 1H), 3.80 (d, $J = 14.8$ Hz, 1H).

$^{13}\text{C}\{^1\text{H}\}$ NMR (150 MHz, C_6D_6): δ 172.9, 163.4 (d, $^2J_{\text{P}} = 12.6$ Hz), 154.5, 149.4, 139.5 (d, $^1J_{\text{P}} = 13.3$ Hz), 138.1 ($^1J_{\text{P}} = 13.4$ Hz), 134.5 ($^1J_{\text{P}} = 22.6$ Hz), 132.9, 132.3, ($^1J_{\text{P}} = 22.4$ Hz), 131.5, 130.4, 129.7, 128.9, 127.1 \times 2, 126.9, 126.0, 125.6, 124.9 ($^2J_{\text{P}} = 19.3$ Hz), 122.0, 115.7, 114.0, 69.1, 35.7 ($^1J_{\text{P}} = 16.9$ Hz) ppm. Two signals of Ph group and three signals of the phenanthroline back-born are obscured in C_6D_6 signal. $^{31}\text{P}\{^1\text{H}\}$ NMR (243 MHz, C_6D_6): δ 42.1 (brs, CHP), -18.7 (s, CH_2P) ppm. HMBC (C_6D_6): $\delta_{\text{P}} 42.1 - \delta_{\text{H}} 4.33$, $\delta_{\text{P}} -18.7 - \delta_{\text{H}} 3.80$, 3.90. IR (ATR): 3048, 2963, 1605, 1575, 1518, 1485, 1426, 1407, 1320, 1212, 1137, 1094, 1026, 864, 836, 802, 737, 695 (cm^{-1}). HRMS (ESI): m/z calcd for $[\text{C}_{38}\text{H}_{48}\text{N}_2\text{P}_2\text{Fe}]^+$ ($2-\text{Cl}^-$): 631.112 ; found 631.115.

$^{31}\text{P}\{^1\text{H}\}$ NMR spectrum of **2** at various temperatures in toluene- d_8 :

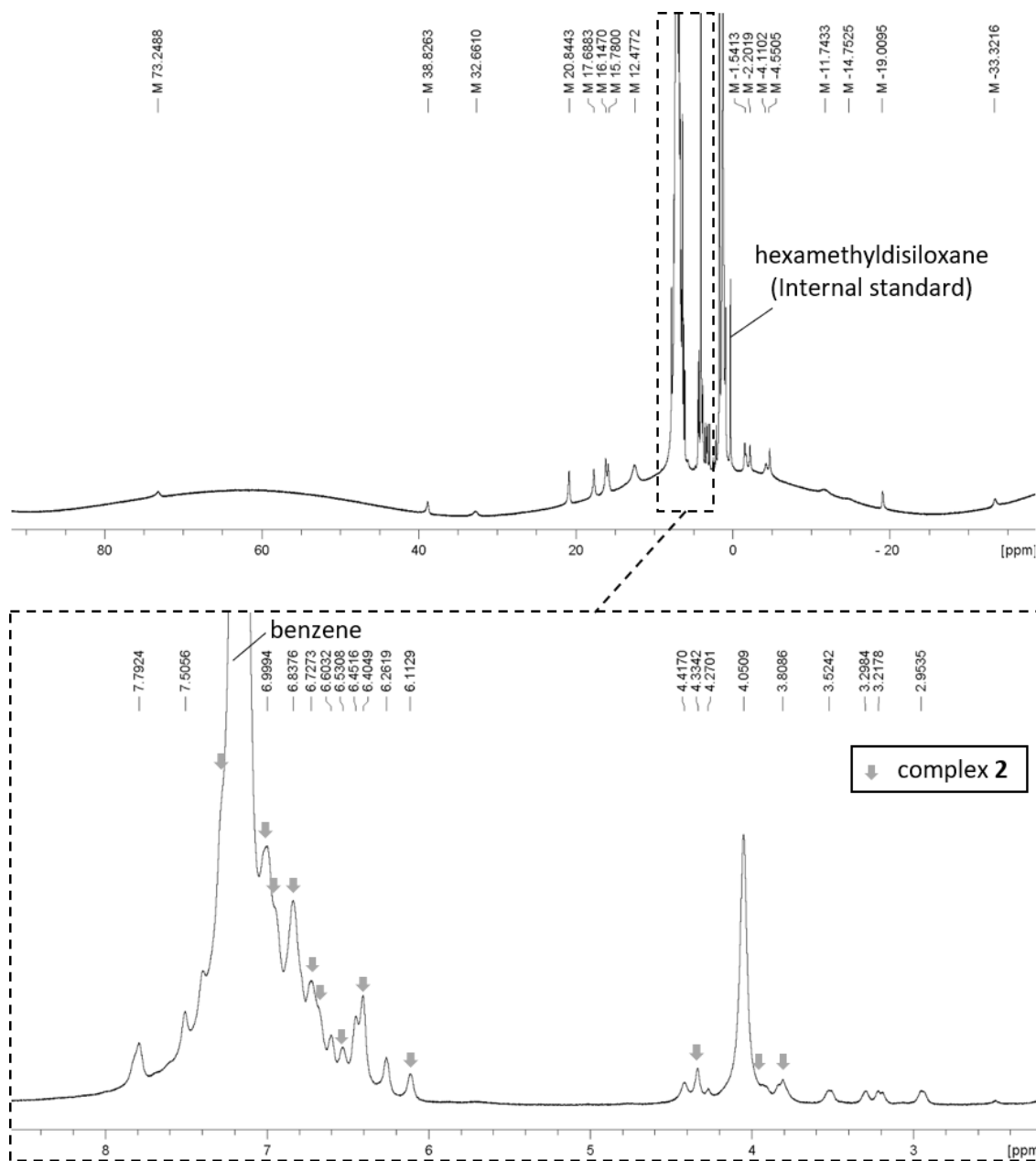


Reaction of **1** with NaOtBu .

Complex **1** (0.020 mg, 0.03 mmol) was suspended in THF (10 ml) and cooled to -78°C . To this solution, THF solution (5 mL) of NaOtBu (0.006 g, 0.06 mmol) was slowly added at the temperature, and then the reaction mixture was slowly warmed to room temperature. After stirred overnight, the volatile was removed *in vacuo*. The red solid was dissolved in C_6H_6 (10 ml), filtered and evaporated. The volatile was removed *in vacuo*. The

^1H and ^{31}P NMR of the crude compounds supported the formation of **2** as well as unidentified products. The crude compound was dissolved in Et_2O /hexane and allowed to stand for one week at room temperature to afford a crystal of **3**.

^1H NMR of the crude compound:



Reaction of **2** with *i*PrOH and AgBF_4 .

Complex **2** (0.040 mg, 0.06 mmol) was dissolved in dehydrated MeCN (1 ml), and *i*PrOH (14.5 mg, 0.16 mmol) was added to the solution. To the solution, was added a MeCN (0.5 ml) solution of AgBF_4 (0.012 g,

0.06 mmol) at room temperature, and the solution was stirred for 1 hour. The reaction mixture was filtered and then concentrated to dryness under vacuum to give the complicated mixture including **5**. The slow Et₂O diffusion into the MeCN solution of the crude compounds afforded **3** as a crystalline solid (9.5 mg, 0.011 mmol, 18%).

Alternative synthesis of **5**

Complex **1** (0.030 mg, 0.04 mmol) was dissolved in MeCN (1 ml). To the solution, was added a MeCN solution (0.5 mL) of AgBF₄ (0.018 g, 0.09 mmol) at room temperature. After the solution was stirred for 10 minutes, the resulting suspension was filtered, and the volatile was removed *in vacuo*. The resulting yellow solid was washed with THF (3 ml×3) and C₆H₆ (3 ml×3) and dissolved in CH₂Cl₂ (2 ml). After recrystallization by CH₂Cl₂/Et₂O, **3** was obtained as yellow crystals (0.029 g, 0.3 mmol, 71%).

¹H NMR (600 MHz, CD₂Cl₂): δ 8.74 (d, *J* = 8.40 Hz, 2H), 8.37 (d, *J* = 8.46 Hz, 2H), 8.21 (s, 2H), 7.56 (t, *J* = 7.86 Hz, 4H), 7.42-7.41 (m, 16H), 5.19 (dd, *J* = 4.75, 5.12, 4H), 1.27 (s, 6H). ¹³C{¹H} NMR (150 MHz, CD₂Cl₂): δ 166.6, 149.6, 138.2, 136.5, 133.3 (t, ²*J*_P = 5.14 Hz), 132.0, 130.7 (m), 129.7, 129.6 (t, ²*J*_P = 9.17 Hz), 127.1, 124.8 (t, ²*J*_P = 5.19 Hz), 47.0, 4.47 ppm. ³¹P{¹H} NMR (243 MHz, CD₂Cl₂): δ 65.7 ppm.

¹H NMR (600 MHz, CD₃CN): δ 8.81 (d, *J* = 8.40 Hz, 2H), 8.32 (d, *J* = 8.40 Hz, 2H), 8.28 (s, 2H), 7.57-7.55 (m, 4H), 7.43-7.39 (m, 16H), 5.14 (dd, *J* = 6.66, 4.81, 4H), 1.14 (s, 3H). ³¹P{¹H} NMR (243 MHz, CD₃CN): δ 66.0 ppm. IR (ATR): 3056, 2981, 2924, 1588, 1505, 1435, 1398, 1276, 1261, 1151, 1057, 1035, 865, 748, 696, 662 (cm⁻¹). HRMS (ESI): *m/z* calcd for [C₄₂H₃₆N₄P₂Fe]²⁺ (**5**-MeCN): 357.088; found 357.081.

Single crystal X-ray diffraction studies.

The single crystal X-ray diffraction measurements of **2-4** was performed under a cold nitrogen stream on a Rigaku XtaLAB P200 diffractometer with a Pilatus 200K detector using multi-layer mirror monochromated Mo Kα radiation. The determination of crystal systems and unit cell parameters and data processing were performed with the *CrystalClear* program package. The data sets were corrected for Lorentz and polarization effects and absorption. The structure was solved by direct methods using SIR2014 program,¹² and refined by full-matrix least squares calculations on F² for all reflections (SHELXL-2014/7)¹³ using Yadokari-XG 2009.¹⁴ Crystallographic data reported in this manuscript have been deposited with Cambridge Crystallographic Data Centre as supplementary publication no. CCDC-000000. Copies of the data can be obtained free of charge via CCDC Website.

Table S1. Crystallographic data of **2**, **3**, **4**, and **5**.

	2	3	4	5
CCDC	1875798	1872788	1872789	1887630
Empirical formula	C ₃₈ H ₂₉ Cl ₁ FeN ₂ P ₂ ·0.5CH ₂ Cl ₂	C ₄₂ H ₃₈ FeN ₂ OP ₂	C ₃₈ H ₂₉ LiN ₂ OP ₂ ·Et ₂ O	2C ₄₂ H ₃₆ B ₂ F ₈ FeN ₄ P ₂ ·C ₂ H ₃ N
Formula weight	709.33	704.53	656.63	1817.37
Temperature / K	93(2)	93(2)	93(2)	93(2)
Crystal system	triclinic	monoclinic	triclinic	monoclinic
Space group	<i>P</i> -1	<i>P</i> 2 ₁ / <i>n</i>	<i>P</i> -1	<i>P</i> 2 ₁ / <i>c</i>
<i>a</i> / Å	10.530(3)	18.672(4)	12.659(5)	12.996(3)
<i>b</i> / Å	11.513(4)	10.613(2)	13.210(5)	34.299(8)
<i>c</i> / Å	14.820(5)	19.039(4)	13.528(3)	18.381(5)
α / °	85.26(2)	90	61.443(19)	90
β / °	86.52(2)	108.382(4)	64.69(2)	92.088(5)
γ / °	75.663(17)	90	89.12(3)	90
Volume / Å ³	1733.2(10)	3580.4(13)	1744.5(11)	8188(3)
<i>Z</i>	2	4	2	4
<i>R</i> ₁ / %	0.0570	0.0605	0.0513	0.1012
<i>wR</i> ₂ / %	0.1679	0.0897	0.1218	0.1922
GOF	0.975	1.076	1.016	1.123

Table S2. Selected bond lengths (Å) and angles (°) of the crystal structures for **2**, **3**, **4**, and **5**.

Complex	2 (M = Fe)	3 (M = Fe)	4 (M = Li)	5 (M = Fe)
C1–C2	1.375(6)	1.374(5)	1.380(3)	1.502(10)
C11–C14	1.500(5)	1.507(4)	1.501(3)	1.494(10)
C2–N1	1.388(5)	1.391(4)	1.333(3)	1.333(9)
C11–N2	1.322(5)	1.333(4)	1.383(5)	1.343(8)
C1–P1	1.777(4)	1.756(4)	1.775(3)	1.877(7)
C14–P2	1.849(4)	1.850(3)	1.865(2)	1.849(7)
C2–C3	1.456(5)	1.440(5)	1.449(3)	1.396(10)
C10–C11	1.407(6)	1.398(4)	1.417(3)	1.397(10)
M–N1	2.078(3)	2.109(3)	1.989(4)	1.972(6)
M–N2	2.179(3)	2.186(3)	2.104(4)	1.973(6)
M–P1	2.5344(14)	2.4927(1)	2.884(4)	2.270(2)
M–P2	2.5010(13)	2.5073(9)	-	2.261(2)
M–X	2.2854(13)	1.865(2)	2.015(4)	1.911 (ave.)
	(X = Cl)	(X = O)	(X = O)	(X = N3, N4)
P1–C1–C2	118.9(3)	117.8(3)	122.57(2)	111.2(5)
P2–C14–C11	109.6(3)	109.9(2)	113.11(2)	111.2(5)

Computational Details

Geometries optimization, energy, and NAO analysis were performed with the DFT method, where the B3LYP function was used. It was ascertained that each optimized geometry of **2** and PNNP exhibited no imaginary frequency. The calculations employed the triple- ζ SDD basis set for iron, 6-31G(d) for P and N,¹⁵ and 6-31G for C and H. Core electrons of Fe (up to 3p) were replaced with effective core potentials (ECPs).¹⁶ The Gaussian 09 program package was used for all calculations.¹⁷ Population analysis was carried out with the method of Weinhold et al.¹⁸ Molecular orbitals were drawn with the GaussView 5.0 program package.

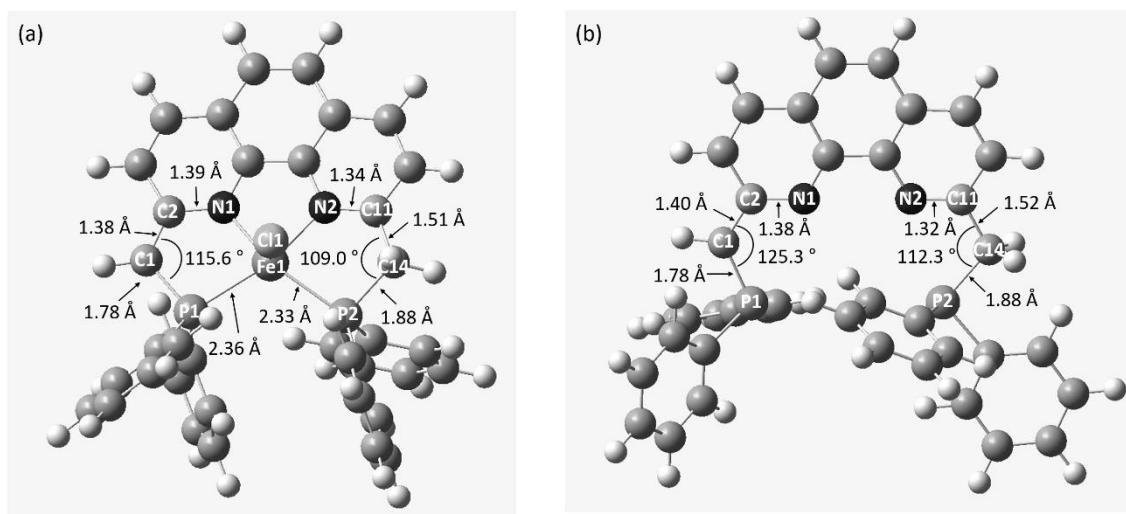


Figure S4. Optimized geometry of **2** (a) and PNNP (b).

Table S7. Natural Charge

	2	PNNP
Fe	-0.06249	-
P1	1.20616	0.92711
P2	1.20586	0.95809
N1	-0.47501	-0.50152
N2	-0.37497	-0.4179
Cl1	-0.46569	-
C1	-0.74362	-0.78711
C14	-0.80289	-0.8143
Phenanthroline moiety	-0.03695	-0.52317

Table S8. Mayer Bond Index

	2	PNNP
C1–C2	1.50	1.42
C11–C14	0.95	0.93
C1–P1	1.04	1.09
C14–P2	0.89	0.93
C2–N1	0.96	1.12
C11–N2	1.25	1.38
Fe1–P1	0.80	-
Fe1–P2	0.78	-
Fe1–N1	0.60	-
Fe1–N2	0.49	-
Fe1–Cl	0.97	-

Table S3. Cartesian Coordinate of **2**

Fe	9.482898	3.694015	2.710539
Cl	8.853070	5.926684	3.046121
N	10.583971	3.922073	1.128756
N	8.035760	3.552985	1.365584
P	11.588247	3.774309	3.771386
P	7.800017	2.897525	4.107976
C	12.612923	4.126760	2.348962
C	11.956739	4.152100	1.130644
C	12.588977	4.378858	-0.163567
C	11.876180	4.353609	-1.328384
C	10.455163	4.109071	-1.312759
C	8.230951	3.865087	-2.334570
C	7.635682	3.684598	-1.047167
C	6.252475	3.497424	-0.777707
C	5.806433	3.377652	0.528779
C	6.727363	3.429298	1.608024

C	8.485516	3.702555	0.086258
C	9.891187	3.912975	-0.036026
C	6.325846	3.432527	3.064423
C	11.755895	1.655062	5.666635
C	12.056439	0.354927	6.084350
C	12.691011	-0.538365	5.210374
C	12.159563	4.862896	5.141291
C	11.391360	5.978390	5.522649
C	11.851359	6.839666	6.526720
C	13.076792	6.601288	7.157732
C	13.848703	5.494319	6.781988
C	13.393567	4.629899	5.782167
C	12.094952	2.089772	4.368390
C	12.734048	1.184724	3.500756
C	7.632459	1.061074	4.112921
C	6.406482	0.405339	4.350902
C	6.321122	-0.988775	4.298612
C	7.459517	-1.752541	4.007019
C	8.682344	-1.116536	3.773637
C	8.768164	0.280488	3.826651
C	7.339922	3.430746	5.808094
C	7.180934	2.524016	6.873000
C	6.874276	2.985713	8.158703
C	6.722294	4.355218	8.398042
C	6.891553	5.265598	7.347481
C	7.205288	4.812734	6.062681
C	13.027389	-0.120386	3.917781
C	9.595077	4.072091	-2.448708
H	13.677057	4.319546	2.423829

H	13.656019	4.573231	-0.174633
H	12.373295	4.526306	-2.278744
H	7.600598	3.849557	-3.217378
H	5.545617	3.463709	-1.601218
H	4.750100	3.259087	0.741882
H	5.429495	2.831622	3.247440
H	6.106497	4.465078	3.367147
H	11.267308	2.338253	6.354698
H	11.796731	0.039095	7.090232
H	12.925016	-1.546920	5.537166
H	10.450039	6.173250	5.020762
H	11.249901	7.697439	6.811577
H	13.430125	7.271713	7.935437
H	14.801649	5.304051	7.266645
H	13.994331	3.769511	5.505080
H	13.011985	1.515980	2.504950
H	5.517804	0.981612	4.589110
H	5.370321	-1.478493	4.484633
H	7.390844	-2.834972	3.964476
H	9.571418	-1.698398	3.554795
H	9.724577	0.762191	3.654600
H	7.295078	1.459554	6.703680
H	6.754469	2.273667	8.969497
H	6.482146	4.711140	9.395048
H	6.789011	6.330994	7.528108
H	7.376885	5.526834	5.263106
H	13.526819	-0.803385	3.236935
H	10.032597	4.221175	-3.432098

Table S4. Cartesian Coordinate of **PNNP**

N	10.45106	3.496883	1.360060
N	7.705683	3.913141	1.593068
P	12.02598	2.912019	4.060603
P	7.085353	3.588101	4.415547
C	12.61713	3.063227	2.386903
C	11.82023	3.332860	1.267327
C	12.46125	3.450868	-0.03633
C	11.73004	3.722022	-1.15305
C	10.31478	3.905910	-1.05797
C	8.151139	4.380496	-2.08808
C	7.522406	4.285461	-0.81146
C	6.126071	4.475781	-0.64376
C	5.558421	4.385091	0.609383
C	6.396155	4.102177	1.719359
C	8.290582	3.992235	0.366777
C	9.742415	3.779542	0.257973
C	5.797889	4.008637	3.113038
C	13.25457	1.369918	6.126910
C	13.94032	0.269749	6.649428
C	14.45856	-0.71236	5.793518
C	12.81872	4.362699	4.946319
C	11.97809	5.438411	5.297178
C	12.49252	6.594853	5.896730
C	13.86217	6.697191	6.166823
C	14.71250	5.635379	5.829150
C	14.19584	4.484199	5.224549
C	13.07404	1.529221	4.734646
C	13.59802	0.529289	3.890605

C	7.329425	1.773100	4.104458
C	6.431663	0.778932	4.540277
C	6.680007	-0.57327	4.277231
C	7.830527	-0.95007	3.573184
C	8.726819	0.030700	3.133410
C	8.484482	1.385137	3.395503
C	6.008298	3.528521	5.934781
C	6.651112	3.191821	7.148471
C	5.960109	3.187088	8.361723
C	4.603316	3.538213	8.401924
C	3.951170	3.885386	7.215566
C	4.644107	3.875601	5.996212
C	14.28010	-0.57734	4.412078
C	9.512930	4.196516	-2.18833
H	13.69390	3.021640	2.216307
H	13.53794	3.315489	-0.09262
H	12.20748	3.807352	-2.12797
H	7.544721	4.601539	-2.96234
H	5.516249	4.694237	-1.51754
H	4.491147	4.527155	0.755154
H	4.978016	3.275163	3.123470
H	5.358302	4.978667	3.392104
H	12.85645	2.120478	6.803892
H	14.06882	0.176012	7.725135
H	14.98945	-1.56958	6.199176
H	10.91406	5.361129	5.091119
H	11.82353	7.411436	6.156069
H	14.26346	7.591997	6.635642
H	15.77805	5.706206	6.035226

H	14.86443	3.667517	4.969731
H	13.46233	0.635693	2.818654
H	5.541303	1.059398	5.094835
H	5.978862	-1.32874	4.623302
H	8.027486	-2.00004	3.372735
H	9.623423	-0.25018	2.589658
H	9.178064	2.139647	3.035497
H	7.706452	2.933630	7.132681
H	6.480349	2.917753	9.276712
H	4.065929	3.543799	9.345982
H	2.899507	4.159822	7.232712
H	4.107147	4.138422	5.091542
H	14.67536	-1.33254	3.736701
H	10.00316	4.272833	-3.15802

Reference

1. a) J. R. Khusnutdinova, D. Milstein, *Angew. Chem. Int. Ed.* **2015**, *54*, 12236. b) J. I. van der Vlugt, *Eur. J. Inorg. Chem.* **2012**, 363. c) P. J. Chirik, K. Wieghardt, *Science* **2010**, *327*, 794. d) V. T. Annibale, D. Song, *RSC Adv.* **2013**, *3*, 11432. e) D. G. A. Verhoeven, M. E. Moret, *Dalton Trans.* **2016**, *45*, 15762.
2. a) C. Gunanathan, D. Milstein, *Acc. Chem. Res.* **2011**, *44*, 588. b) C. Gunanathan, D. Milstein, *Science* **2013**, *341*, 1229712. c) C. Gunanathan, D. Milstein, *Chem. Rev.* **2014**, *114*, 12024. d) F. Ozawa, Y. Nakajima, *Chem. Rec.* **2016**, *16*, 2314.
3. B. Bichler, C. Holzhaacker, B. Stöger, M. Puchberger, L. F. Veios, K. Kirchner, *Organometallics* **2013**, *32*, 4114. b) T. P. Gonçalves, K.-W. Huang, *J. Am. Chem. Soc.* **2017**, *139*, 13442.
4. a) S. W. Kohl, L. Weiner, L. Schwartzburd, L. Konstantinovski, L. J. W. Shimon, Y. Ben-David, M. A. Iron, D. Milstein, *Science* **2009**, *324*, 74. b) M. Montag, J. Zhang, D. Milstein, *J. Am. Chem. Soc.* **2012**, *134*, 10325.
5. a) E. Khaskin, M. A. Iron, L. J. W. Shimon, J. Zhang, D. Milstein, *J. Am. Chem. Soc.* **2010**, *132*, 8542. b) Y.-H. Chang, Y. Nakajima, H. Tanaka, K. Yoshizawa, F. Ozawa, *J. Am. Chem. Soc.* **2016**, *138*, 6985.
6. a) . Zhang, G. Leitius, Y. Ben-David, D. Milstein, *Angew. Chem. Int. Ed.* **2006**, *45*, 1113. b) N. Gorgas, B. Stöger, L. F. Veios, E. Pittenauer, G. Allmaier, K. Kirchner, *Organometallics* **2014**, *33*, 6905. c) T. Zell, Y. Ben-David, D. Milstein, *Angew. Chem. Int. Ed.* **2014**, *53*, 4685. f) R. Langer, G. Leitius, Y. Ben-David, D. Milstein, *Angew. Chem. Int. Ed.* **2011**, *50*, 2120. d) J. A. Luque-Urrutia, A. Poater, *Inorg. Chem.* **2017**, *56*, 14383. c) E. Balaraman,

- C. Gunanathan, J. Zhang, L. J. W. Shimon, D. Milstein, *Nat. Chem.* **2011**, *3*, 609 W. Addison, T. N. Rao, J. Reedijk, J. van Rijn and G. C. Verschoor, *J. Chem. Soc., Dalton Trans.* **1984**, 1349.
7. a) C. Gunanathan, Y. Ben-David, D. Milstein, *Science* **2007**, *317*, 790. b) E. Balaraman, E. Khaskin, G. Leituss, D. Milstein, *Nat. Chem.* **2013**, *5*, 122. c) P. Hu, E. Fogler, Y. Diskin-Posner, M. A. Iron, D. Milstein, *Nat. Commun.* **2015**, *6*, 6859. d) M. Feller, E. Ben-Ari, Y. Diskin-Posner, R. Carmieli, L. Weiner, D. Milstein, *J. Am. Chem. Soc.* **2015**, *137*, 4634. e) Y.-H. Chang, K. Takeuchi, M. Wakioka, F. Ozawa, *Organometallics* **2015**, *34*, 1957. f) S. R. M. M. de Aguiar, Ö. Öztöpcü, B. Stöger, K. Mereiter, L. F. Veiros, E. Pittenauer, G. Allmaier, K. Kirchner, *Dalton Trans.* **2014**, *43*, 14669. g) A. Nerush, M. Vogt, U. Gellrich, G. Leituss, Y. Ben-David, D. Milstein, *J. Am. Chem. Soc.* **2016**, *138*, 6985.
 8. a) R. Langer, I. Fuchs, M. Vogt, E. Balaraman, Y. Diskin-Posner, L. J. W. Shimon, Y. Ben-David, D. Milstein, *Chem. Eur. J.* **2013**, *19*, 3407. b) T. Miura, M. Naruto, K. Toda, T. Shimomura, S. Saito, *Sci. Rep.* **2017**, *7*, 1586. c) S. Saito, N. Ryoji, T. Miura, M. Naruto, K. Iida, Y. Takada, K. Toda, S. Nimura, S. Agrawal, S. Lee, U.S. Patent 0107151A1, **2016**.
 9. T. Simler, L. Karmazin, C. Bailly, P. Braunstein, A. A. Danopoulos, *Organometallics* **2016**, *35*, 903.
 10. T. Zell, R. Langer, M. A. Iron, L. Konstantinovski, L. J. W. Shimon, Y. Diskin-Posner, G. Leituss, E. Balaraman, Y. Ben-David, D. Milstein, *Inorg. Chem.* **2013**, *52*, 9636.
 11. a) A. Sacco, G. Vasapollo, C. F. Nobile, A. Piergiovanni, M. A. Pellinghelli, M. Lanfranchi, *J. Organomet. Chem.* **1988**, *356*, 397. b) H. Qichen, X. Minzhi, Q. Yanlong, X. Weihua, *J. Organomet. Chem.* **1985**, *287*, 419. c) M. Feller, E. Ben-Ari, M. A. Iron, Y. Diskin-Posner, G. Leituss, L. J. W. Shimon, L. Konstantinovski, D. Milstein, *Inorg. Chem.* **2010**, *49*, 1615. d) Y. Nakajima, F. Ozawa, *Organometallics* **2012**, *31*, 2009.
 12. M. C. Burla, R. Caliandro, B. Carrozzini, G. L. Cascarano, C. Cuocci, C. Giacovazzo, M. Mallamo, A. Mazzone and G. Polidori, *J. Appl. Cryst.* **2015**, *48*, 306.
 13. G. M. Sheldrick, SHELXL-2014/7, University of Göttingen, Göttingen, Germany, **2014**.
 14. C. Kabuto, S. Akine, T. Nemoto, E. Kwon, Release of software (Yadokari-XG 2009) for crystal structure analyses. Nippon Kessho Gakkaishi **2009**, *51*, 218.
 15. a) P. C. Hariharan, J. A. Pople, *Theor. Chim. Acta* **1973**, *28*, 213. b) P. C. Hariharan, J. A. Pople, *Mol. Phys.* **1974**, *27*, 209.
 16. D. Andrae, U. Haussermann, M. Dolg, H. Stoll, H. Preuss, *Theor. Chim. Acta* **1990**, *77*, 123.
 17. M. J. Frisch, G. W. Trucks, H. B. Schlegel, G. E. Scuseria, M. A. Robb, J. R. Cheeseman, G. Scalmani, V. Barone, G. A. Petersson, H. Nakatsuji, X. Li, M. Caricato, A. Marenich, J. Bloino, B. G. Janesko, R. Gomperts, B. Mennucci, H. P. Hratchian, J. V. Ortiz, A. F. Izmaylov, J. L. Sonnenberg, D. Williams-Young, F. Ding, F. Lipparini, F. Egidi, J. Goings, B. Peng, A. Petrone, T. Henderson, D. Ranasinghe, V. G. Zakrzewski, J. Gao, N. Rega, G. Zheng, W. Liang, M. Hada, M. Ehara, K. Toyota, R. Fukuda, J. Hasegawa, M. Ishida, T. Nakajima, Y. Honda, O. Kitao, H. Nakai, T. Vreven, K. Throssell, J. A. Montgomery, Jr., J. E. Peralta, F. Ogliaro, M. Bearpark, J. J. Heyd, E. Brothers, K. N. Kudin, V. N. Staroverov, T. Keith, R. Kobayashi, J. Normand, K. Raghavachari, A. Rendell, J. C. Burant, S. S. Iyengar, J. Tomasi, M. Cossi, J. M. Millam, M. Klene, C. Adamo, R. Cammi, J. W.

Ochterski, R. L. Martin, K. Morokuma, O. Farkas, J. B. Foresman, and D. J. Fox, *Gaussina 09, Revision D.01*, Gaussian, Inc., Wallingford CT, **2016**.

18. A. E. Reed, L. A. Curtiss, F. Weinhold, *Chem. Rev.* **1988**, 88, 899.

Chapter 3

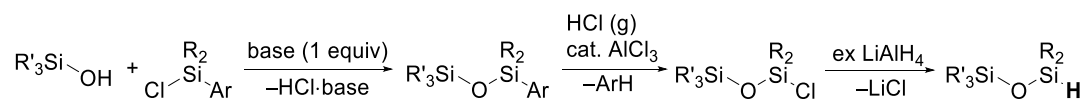
Selective Synthesis of Hydrosiloxanes via Dehydrogenative Coupling of Silanols with Hydrosilanes Catalyzed by PNNP-Iron Complexes

Abstract

The Fe(0) complex bearing a PNNP-R ligand, **2a**, **2b**, and **3** catalyzed dehydrogenative coupling of silanols with silanes to selectively form various hydrosiloxanes, which are important building blocks for the synthesis of a range of siloxane compounds. This system exhibited higher catalytic efficiency than the previously reported precious-metal-catalyzed systems.

Introduction

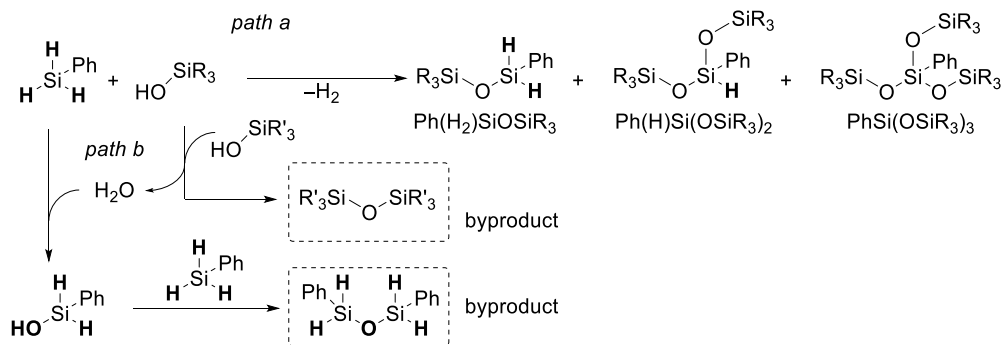
Silicones, which is composed of siloxane bonds (Si–O–Si) and organic groups substituted on the silicon, exhibit unique characters like thermal-, oxidation-, and chemical-resistance etc.¹ Therefore, silicones are applied for various purposes in our life. One common method to synthesize silicones is dehydration condensation of silicon raw materials such as chlorosilane and alkoxyasilane.¹ In this system, the reaction is sometimes highly exothermic and it is difficult to control. As a result, the structure and the arrangement of the obtained silicone molecules are not uniformed. In recent years, it was attempted to precisely synthesize the arrangement-controlled silicones aiming at preparation of silicones with higher performance.² However, the synthesis of such the silicones are multistep reactions, which requires the highly reactive and expensive reagents, accompanied by more than equimolar amount of by-products (Scheme 3-1). To obtain sequence-controlled oligohydrosiloxanes, an oligomer of silicone having a reactive Si–H bond, has recently draw an increasing attention as the starting material.



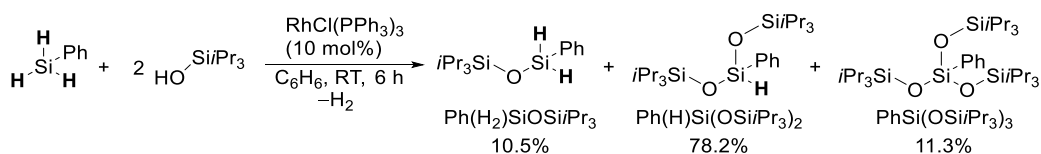
Scheme 3-1. Classical synthesis of hydrosiloxanes.

Dehydrogenative coupling of hydrosilanes with silanols is a simple synthetic method using commercially available precursors. However, the number of examples that afford high reaction selectivity is extremely limited. One reason for this is the complicated reactivity of silanols; i.e. silanols easily undergo dehydrative condensation to form a homo-coupling product. In addition, the by-product, H₂O further reacts with unreacted hydrosilanes to generate various silanol molecules, which are also quickly converted to homo-coupled-siloxanes (Scheme 3-2, path b).³ Furthermore, the reactive SiH terminus is another problem to achieve high reaction selectivity; i.e. dehydrogenative coupling of hydrosilanes and alcohols easily consumes the remaining Si–H moieties (Scheme 3-2, path a). In fact, Michalska reported that the dehydrogenative coupling reaction of PhSiH₃ with silanols (R₃SiOH, R = Et or Pr) by Rh catalysts, affording the mixture of Ph(H₂)SiOSiPr₃ (10.5%), Ph(H)Si(OSiPr₃)₂ (78.2%) and PhSi(OSiPr₃)₃ (11.3%) (Scheme 3-3).^{4a} In addition, selectivities of siloxane were depended on the kinds of

hydrosilanes and/or silanols used in the reactions.

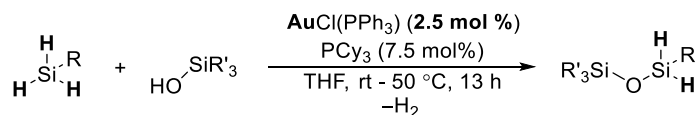


Scheme 3-2. Synthesis of the hydrosiloxanes via dehydrogenative coupling and the side reaction.

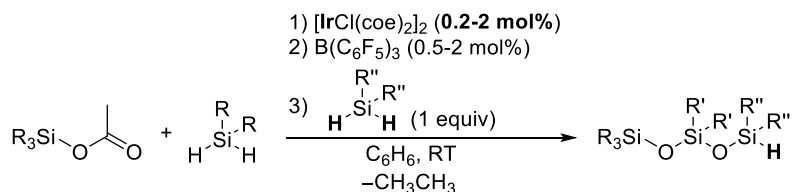


Scheme 3-3. The reaction of Phenylsilane with $i\text{Pr}_3\text{SiOH}$ catalyzed by $\text{RhCl(PPh}_3)_3$.

To the best of my knowledge, the examples of selective synthesis of hydrosiloxanes were limited to only two: One of them was achieved by dehydrogenative coupling of silanols with hydrosilanes using gold catalysts with the turn over number (TON) of $< 5,000$ (Scheme 3-4).^{4b} The other example demonstrated the selective synthesis of sequence-controlled hydrosiloxanes via in-situ sequential reactions composed of hydrosilylation of acetoxyethylsilane, rearrangement, and dealkylation, catalyzed by 0.5-2.5 mol% of iridium complex and 0.1 mol% of $\text{B(C}_6\text{F}_5)_3$, respectively (Scheme 3-5)^{4c} Considering that both of the two examples requires precious metal catalysts, it is challenging to perform dehydrogenative coupling of hydrosilanes with silanols to form hydrosiloxanes selectively using by cheap and abundant metal catalysts.

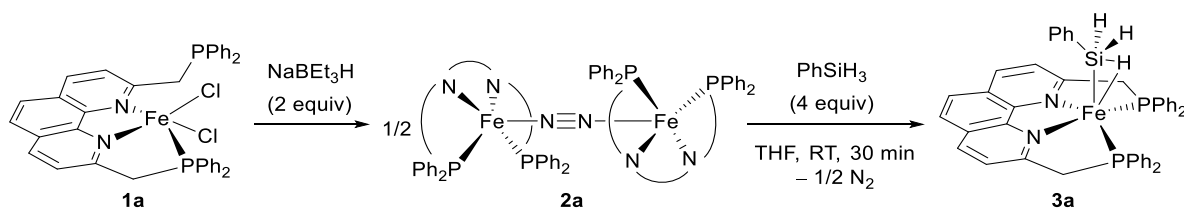


Scheme 3-4. Synthesis of the hydrosiloxane catalyzed by $\text{AuCl(PPh}_3)_3$.



Scheme 3-5. Synthesis of the hydrosiloxane catalyzed by $\text{AuCl(PPh}_3)_3$ and $\text{B(C}_6\text{F}_5)_3$.

In chapter 1, the author succeeded in the synthesis of the iron(0) complexes $[\text{Fe}(\text{PNNP-Ph})]_2(\mu\text{-N}_2)$ (**2a**; R = Ph, **2b**; R = Cy) and $[\text{Fe}(\text{SiH}_3\text{H})(\text{PNNP-Ph})]$ (**6**) (Scheme 3-6). The latter complex has the agositic Si–H bond, which is elongated due to the back donation to the Si–H σ^* bond. The author assumed that such the activated Si–H bond in **3** selectively reacts with silanols to form a dehydrogenative coupling product, and thus the occurrence of other side-reactions could be suppressed.



Scheme 3-6. Synthesis of **3a**.

In this chapter, the author succeeded in the synthesis of various hydrosiloxanes by dehydrogenative coupling of hydrosilanes with silanols using PNNP-iron complexes. The reaction achieved the highest TON of > 18,000 among the previously reported systems.

Results and discussion

First, the reaction was carried out using PhSiH_3 and Me_3SiOH as substrates, since both Me and Ph groups are significantly important substituents for the production of various siloxanes.¹ The reaction was carried out in THF at room temperature for 12 h. The reaction did not proceed without catalysts (Table 1, entry 1). It was also confirmed that **1a** did not catalyze the reaction, either (Table 1, entry 2). By using the combination of **1a** (0.1 mol%) and NaBEt_3H (0.2 mol%) as a catalyst, PhSiH_3 reacted with 2 equiv of Me_3SiOH to form hydrotrisiloxane $(\text{Me}_3\text{SiO})_2(\text{SiHPh})$ in an excellent yield (Table 1, entry 3). Notably, neither disiloxane $(\text{Me}_3\text{SiO})(\text{SiH}_2\text{Ph})$ nor tetrasiloxane $(\text{Me}_3\text{SiO})_3(\text{SiPh})$ was obtained in the reaction. It was also confirmed that hydrotrisiloxane $(\text{Me}_3\text{SiO})_2(\text{SiHPh})$ was obtained in the reaction of PhSiH_3 with 3 equiv of Me_3SiOH as the sole product even at a

higher catalyst loading, **1a** (1 mol%) and NaBEt₃H (2 mol%).

Table 1. Dehydrogenative coupling of Me₃SiOH with PhSiH₃ catalyzed by Fe complexes

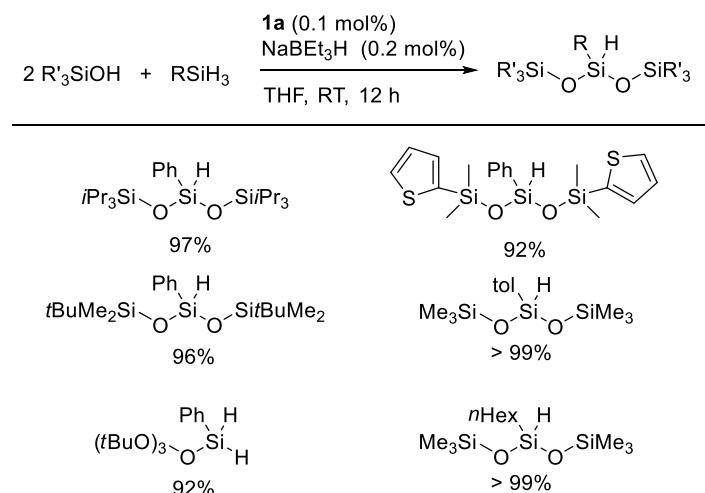
$$2 \text{ Me}_3\text{SiOH} + \text{PhSiH}_3 \xrightarrow[\text{THF, RT, 12 h}]{\text{1a,b} / 2 \text{ NaBEt}_3\text{H} \text{ (x mol\%)}} \text{Me}_3\text{Si}-\text{O}-\text{Si}(\text{Ph})(\text{H})-\text{O}-\text{SiMe}_3 + \text{Me}_3\text{Si}-\text{O}-\text{Si}(\text{Ph})(\text{H})-\text{H}$$

entry	[Fe] cat (X mol%)	Product yields NMR ^b (isolated)
1	–	(Me ₃ SiO) ₂ (SiHPh) – (Me ₃ SiO)(SiH ₂ Ph) –
2	1a (1 mol%)	(Me ₃ SiO) ₂ (SiHPh) – (Me ₃ SiO)(SiH ₂ Ph) < 5
3	1a + 2 NaBEt ₃ H (0.1 mol%)	(Me ₃ SiO) ₂ (SiHPh) > 99 (Me ₃ SiO)(SiH ₂ Ph) –
4	1a + 2 NaBEt ₃ H (0.01 mol%)	(Me ₃ SiO) ₂ (SiHPh) 89 (Me ₃ SiO)(SiH ₂ Ph) 8
5	[FeBr ₂ (PNNP-Cy)] 1b + 2 NaBEt ₃ H (0.01 mol%)	(Me ₃ SiO) ₂ (SiHPh) 28 (Me ₃ SiO)(SiH ₂ Ph) 28
6	NaBEt ₃ H (0.1 mol%)	(Me ₃ SiO) ₂ (SiHPh) – (Me ₃ SiO)(SiH ₂ Ph) 55 (Me ₃ SiO) ₃ SiPh 30 Me ₃ SiOSiMe ₃ 4
7	3 (0.01 mol%)	(Me ₃ SiO) ₂ (SiHPh) 83 (Me ₃ SiO)(SiH ₂ Ph) 9

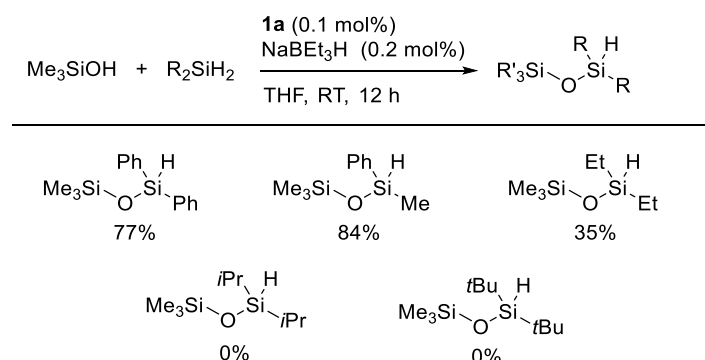
a Reaction conditions: PhSiH₃ (32.4 mg, 0.30 mmol) and Me₃SiOH (56.8 mg, 0.63 mmol) in THF (5 mL) at room temperature for 12 h. *b* Yields are determined by ¹H NMR with mesitylene as an internal standard.

The catalyst loading could be reduced to 0.01 mol% to give (Me₃SiO)₂(SiHPh) in a highly selective manner (89% yield) accompanied by the formation of disiloxane (Me₃SiO)(SiH₂Ph) (8% yield) as a minor product (Table 1, entry 3). The reaction suggests a much higher turnover number (TON) of >18, 000 than those of the previous reports, which are catalyzed by precious-metal complexes (TON 1000–4000).^{4a,4b} Complex **1b** reacts with NaBEt₃H at a slower rate to form active **2b** (vide supra) and thus exhibited less activity, resulting in the formation of (Me₃SiO)₂(SiHPh) (28%) and (Me₃SiO)(SiH₂Ph) (28%) in the presence of **1b** (0.01 mol%) and NaBEt₃H (0.02 mol%) (Table 1, entry 3). The reaction catalyzed by NaBEt₃H was also performed, leading to the formation of a mixture of disiloxane (Me₃SiO)(SiH₂Ph) (55%) and trisiloxane (Me₃SiO)₃(SiPh) (30%), accompanied by the homo-coupling product Me₃SiOSiMe₃ (4%) (Table 1, entry 6). As mentioned above, the reaction catalyzed by **1a**/2NaBEt₃H didn't form either trisiloxane (Me₃SiO)₃(SiPh) or Me₃SiOSiMe₃. Thus, it is likely that the added NaBEt₃H was completely consumed for the activation of **1a** to provide **2a**. Notably, when **3** (0.01 mol%) was used

as a catalyst, the yields of $(\text{Me}_3\text{SiO})_2(\text{SiHPh})$ and $(\text{Me}_3\text{SiO})(\text{SiH}_2\text{Ph})$ were 83% and 9% (Table 1, entry 7). Therefore, it was confirmed that **3** catalyzed the dehydrogenative coupling of Me_3SiOH with PhSiH_3 to the same level as **1a**/ $2\text{NaBEt}_3\text{H}$.



Scheme 3-7. Reaction of silanols with primary silanes catalyzed by **1a**/ NaBEt_3H .



Scheme 3-8. Reaction of silanols with primary silanes catalyzed by **1a**/ NaBEt_3H .

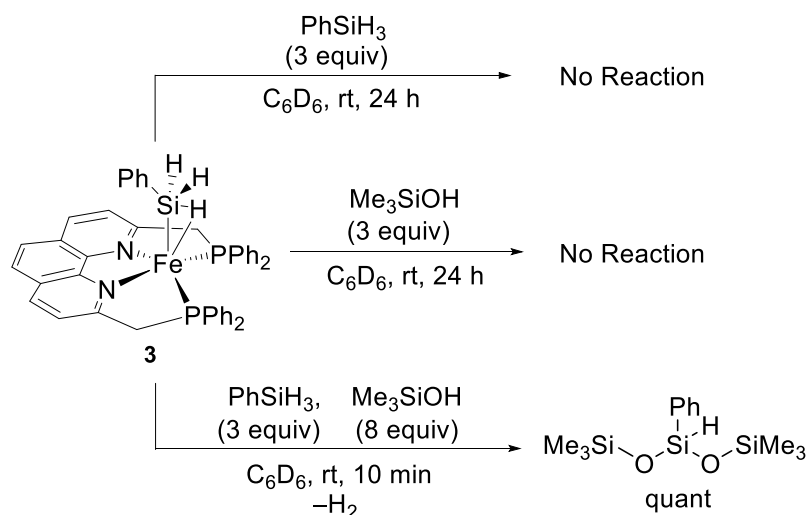
With the optimized conditions using 0.1 mol% of the **1a**/ $2\text{NaBEt}_3\text{H}$ combination, the author next examined the substrate scope of the dehydrogenative coupling of silanols with primary silanes (Scheme 3-7). PhSiH_3 reacted with various aliphatic silanols. When using $i\text{Pr}_3\text{SiOH}$ and $t\text{BuMe}_2\text{SiOH}$, the corresponding trisiloxanes $(\text{R}_3\text{SiO})_2(\text{SiHPh})$ were formed in excellent yields. Reaction of PhSiH_3 with bulky $(t\text{BuO})_3\text{SiOH}$ resulted in the selective formation of hydrodisiloxane $((t\text{BuO})_3\text{SiO})(\text{SiH}_2\text{Ph})$ in 92%. Interestingly, the silanol with a coordinating thiophenyl substituent, $\text{Me}_2(2\text{-thiophenyl})\text{SiOH}$ was also applicable in the reaction to furnish the corresponding hydrotrisiloxane in 92% yield. $4\text{-MeC}_6\text{H}_4\text{SiH}_3$ and $n\text{-HexSiH}_3$ were also subjected to the reaction, leading to the

quantitative formation of the corresponding hydrotrisiloxane $(\text{Me}_3\text{SiO})_2(\text{SiHR})$ ($\text{R} = 4\text{-MeC}_6\text{H}_4, n\text{Hex}$).

The combination of **1a**/2NaBEt₃H also catalyzed the coupling of Me₃SiOH with secondary silanes (Scheme 3-8). In the presence of **1a** (0.1 mol%) and NaBEt₃H (0.2 mol%), Me₃SiOH reacted with Ph₂SiH₂ and PhMeSiH₂ to selectively form the corresponding hydrotrisiloxanes in good yields, (Me₃SiO)SiHPh₂ (77%) and (Me₃SiO)SiHPhMe (84%), respectively. However, the reactivity of the dialkylsilane Et₂SiH₂ towards Me₃SiOH was very low, (Me₃SiO)SiHEt₂ (35%). Bulky dialkylsilanes such as *i*Pr₂SiH₂ and *t*Bu₂SiH₂ did not react with Me₃SiOH.

Since complex **3** efficiently catalyzed the dehydrogenative coupling of silanes with silanols (vide supra), the author postulated that **3** could be a key intermediate in the catalytic cycle. To shed light on the reaction mechanism, the following experiments were performed.

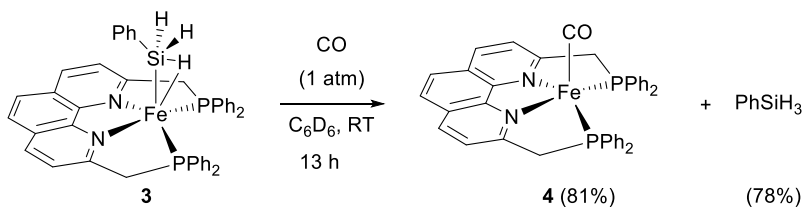
First, stoichiometric reactions of **3** with PhSiH₃ or Me₃SiOH were performed and followed by ¹H NMR in C₆D₆. However, the reaction did not proceed and **3** remained unchanged in both cases (Scheme 3-9). On the other hand, treatment of **3** with 3 equiv of PhSiH₃ and 8 equiv of Me₃SiOH provided quantitative trihydrosiloxane (Scheme 3-9).



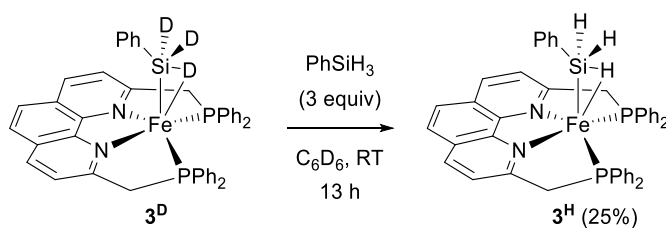
Scheme 3-9. Stoichiometric reactions of **3** with phenylsilane and/or trimethylsilanols.

It was revealed that **3** is active for ligand exchange. The treatment of **3** under CO atmosphere slowly proceeded to form **4** (81% yield) as well as free PhSiH₃ (78%) (Scheme 3-10). Complex **3** also underwent ligand

exchange with free PhSiH_3 ; the reaction of deuterated **3^D** bearing a PhSiD_3 ligand with 3 equiv of PhSiH_3 slowly proceeded at room temperature, resulting in the formation of **3^H** (25% for 13h) (Scheme 11). In the reaction, no H/D mixing of PhSiH_3 was detected.

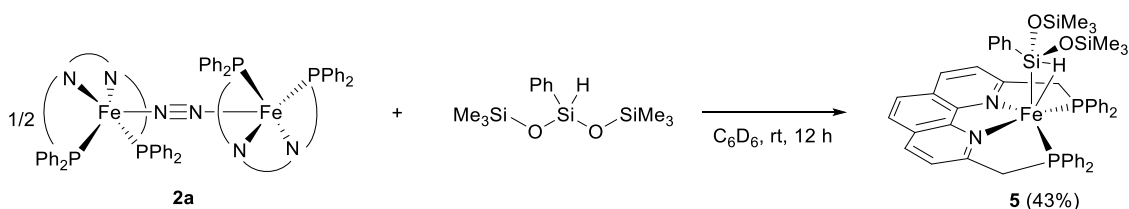


Scheme 3-10. The reaction of **3** under carbon monoxide atmosphere.

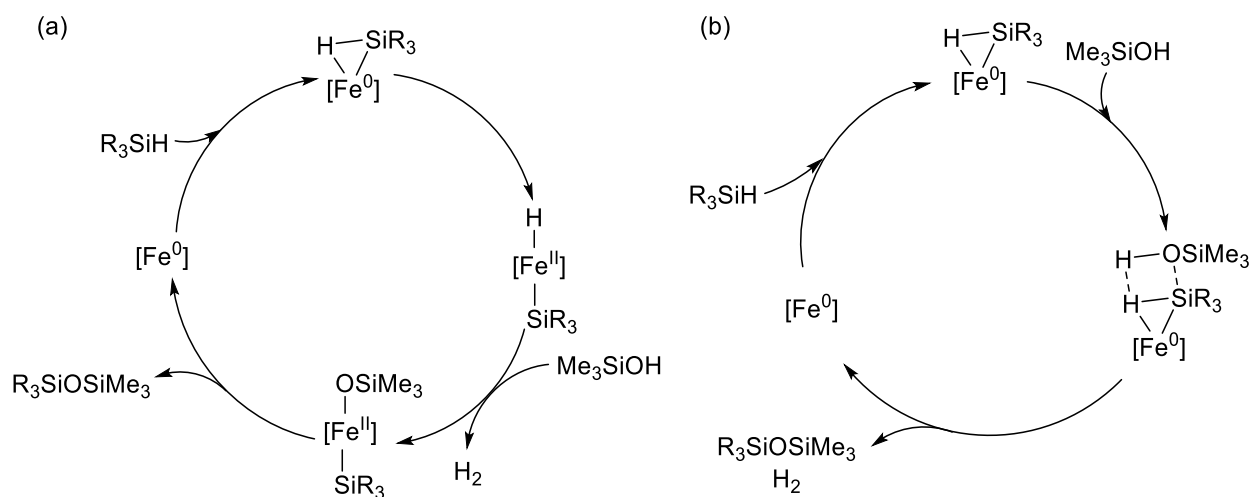


Scheme 3-11. The reaction of **3^D** with phenylsilane.

Nest, the reaction of **2a** with $(\text{Me}_3\text{SiO})_2(\text{SiHPh})$ as a bulky hydrosilane was performed to afford the corresponding hydrosilane complex **5** only in 43% yield (NMR) (Scheme 3-12). Therefore, the incorporation of substrates in the reaction sphere of $[\text{Fe}(\text{PNNP-R})]$ is somewhat dependent on the steric hinderance of the substrates.



Scheme 3-12. The reaction of **2a** with $\text{PhSiH}(\text{OSiMe}_3)_2$ with phenylsilane.



Scheme 3-13. Hypothesis of the reaction mechanism.

As mentioned above, the catalytic reaction did not proceed only in the presence of excess hydrosilane. The results strongly indicated the involvement of the second $PhSiH_3$ molecule to assist the catalytic cycle. The author tentatively ascribe the role of $PhSiH_3$ molecule to stabilization effect of the active $Fe(0)$ species during the reaction. One possible mechanism is including an $Fe(0)/Fe(II)$ cycle (Scheme 3-13 (a)); i.e. the reaction initiates with the oxidative addition of $PhSiH_3$ to form a silyl(hydride) intermediate, which successively reacts with silanol, resulting in the formation of siloxanes, H_2 and the active $Fe(0)$ species.⁵ Alternatively, the activated $PhSiH_3$ of **3** is directly attacked by silanol to form siloxane, in which step, the Si-H bond cleavage and the Si-O bond formation proceeded in a concerted fashion (Scheme 3-13 (b)). This mechanism is also demonstrated in the transition-metal-catalysed dehydrogenative coupling of hydrosilanes with alcohols. The mechanistic study is still underway in the laboratory.

Conclusion

Selective formation of hydrotrisiloxanes was achieved through dehydrogenative coupling of silanols with silanes using **1a** as the catalyst precursor. The reaction proceeded with high efficiency and good reaction selectivity. The reactions underwent iron(silane) complex and the silane ligand and reaction selectivity were affected by silanes steric.

Experimental section

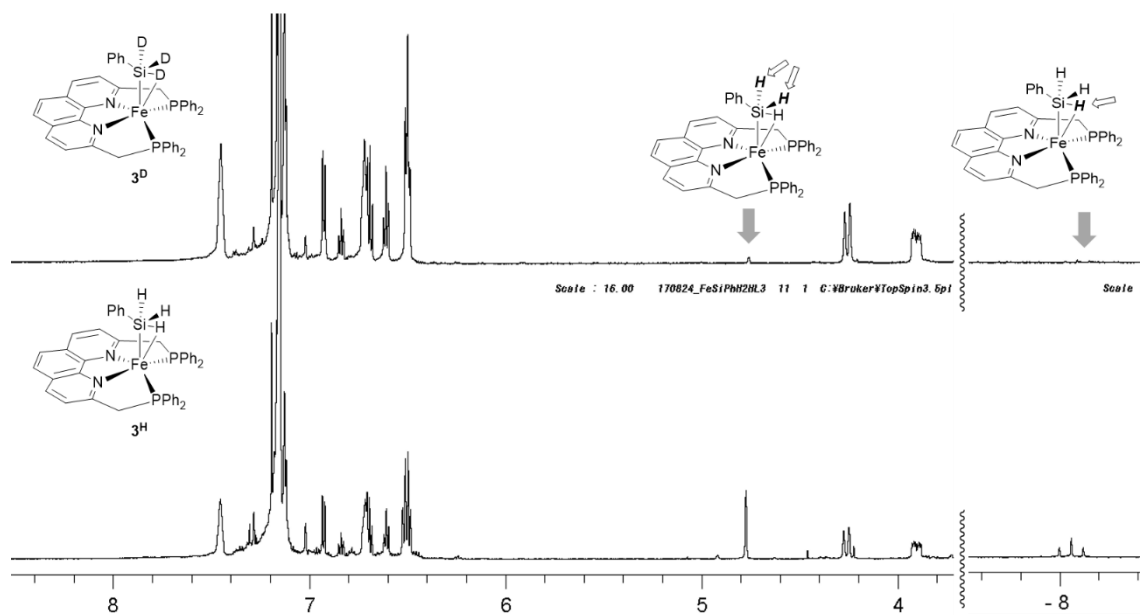
General considerations

All experiments were performed under nitrogen atmosphere using Schlenk techniques or a glove box unless otherwise noted. *n*-Hexane, tetrahydrofuran, benzene and dichloromethane were purified by a solvent purification system (MBraun SPS-800 or Glass Contour Ultimate Solvent System). C₆D₆ was dried over sodium benzophenone ketyl and distilled. (Trimethylsilyl) methyl lithium was crystallized at -40 °C from (Trimethylsilyl)methyl lithium solution 1.0 M in pentane. PhSiD₃⁶ and 4-Methylphenylsilane⁷ were synthesized by following the reported procedures. All other reagents were purchased from commercial suppliers and used without further purification unless otherwise noted. ¹H, ¹³C{¹H}, and ³¹P{¹H} NMR spectra (¹H, 600 MHz; ¹³C, 150 MHz; ²⁹Si, 119 MHz; ³¹P, 243 MHz) were recorded on a Bruker AVANCE III HD 600 spectrometer. Chemical shifts are reported in δ (ppm) and referenced to the residual solvent signals for ¹H and ¹³C and 85% H₃PO₄ as an external standard for ³¹P. The high-resolution ESI mass spectra were obtained on a Bruker microTOF II.

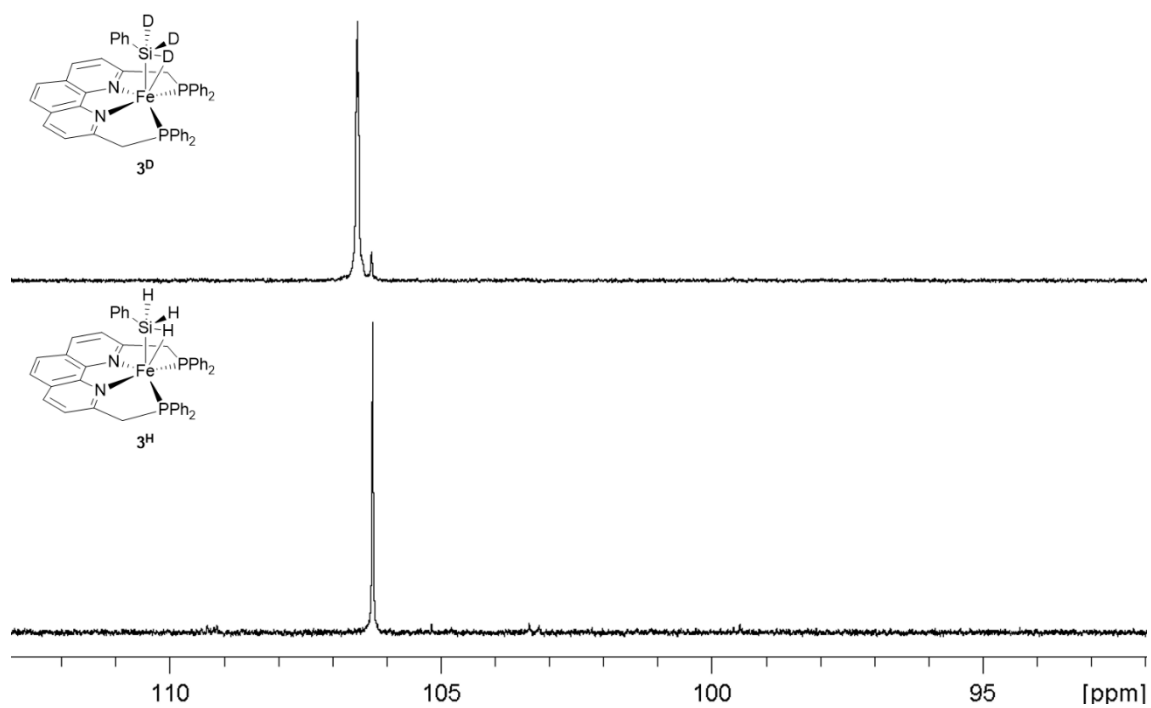
Synthesis of [Fe(η²-HSiH₂Ph)(PNNP-Ph)] (**3^D**)

To a THF suspension of **1a** (0.030 g, 43 μmol) (3 mL), was added NaBEt₃H (1 M in THF, 86 μL, 86 μmol) at room temperature. The mixture was stirred for 30 minutes, added phenylsilane (18.4 mg, 171 μmol), and further stirred for 30 minutes at the temperature. The solution was concentrated to dryness under vacuum, and the resulting solid was washed by hexane (1 mL × 3) and dried. The resulting compound was extracted with C₆H₆ and filtered. After evaporation, **5a** was obtained as a black solid (0.024 g, 76 %). **5a** was crystallized from cold Et₂O/*n*-hexane to form block crystals. ¹H NMR (600 MHz, C₆D₆): δ 7.54 (br, 4H, PPh-*H*), 7.20 (s, 2H, Phen-*H*), 7.13-7.05 (m, 8H, Ar-*H*), 6.93 (d, 2H, *J* = 7.26 Hz, Phen-*H*), 6.83 (t, 1H, *J* = 7.26, SiPh), 6.71-6.69 (m, 6H, Ar-*H*), 6.61 (t, *J* = 7.32 Hz, 2H), 6.51-6.49 (m, 6H), 4.26 (d, 2H, *J* = 15.84 Hz, PCH₂), 3.81 (dt, 2H, *J* = 16.5, 5.28 Hz, PCH₂). ¹³C{¹H} NMR (150 MHz, C₆D₆): δ 155.9, 140.8, 140.6, 133.1, 132.9, 132.8, 131.3, 131.2, 129.5, 128.3, 126.7, 126.0, 118.8, 114.6, 47.1 ppm. ³¹P{¹H} NMR (243 MHz, C₆D₆): δ 106.5 (t, ²*J*_{DP} = 10.5 Hz) ppm.

^1H NMR (600 MHz, C_6D_6):



^{31}P NMR (243 MHz, C_6D_6):

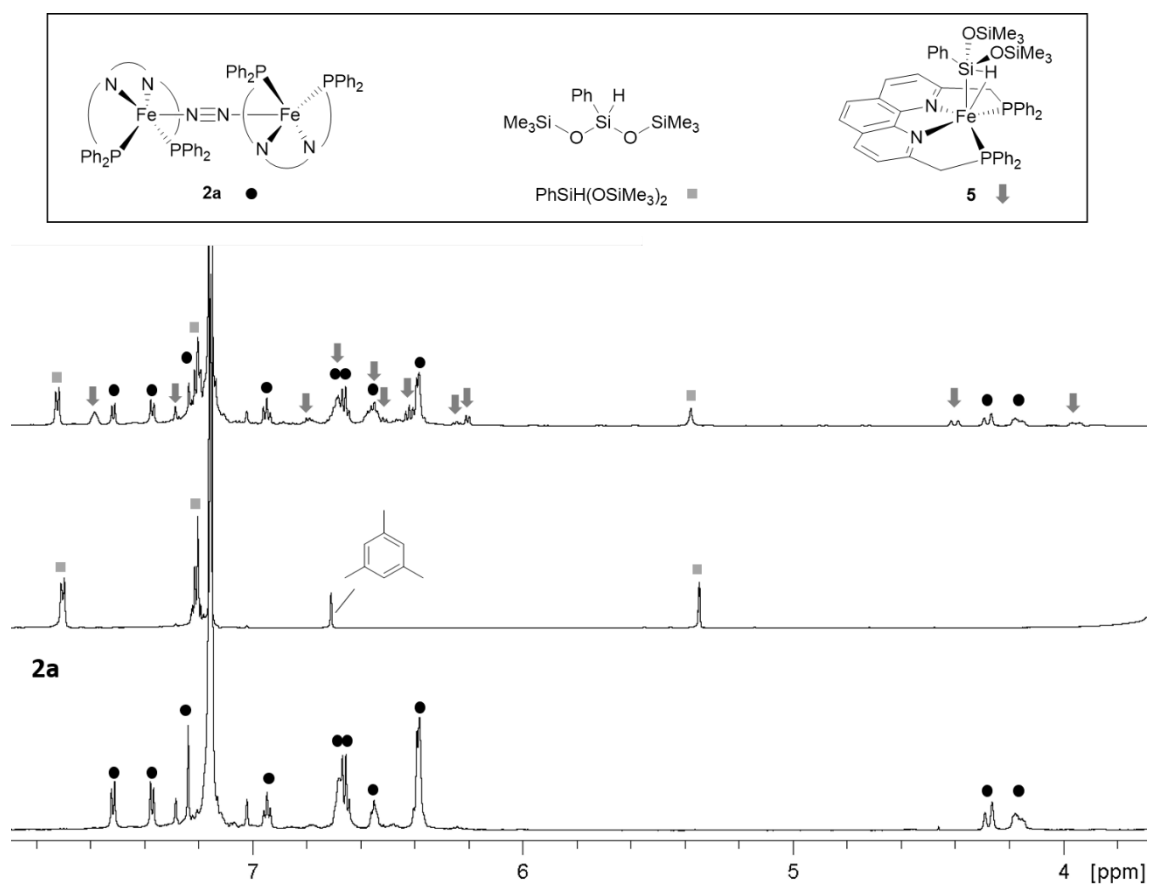


The reaction of **2** with $\text{PhSiH(OSiMe}_3)_2$ (Synthesis of **5**)

1 (0.010 g, 14 μmol) (3 mL), NaBEt_3H (1 M in THF, 28 μL , 28 μmol) and $\text{PhSiH(OSiMe}_3)_2$ (4.6 mg, 28 μmol) in 0.4 mL of C_6D_6 were added to *J-Young* NMR tube. After 12 h at room temperature, ^1H NMR spectra was measured.

The spectra was shown below.

^1H NMR (600 MHz):



Catalytic dehydrogenation of silanes with silanols

A typical procedure (Table 1, entry 1) is as follows. All reactions were carried out under a nitrogen atmosphere. To a vial were added a THF solution (0.5 mL) of PhSiH_3 (32.4 mg, 0.30 mmol) and a 0.1 M stock solution of **1a**/ NaBEt_3H (30 μL , 0.030 μmol).¹⁸ After stirring for 5 minutes, Me_3SiOH (56.0 mg, 0.62 mmol) was added, and

the mixture was stirred at room temperature for 12 h. Mesitylene (36.0 mg, 0.30 mmol) as an internal standard was added to the reaction mixture, and ^1H NMR spectra were recorded to determine the NMR yield of $(\text{Me}_3\text{SiO})_2(\text{SiHPh})$ (>99%).

Compounds characterization data of hydrosiloxanes

The final product was characterized by ^1H , $^{13}\text{C}\{^1\text{H}\}$ and $^{29}\text{Si}\{^1\text{H}\}$ NMR as well as HRMS. $(\text{Me}_3\text{SiO})(\text{SiH}_2\text{Ph})$,^{4b} $(\text{Me}_3\text{SiO})_2(\text{SiHPh})$,^{4b,9} $((t\text{BuO})_3\text{SiO})(\text{SiH}_2\text{Ph})$,^{4b} $(\text{Me}_3\text{SiO})(\text{SiHPh}_2)$ ¹⁰ and $(\text{Me}_3\text{SiO})(\text{SiHPhMe})$ ⁹ were identified by comparing their ^1H , $^{13}\text{C}\{^1\text{H}\}$ and $^{29}\text{Si}\{^1\text{H}\}$ NMR data with those previously reported. 4-Methylphenylsilane¹¹ was synthesized by following the reported procedures.

$(i\text{Pr}_3\text{SiO})_2(\text{SiHPh})$ Using PhSiH_3 (32.4 mg, 0.30 mmol) and $i\text{Pr}_3\text{SiOH}$ (108.1 mg, 0.62 mmol). ^1H NMR (600 MHz, C_6D_6 , 25 °C): δ 7.72 (d, 2H, $J = 1.50$ Hz, Ar- H), 7.21-7.18 (m, 3H, Ar- H), 5.39 (s, 1H, $^1J_{\text{SiH}} = 246.6$ Hz), 0.98-0.89 (m, 42H) ppm. $^{13}\text{C}\{^1\text{H}\}$ NMR (150 MHz, C_6D_6 , 25 °C): δ 137.6, 132.8, 130.1, 128.1, 17.7, 12.8 ppm. $^{29}\text{Si}\{^1\text{H}\}$ NMR (119 MHz, C_6D_6 , 25 °C): δ 9.5, -49.2 ppm.

HRMS (ESI): m/z calcd for $[\text{C}_{23}\text{H}_{48}\text{O}_2\text{Si}_3\text{H}]^+$ (M+H): 453.3040 ; found 453.3029.

$(t\text{BuMe}_2\text{SiO})_2(\text{SiHPh})$ Using PhSiH_3 (32.4 mg, 0.30 mmol) and $t\text{BuMe}_2\text{SiOH}$ (108.1 mg, 0.62 mmol). ^1H NMR (600 MHz, C_6D_6 , 25 °C): δ 7.73 (dd, 2H, $J = 7.74, 1.62$ Hz, Ar- H), 7.23-7.19 (m, 3H, Ar- H), 5.39 (s, 1H, $^1J_{\text{Si, H}} = 243.8$ Hz, SiH), 0.96 (s, 18H), 0.14 (s, 6H), 0.12 (s, 6H) ppm. $^{13}\text{C}\{^1\text{H}\}$ NMR (150 MHz, C_6D_6 , 25 °C): δ 137.4, 133.4, 130.5, 128.2, 25.9, 18.4, -2.8 ppm. $^{29}\text{Si}\{^1\text{H}\}$ NMR (119 MHz, C_6D_6 , 25 °C): δ 13.2, -48.5 ppm.

HRMS (ESI): m/z calcd for $[\text{C}_{18}\text{H}_{36}\text{O}_2\text{Si}_3\text{H}]^+$ (M+H): 369.2101 ; found 369.2111.

$(\text{Me}_3\text{SiO})_2(\text{SiHTol})$ Using TolSiH_3 (36.6 mg, 0.30 mmol) and Me_3SiOH (56.1 mg, 0.62 mmol).

^1H NMR (600 MHz, C_6D_6 , 25 °C): δ 7.67 (d, 2H, $J = 7.87$, Ar- H), 7.07 (d, 2H, $J = 7.07$, Ar- H), 5.41 (s, 1H, $^1J_{\text{Si, H}} = 243.3$ Hz, SiH), 2.08 (s, 3H, PhCH_3), 0.17 (s, 18H, $\text{Si}(\text{CH}_3)_3$) ppm. $^{13}\text{C}\{^1\text{H}\}$ NMR (150 MHz, C_6D_6 , 25 °C): δ 139.9, 133.6, 133.2, 128.7, 25.4, 1.5 ppm. $^{29}\text{Si}\{^1\text{H}\}$ NMR (119 MHz, C_6D_6 , 25 °C): δ 10.2, -48.1 ppm.

HRMS (ESI): m/z calcd for $[C_{18}H_{36}O_2Si_3H]^+$ (M+H): 369.2101 ; found 369.2111.

(Me₃SiO)₂(SiH_{*n*}Hex) Using *n*HexSiH₃ (34.8 mg, 0.30 mmol) and Me₃SiOH (56.0 mg, 0.62 mmol). ¹H NMR (600 MHz, C₆D₆, 25 °C): δ 5.0 (s, 1H, ¹J_{Si, H} = 232.4 Hz, SiH), 1.50 (quin, 2H, *J* = 7.80, SiCH₂CH₂), 1.35 (quin, 2H, *J* = 7.35, SiCH₂CH₂CH₂), 1.32-1.23 (m, 4H, CH₂CH₂CH₃), 0.89 (t, 3H, *J* = 7.02, CH₃), 0.66 (t, 2H, *J* = 8.01, SiCH₂), 0.19 (s, 18H, Si(CH₃)₃) ppm. ¹³C{¹H} NMR (150 MHz, C₆D₆, 25 °C): δ 32.6, 31.7, 22.6, 22.2, 17.5, 14.0, 1.5 ppm. ²⁹Si{¹H} NMR (119 MHz, C₆D₆, 25 °C): δ 9.00, −36.0 ppm.

HRMS (ESI): m/z calcd for $[C_{12}H_{32}O_2Si_3H]^+$ (M+H): 293.1788 ; found 293.1787.

(thiophen-2-ylMe₂SiO)₂(SiHPh) Using PhSiH₃ (32.4 mg, 0.30 mmol) and thiophen-2-ylMe₂SiOH (98.1 mg, 0.62 mmol). ¹H NMR (600 MHz, CD₃CN): δ 7.72 (dd, 2H, *J* = 4.59, 0.87 Hz, Ar-*H*), 7.55 (dd, 2H, *J* = 7.21, 1.38 Hz, Ar-*H*), 7.42 (dt, 2H, *J* = 7.47, 1.41 Hz, Ar-*H*), 7.34 (t, 2H, *J* = 7.32 Hz, Ar-*H*), 7.31 (dd, 2H, *J* = 3.36, 0.84 Hz, Ar-*H*), 7.23-7.21 (m, 2H, Ar-*H*), 5.45 (s, 1H, ¹J_{SiH} = 248.9 Hz, SiH), 0.39 (s, 6H, SiCH₃), 0.38 (s, 6H, SiCH₃) ppm. ¹³C{¹H} NMR (150 MHz, C₆D₆): δ 138.2, 136.1, 134.7, 133.2, 130.8, 130.3, 128.0, 1.27, 1.26 ppm. ²⁹Si{¹H} NMR (119 MHz, C₆D₆): δ −3.5, −47.7 ppm. HRMS (ESI): m/z calcd for $[C_{18}H_{24}O_2S_2Si_3H]^+$ (M+H): 421.0604 ; found 421.0604.

Reference

1. a) R. G. Jones, W. Ando and J. Chojnowski, *Silicon-Containing Polymers*, Kluwer Academic Publishers, Dordrecht, **2000**. b) M. A. Brook, *Silicon in Organic, Organometallic, and Polymer Chemistry*, Wiley-Interscience, New York, **2000**.
2. a) D. B. Thompson and M. A. Brook, *J. Am. Chem. Soc.* **2008**, *130*, 32. b) J. B. Grande, T. Ulrich, T. Dickie and M. A. Brook, *Polym. Chem.* **2014**, *5*, 6728. c) R. Wakabayashi, K. Kawahara and K. Kuroda, *Angew. Chem., Int. Ed.* **2010**, *49*, 5273. d) S. Saito, N. Yamasue, H. Wada, A. Shimojima and K. Kuroda, *Chem. Eur. J.* **2016**, *22*, 13857. e) Y. Li and Y. Kawakami, *Macromolecules* **1999**, *32*, 6871. f) D. Zhou and Y. Kawakami, *Macromolecules* **2005**, *38*, 6902. g) Z. Chang, M. C. Kung and H. H. Kung, *Chem. Commun.* **2004**, 206. h) A. V. Arzumanyan, I. K. Goncharova, R. A. Novikov, S. A. Milenin, K. L. Boldyrev, P. N. Sol'yev, Y. V. Tkachev, A. D. Volodin, A. F. Smol'yakov, A. A. Korlyukovae and A. M. Muzafarov, *Green Chem.* **2018**, *20*, 1467.

3. a) R. Ciriminna, A. Fidalgo, V. Pandarus, F. Béland, L. M. Ilharco and M. Pagliaro, *Chem. Rev.* **2013**, *113*, 6592. b) V. Chandrasekhar, R. Boomishankar and S. Nagendran, *Chem. Rev.* **2004**, *104*, 5847.
4. a) Z. M. Michalska, *Transition Met. Chem.* **1980**, *5*, 125. b) Y. Satoh, M. Igarashi, K. Sato and S. Shimada, *ACS Catal.* **2017**, *7*, 1836. c) K. Matsumoto, K. V. Sajna, Y. Satoh, K. Sato and S. Shimada, *Angew. Chem., Int. Ed.*, **2017**, *56*, 3168. d) K. Matsumoto, Y. Oba, Y. Nakajima, S. Shimada and K. Sato, *Angew. Chem., Int. Ed.* **2018**, *57*, 4637.
5. a) L. H. Sommer and J. E. Lyons, *J. Am. Chem. Soc.* **1969**, *91*, 7061. b) X.-L. Luo and R. H. Crabtree, *J. Am. Chem. Soc.* **1989**, *111*, 2527. c) E. Scharrer, S. Chang and M. Brookhart, *Organometallics* **1995**, *14*, 5686. d) M. Bühl and F. T. Mauschick, *Organometallics* **2003**, *22*, 1422. e) D. Ventura-Espinosa, A. Carretero-Cerdán, M. Baya, H. García and J. A. Mata, *Chem. Eur. J.* **2017**, *23*, 10815.
6. A. Kumar, A. Kumar Pandiakumar and A.G. Samuelson, *Tetrahedron* **2014**, *70*, 3185.
7. B.-H. Kim, M.-S. Cho, M.-A. Kim and H.-G. Woo, *J. Organomet. Chem.* **2003**, *685*, 93.
8. A. V. Arzumanyan, I. K. Goncharova, R. A. Novikov, S. A. Milenin, K. L. Boldyrev, P. N. Sol'yev, Y. V. Tkachev, A. D. Volodin, A. F. Smol'yakov, A. A. Korlyukovae and A. M. Muzafarov, *Green Chem.* **2018**, *20*, 1467.
9. J. Hao, B. Vabre, and D. Zargarian, *J. Am. Chem. Soc.* **2015**, *137*, 15287.

Chapter 4

Synthesis and properties of chloro(silyl)iron complexes via oxidative addition reaction of Si–Cl bond

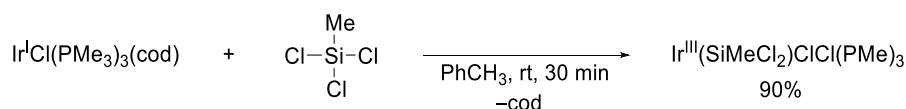
Abstract

[{Fe(PNNP-Ph)}₂(μ-N₂)] (**1**) underwent the Si–Cl bond cleavage of chlorosilanes to form [Fe(SiR₃)(Cl)(PNNP-Ph)] (SiR₃ = SiCl₃ (**2a**), SiMeCl₂ (**3**) and SiPhCl₂ (**4**)) as the oxidative additive complexes. According to single crystal X-ray diffraction study, **2a** adopt an octahedral geometry with the silyl and chloro ligands at the axial positions. The results demonstrated the first example of a well-defined Si–Cl oxidative addition reaction by a 3d transition metal complex. It was also revealed that the reaction of **1** with SiCl₄ in presence of dihydroanthracene (DHA) resulted in the formation of [Fe(HSiCl₃)(PNNP-Ph)] (**6**), indicating that the oxidative additive reaction of Si–Cl bond by **1** proceeded via radical pathway.

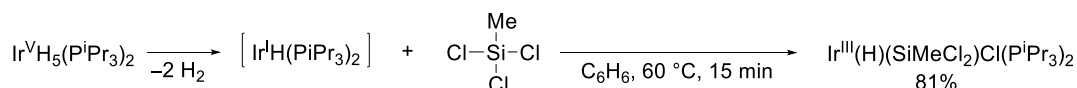
Introduction

Chlorosilanes are important raw materials for various organosilicon materials (e.g. silicones).¹ It is known that the diverse properties of silicones are highly dependent on the substituents on the silicon atom. Therefore, to produce various silicone products with higher performances, it is of great importance to prepare chlorosilanes with a variety of organic substituents. The common synthetic procedures of organochlorosilanes are as follows, 1) methyl-, ethyl-, and phenylchlorosilanes are synthesized by Müller–Rochow “direct process”, in which silicon metal reacts with alkyl-, or aryl chloride in the presence of a copper catalyst;¹ 2) treatment of the chlorosilanes with organometallic reagents or metal hydrides, such as organomagnesium, organolithium, and LiAlH_4 , etc.¹ However, these methods tend to suffer from limited functional-group tolerance due to the harsh reaction conditions that require reactive organometallic reagents. Another problem of this method is its low reaction selectivity, namely, the nucleophilic substitution reactions of di- and trichlorosilanes usually produce mixtures of mono-, di-, and tri-substituted products. In these regards, catalytic Si–C-bond-forming reactions with chlorosilanes as starting materials are one of attractive strategies to efficiently prepare a series of organochlorosilanes with a high selectivity. However, bond dissociation energy (BDE) of Si–Cl bonds is extremely high ($\text{Me}_3\text{Si–Cl}$: 113 kcal/mol);² the value is much higher than those of Si–I bonds ($\text{Me}_3\text{Si–I}$: 77 kcal/mol)² and the carbon counterpart, C–Cl bonds ($\text{Me}_3\text{C–Cl}$: 80 kcal/mol).² Thus, only limited numbers of reports on catalytic transformation of Si–Cl to Si–R have been reported to date.³ In most cases, pre-treatment of chlorosilane with lithium iodide was required for the *in-situ* halogen exchange to provide the corresponding iodosilanes.³ In this context, a nickel-catalyzed direct silyl–Heck reaction of chlorosilanes was recently demonstrated.⁴ This reaction was assumed to be initiated with the oxidative addition of Si–Cl bond by an electrophilic nickel(0) complex. The piece of work is of great significance as the first example of the direct transformation of chlorosilanes via oxidative addition of a Si–Cl bond. Indeed, only four examples of the well-defined Si–Cl oxidative addition reaction have been reported to date using complexes of electron rich Ir (Schemes 4-1, 4-2),^{5a,5b} Pt (Scheme 4-3),^{5c} and Rh^{5d} (Scheme 4-4). In addition, the detailed mechanistic studies had rarely performed. Therefore, to elucidate the detailed mechanism of Si–Cl bond cleavage is still a big challenge in this

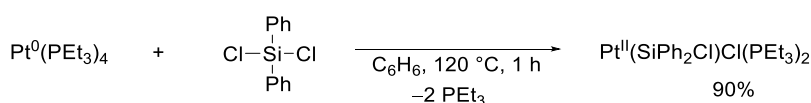
area.



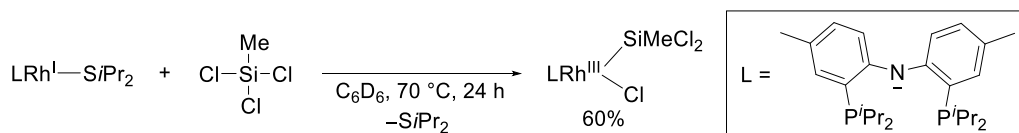
Scheme 4-1. Reaction of $\text{IrCl}(\text{PMe}_3)_3(\text{cod})$ with MeSiCl_3 .



Scheme 4-2. Reaction of $\text{IrH}_5(\text{P}^i\text{Pr}_3)_2$ with MeSiCl_3 .



Scheme 4-3. Reaction of $\text{Pt}(\text{PEt})_4$ with PhSiCl_3 .



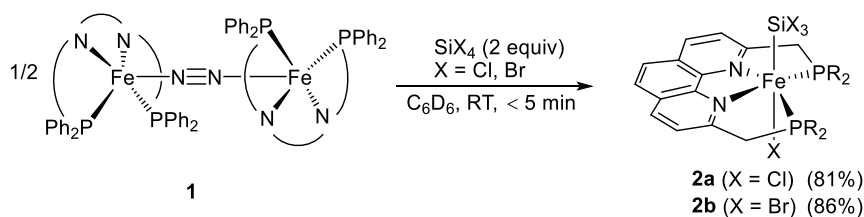
Scheme 4-4. Reaction of $\text{Rh}(\text{SiPr})\text{L}$ with MeSiCl_3 .

In this chapter, the author disclosed that $[\text{Fe}(\text{PNNP-Ph})_2(\mu\text{-N}_2)]$ (**1**) smoothly underwent oxidative addition of Si–Cl bond to form silyl(chloro) complex. Mechanistic study was conducted to disclose the radical pathway for the Si–Cl bond cleavage. The reactivity of silyl(chloro) complex was further investigated.

Results and discussion

Treatment of $[\{\text{Fe}(\text{PNNP-Ph})\}_2(\mu\text{-N}_2)]$ (**1**) with SiX_4 ($\text{X} = \text{Cl}, \text{Br}$) in C_6D_6 at room temperature quickly proceeded to result in the stoichiometric formation of purple complexes $[\text{FeSiCl}_3(\text{Cl})(\text{PNNP-Ph})]$ (**2a**) and $[\text{FeSiBr}_3(\text{Br})(\text{PNNP-Ph})]$ (**2b**), respectively (Scheme 4-5). These complexes were diamagnetic and characterized by ^1H , ^{13}C , ^{31}P and ^{29}Si NMR spectra. The ^{31}P NMR spectra (C_6D_6) of **2a** and **2b** exhibited one sharp singlet, which was assignable to two phosphine side-arms. Therefore, symmetrical structures of PNNP-Ph ligand were supported

in **2a** and **2b**. Likewise, ^1H NMR spectra of **2a** and **2b** also supported the existence of the symmetry plane containing the Fe atom, the Si atom, and the midpoint of two N atoms. In the ^1H NMR spectra, the CH_2 moieties exhibited two doublets with germinal coupling constant at $\delta = 4.81$ (d, $J = 15.7$ Hz) and $\delta = 4.35$ (d, $J = 14.3$ Hz) ppm (**2a**) and $\delta = 4.96$ (d, $J = 18.4$ Hz) and $\delta = 4.44$ (d, $J = 17.8$ Hz) ppm (**2b**). The spectra supported the different magnetic environments, which was bisected with the phenanthroline plane of PNNP-R. The ^{29}Si NMR signals of **2a** appeared at $\delta = 46.9$, respectively. According to single crystal X-ray diffraction studies, the geometries of both **2a** and **2b** were revealed to be octahedral with tetradentate PNNP-Ph ligand at equatorial plane and the SiX_3 ($\text{X} = \text{Cl}$: **2a**, = Br: **2b**) and the halogen groups at the axial positions (Figure 4-1). The Fe–Si bond lengths were 2.285(6) Å (**2a**) and 2.275(17) Å (**2b**), which were in the common range of Fe–Si single bonds of iron(II) silyl complexes with a low-spin state.



Scheme 4-5. Reaction of **1** with SiX_4 ($\text{X} = \text{Cl}, \text{Br}$).

Reactions of **1** with various chlorosilanes were summarized in Scheme 4-6. Complex **1** similarly reacted with MeSiCl_3 , leading to the formation of the corresponding oxidative addition product of $[\text{Fe}(\text{Cl})(\text{SiMeCl}_2)(\text{PNNP-Ph})]$ (**3**) in 83% yield (Figure 4-S1). In contrast, the reactions of **1** with bulkier PhSiCl_3 did not proceed at room temperature, but, the reactions performed at higher 50 °C provided $[\text{Fe}(\text{Cl})(\text{SiPhCl}_2)(\text{PNNP-Ph})]$ (**4**) in 43% yield, accompanied by thermal decomposition products of **1**. The reactions of **1** with Ph_2SiCl_2 or Me_3SiCl didn't undergo, and the chlorosilanes were fully recovered only to provide thermal decomposition products of **1**. It is reported that the reactivity of chlorosilane towards oxidative addition is highly dependent on the number of Cl substituents. The electron-withdrawing Cl groups make the LUMO energy level lower, and thus enhance the Lewis acidity of the Si

atom.⁶ As a result, the SiCl₄ and RSiCl₃ (R = Me, Ph) could interact with the electron rich iron(0) metal center more easily than Ph₂SiCl₂ or Me₃SiCl.

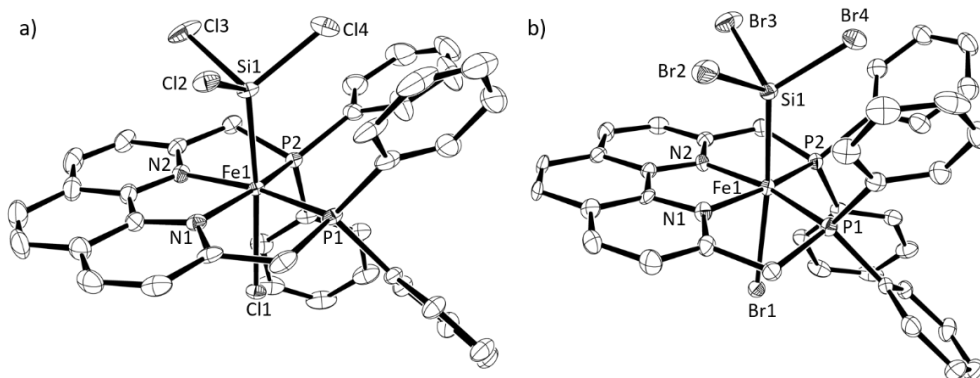
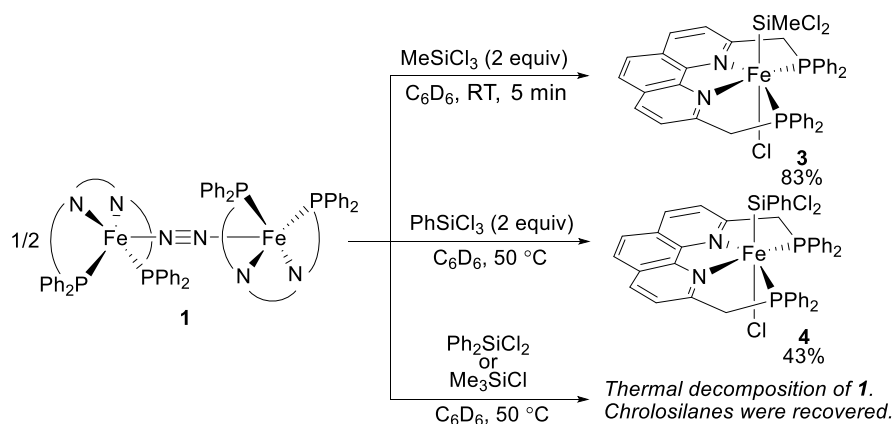
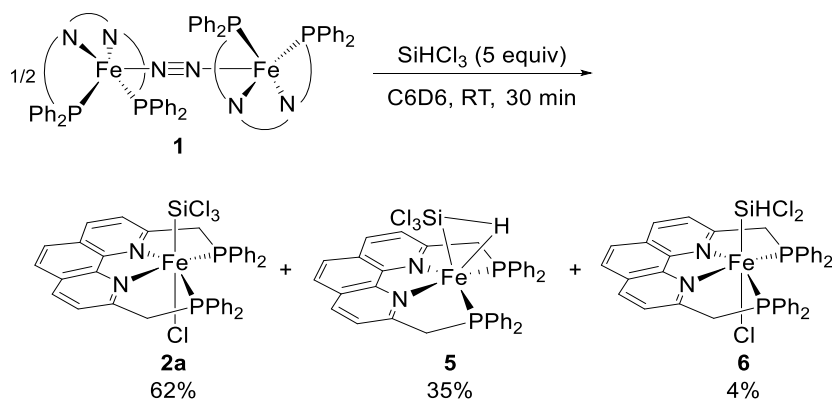


Figure 4-1. Molecular structures of **2a** and **2b** with 50% probability ellipsoids. Hydrogen atoms are omitted for clarity. Selected bond lengths (Å) and bond angles (°) of **2a**: Fe1–N1 1.973(3), Fe1–N2 1.960(3), Fe1–P1 2.2338(10), Fe1–P2 2.2459(10), Fe1–Si1 2.2480(10), Fe1–Cl1 2.3891(9), Si1–Cl2 2.0950(14), Si1–Cl3 2.1145(13), Si1–Cl4 2.1243(13), N1–Fe1–N2 81.73(12), P1–Fe1–P2 112.34(4), Si1–Fe1–Cl1 172.32(4). Selected bond lengths (Å) and bond angles (°): Fe1–N1 1.961(4), Fe1–N2 1.954(4), Fe1–P1 2.2472(17), Fe1–P2 2.2459(16), Fe1–Si1 2.2876(18), Fe1–Br1 2.5290(10), Si1–Br2 2.2571(17), Si1–Br3 2.2948(17), Si1–Br4 2.3048(17), N1–Fe1–N2 82.17(19), P1–Fe1–P2 111.83(6), Si1–Fe1–Br1 174.38(6).



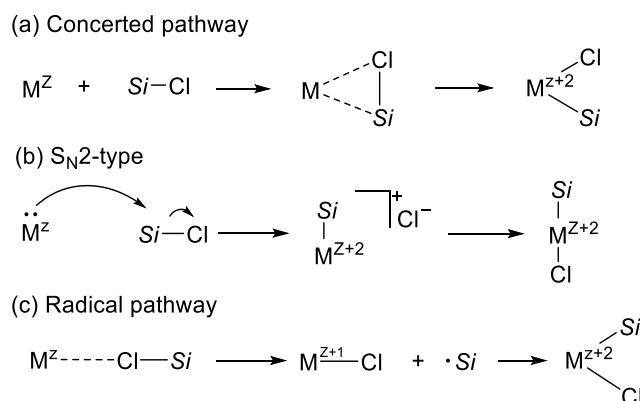
Scheme 4-6. Reactions of **1** with MeSiCl₃, PhSiCl₃, Ph₂SiCl₂ and Me₃SiCl.

In the reaction of **1** with HSiCl₃, which contains both a Si–Cl bond and a Si–H bond, oxidative addition product **7** was obtained in only 4%, accompanied by the hydrosilane-adducted iron(0) complex [Fe(HSiCl₃)(PNNP-Ph)] (**5**) in 35% yield at room temperature after 30 minutes (Scheme 4-7). In addition, complex **2a** was obtained as a major product (62%). After 12 h, the yields of **5** decreased to 52%, and that of **2a** increased to 40%. The observed formation of **2a** supported the occurrence of disproportionation of HSiCl₃ to form SiCl₄ *in-situ*.

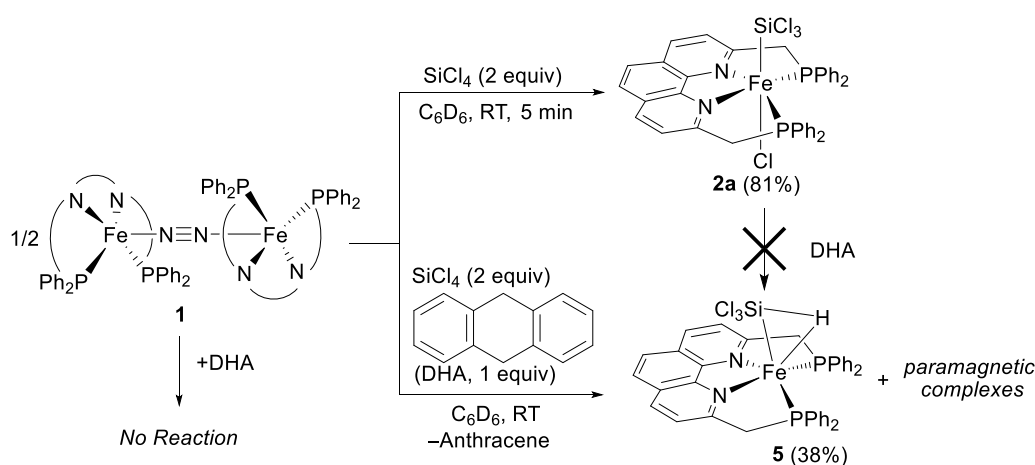


Scheme 4-7. Reaction of **1** with HSiCl_3 .

Generally, three mechanisms are established for oxidative addition as follows;⁷ 1) concerted pathway (Scheme 4-8 (a)),^{7b} 2) $\text{S}_{\text{N}}2$ -type pathway (Scheme 4-8 (b)),^{7c} and 3) radical pathway (Scheme 4-8 (c)).^{7d} To shed light on the reaction mechanism, the author performed the reaction of **1** with SiCl_4 in the presence of 9,10-dihydroanthracene (DHA) (Scheme 4-9). It was surprising that the reaction resulted in the formation of **5** (38% yield) as well as several unidentified paramagnetic species and anthracene. The result indicated that the oxidative addition of the Si–Cl bond by **2a** proceeded via the radical pathway, in which a silyl radical was formed *in-situ* and successively abstracted a H atom from DHA to form HSiCl_3 . The resulting HSiCl_3 was trapped by unreacted **2a**, then **5** and anthracene were formed. The reaction is of great significance as the first example to demonstrate the Si–Cl bond cleavage via the radical mechanism. Furthermore, it should be noted that such the hemolytic cleavage of Si–Cl bond is highly useful for the hydrogenation of chlorosilanes as discussed below.



Scheme 4-8. Mechanisms of oxidative addition.

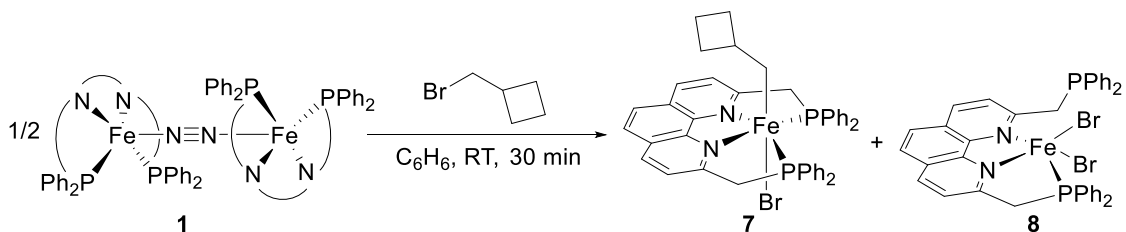


Scheme 4-9. Reactions of **1** with $SiCl_4$, and/or DHA.

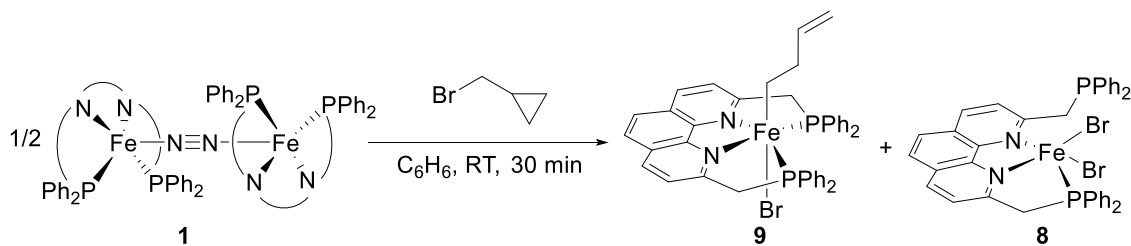
To further shed light on the reaction mechanism, the radical clock experiments⁸ were carried out. The reaction of **1** with (bromomethyl)cyclobutane in C_6H_6 quickly provided oxidative addition product of **7** as well as **8** (Scheme 4-10). Complex **7** was identified by NMR and ESI-MS. Luckily, green block crystals were obtained and single-crystal X-ray diffraction study was carried out. Complex **7** exhibited a distorted octahedral structure, in which bromo and cyclobutylmethyl ligands were located at the axial positions (Figure 4-2).

The reaction of **1** with (bromomethyl)cyclopropane was also carried out in C_6H_6 at room temperature for 30 min to give the complicated mixture containing **9** (Scheme 4-11). The 1H NMR spectrum of the resulting mixture exhibited same integral as $\delta = 6.23$ (m, 1H), 5.04 (m, $J = 15.0$ Hz, 1H), and 4.95 (d, $J = 9.65$ 1H) ppm, which ascribed to terminal alkene and the CH_2 moieties in the PNNP-Ph ligand ($\delta = 4.58$ (m, 2H) and 4.39 (m, 2H)). It was indicating the formation of oxidative addition product **9**, which possesses 1-butenyl ligand formed via ring

opening of the cyclopropyl ring.



Scheme 4-10. Reactions of **1** with (bromomethyl)cyclobutane.



Scheme 4-11. Reactions of **1** with (bromomethyl)cyclopropane.

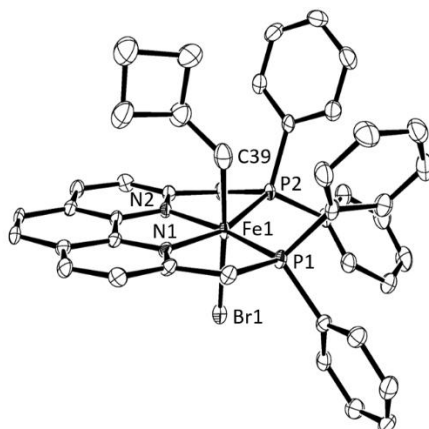
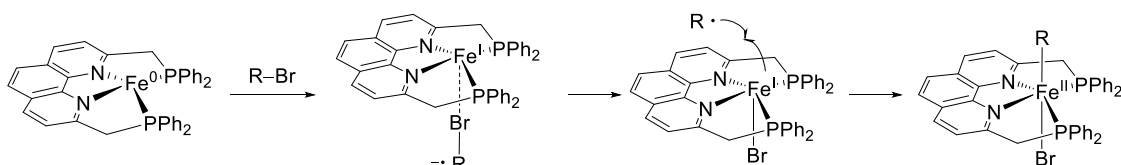


Figure 4-3. Molecular structure of **6** with 50% probability ellipsoids. Hydrogen atoms are omitted for clarity. Selected bond lengths (Å) and bond angles (°) of **6**: Fe1–N1 1.931(3), Fe1–N2 1.952(3), Fe1–P1 2.2341(12), Fe1–P2 2.2257(10), Fe1–C39 2.096(4), Si1–Cl1 2.131(4), Fe1–Br1 2.5770(8), N1–Fe1–N2 82.08(12), P1–Fe1–P2 110.94(4), Si1–Fe1–N3 175.88(11).

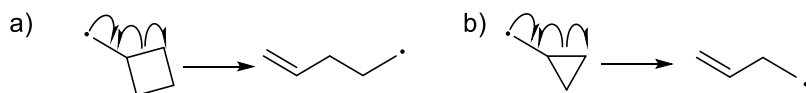
Generally, when the oxidative reaction of alkyl halides proceeds via the radical pathway, low valent metal center (LM^n) coordinated to halide of alkyl halide to form the adduct. Then, single electron transfer occurs to provide $LM^{n+1}(X)$ and alkyl radical ($R\cdot$). Next, $R\cdot$ combines with $LM^{n+1}(X)$ to give oxidative addition product ($LM^{n+1}(X)(R)$) (Scheme 4-12).^{7d}

In such the radical process of oxidative additions of (bromomethyl)cyclobutane or (bromomethyl)cyclopropane, the ring-opening reaction proceeds to provide 1-pentene and 1-butene, respectively, when the radicals exist at the α -position of methylcyclobutane or methylcyclopropane with a certain lifetime

(Scheme 4-13). It was reported that the rate constants (k_{RO} (S^{-1})) of methylcyclobutane radical or methylcyclopropane radical were calculated to be 4.7×10^3 and 1.0×10^8 , respectively.⁸ Since the ring-opening was observed only in the case of (boromomethyl)cyclopropane in this study, the author estimated the lifetime of the alkyl radical formed in the oxidative addition reaction by **1** between 4.7×10^3 and 1.0×10^8 .

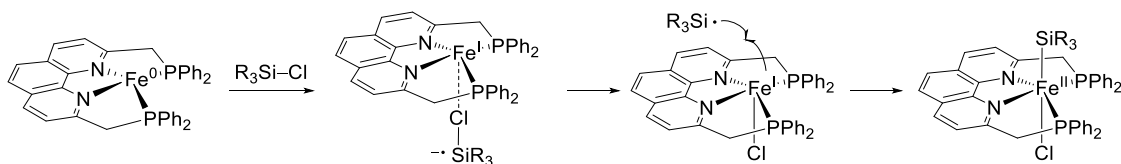


Scheme 4-12. Reaction mechanisms of **1** with alkyl bromide.



Scheme 4-13. Radical clock reactions of cyclobutylmethyl radical and cyclopropylmethyl radical.

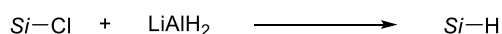
Overall, the mechanistic study using radical clocks supported that the oxidative addition reactions of Si–Cl bond proceed via radical pathway. The possible mechanism was shown in Scheme 4-14. First, starting from chlorosilane adducts of **1**, one electron was transferred to chlorosilane to form an iron(I) chloride intermediate and a silyl radical. Next, the silyl radical coordinated to the iron(I) metal, then oxidative addition product was generated. It was assumed that key step of the reaction was the single electron transfer step. Thus, the reactivity towards oxidative addition increase in the order of $SiCl_4 > RSiCl_3 > R_2SiCl_2 > R_3SiCl$; $SiCl_4$ is the most reactive because it is least sterically hindered and possesses lowest LUMO energy.



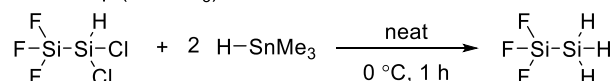
Scheme 4-14. Reaction mechanisms of **1** with chlorosilane.

Next, the author set out for the development of facile Si–H bond formation of chlorosilanes. Direct substitution reaction of Si–Cl bond to Si–H bond under mild conditions is attractive to provide hydrosilanes. The conventional synthetic method for the production of hydrosilanes relies on the use of reactive hydride reagents, such as LiAlH_4 and DIBAL-H.^{1,9a} (Scheme 4-15 (a)). In addition, the substitute reactions using HSnMe_3 ^{9b} (Scheme 4-15 (b)) and NaBH_4 ^{9c} (Scheme 4-15 (c)) as mild reagents are also known as a laboratory scale methods. However, it is necessary to use excess amounts of hydride reagents. Recently, some groups reported hydrogenation of halosilanes including chlorosilanes using iridium or ruthenium catalysts (Scheme 4-15 (d), (e)). In these reactions, it was necessary to add NaI or $\text{NaBAR}^{\text{F}}_4$, which undergo halogen-exchange with chlorosilanes to form reactive iodosilanes or silylcations.^{9d,e} In this context, the author was motivated to engage in the direct hydrogenation of chlorosilanes.

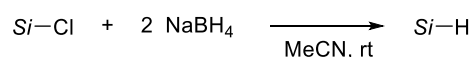
(a) classical reaction



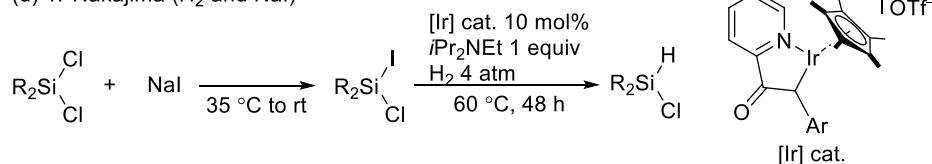
(b) K. G. Sharp (HSnMe_3)



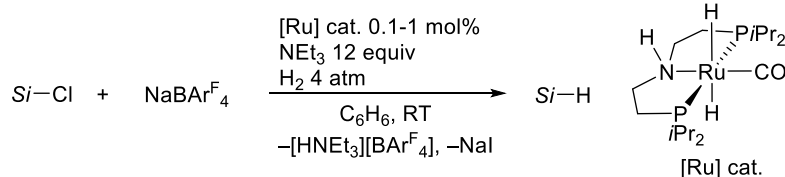
(c) H. Nakazawa (NaBH_4)



(d) Y. Nakajima (H_2 and NaI)



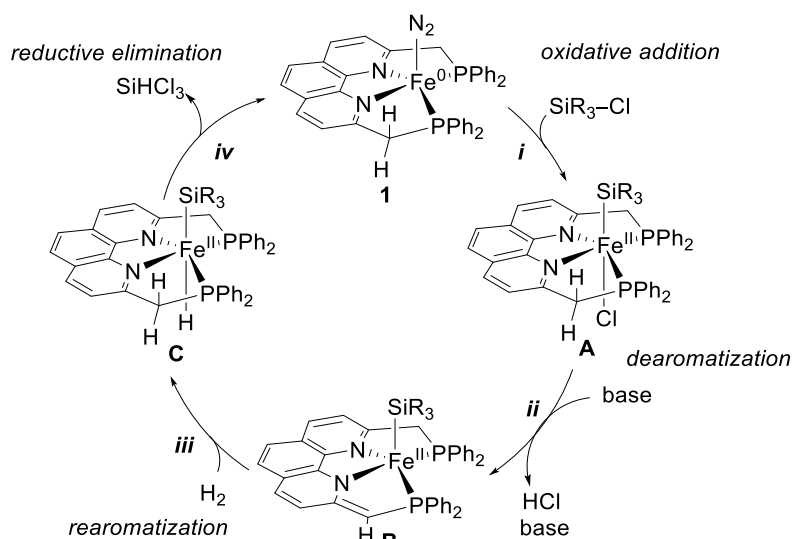
(e) S. Schneider (H_2 and $\text{NaBAR}^{\text{F}}_4$)



Scheme 4-15. Substitute reaction of Si–Cl to Si–H.

The author applied to utilize the concept of MLC for the hydrogenolysis of chlorosilanes in the iron PNNP-R system, which was inspired by the previous reports on MLC-supported hydrogenolysis of carbonyl compounds by Milstein and co-workers.¹⁰ The author's working hypothesis was shown in Scheme 4-16. (i) Iron(0)

complex **A** dissociates molecular N_2 to form coordinatively unsaturated iron(0) species **1** (dissociative path). **1** reacts with a cleave of Si–Cl bond in chlorosilanes to form the corresponding iron silyl(chloro) complex **A**. (ii) Deprotonation of **A** by base leads to dearomatization of the ligand backbone moiety to form **B**. (iii) Treatment of **B** with hydrogen undergoes rearomatization to form silyl(hydrido) complex **C**. (iv) **C** undergoes reductive elimination to give hydrosilane and recovered **1**.

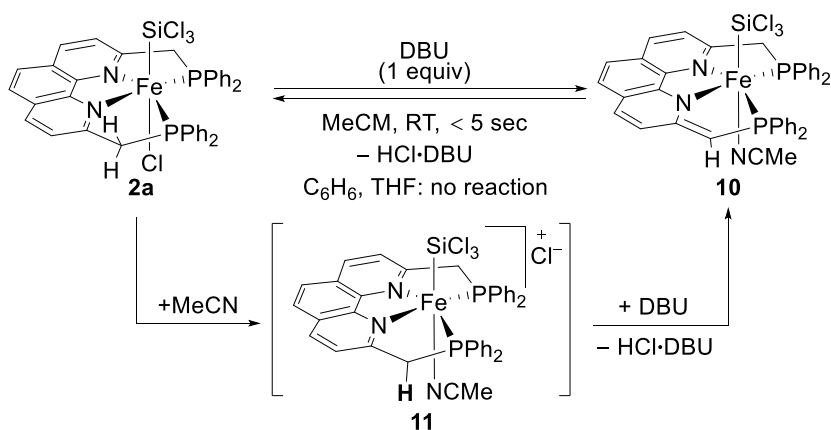


Scheme 4-16. Proposed catalytic reaction to provide hydrosilane from chlorosilane using hydrogen as a reductant.

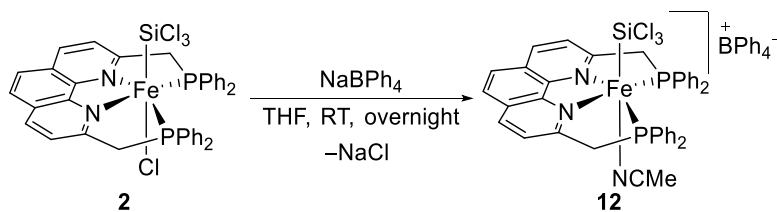
First, to obtain the dearomatized complex **A**, reactions of **2a** with NaOtBu or NaH were performed. However, the efficient deprotonation of the PNNP-Ph ligand did not proceed and the substitution reaction of chloro groups on the Si atom proceeded. The dearomatization reaction was carried out using 1,8-diazabicyclo[5.4.0]undec-7-ene (DBU) as a milder base. The reaction of **2a** with DBU in C_6H_6 or THF did not proceed. In contrast, treatment of **2a** with DBU in CD_3CN at room temperature resulted in the formation of dearomatized complex **10**, which exhibited two doublet signals at δ 69.2 ppm ($^2J_{\text{P}} = 28.7$ Hz) and δ 54.6 ppm ($^2J_{\text{P}} = 27.7$ Hz) in ^{31}P NMR spectrum. Complex **10** was converted again to **2a** after the removal of CD_3CN (Scheme 14-6). The red plate crystals of **10** were obtained by treatment **2a** with DBU in presence of 1,8-bis(dimethylamino) naphthalene (proton sponge). Since the deprotonation reaction proceeded only in the polar acetonitrile solvent, it is postulated that the Cl ligand dissociation occur in the polar acetonitrile. To investigate this point, cationic complex **12** was alternatively

synthesized by the reaction of **2a** with NaBPh₄ (Scheme 4-18).

Complex **12** was fully identified by NMR. It should be mentioned that **11** exhibited similar signals to those of **12** in CD₃CN, although the spectra of **2a** and **12** were significantly different in other solvent. Therefore, it was indicated that both **10** and **11** exhibited the similar core structure, [Fe(SiCl₃)(PNNP-Ph)(CH₃CN)]⁺ in CD₃CN.



Scheme 4-17. Dearomatization reaction of **2a**.



Scheme 4-18. Reaction of **2a** with NaBPh₄.

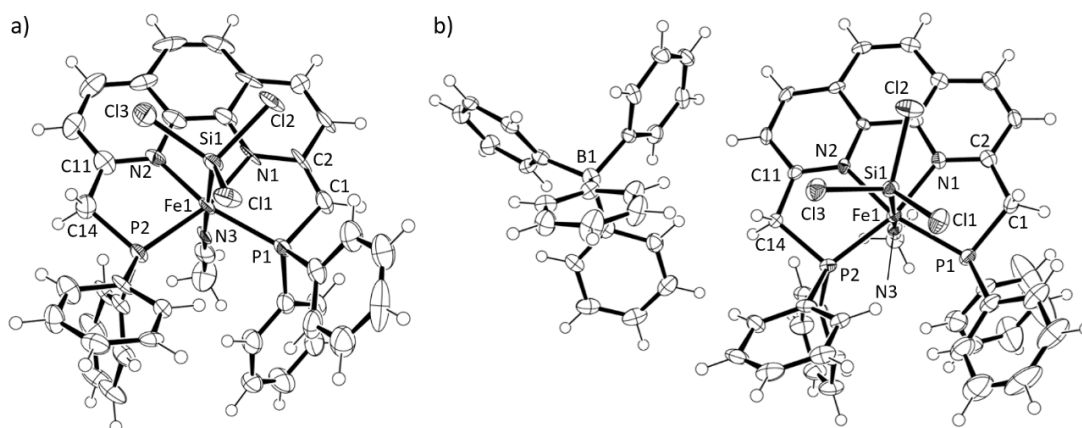
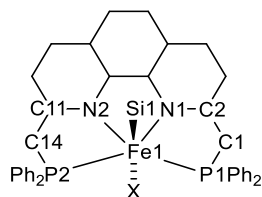


Figure 4-3. Molecular structures diagram of **10** (a) and **12** (b) with 50% probability ellipsoids. Selected bond lengths (Å) and bond angles (°) of **10**: Fe1–N1 1.952(9), Fe1–N2 1.957(8), Fe1–P1 2.239(3), Fe1–P2 2.264(3), Fe1–Si1 2.254(4), Fe1–N3, 1.943(10), Si1–Cl1 2.131(4), Si1–Cl2 2.119(4), Si1–Cl3 2.098(4), N1–Fe1–N2 81.1(4), P1–Fe1–P2 113.13(11), Si1–Fe1–N3 175.0(2). Selected bond lengths (Å) and bond angles (°) of **12**: Fe1–N1 1.961(4), Fe1–N2 1.954(4), Fe1–P1 2.2316(17), Fe1–P2 2.2599(17), Fe1–Si1 2.2719(18), Fe1–N3 1.976(5), Si1–Cl1 2.087(2), Si1–Cl2 2.107(2), Si1–Cl3 2.110(2), N1–Fe1–N2 82.01(18), P1–Fe1–P2 112.47(7), Si1–Fe1–N3 172.79(14).

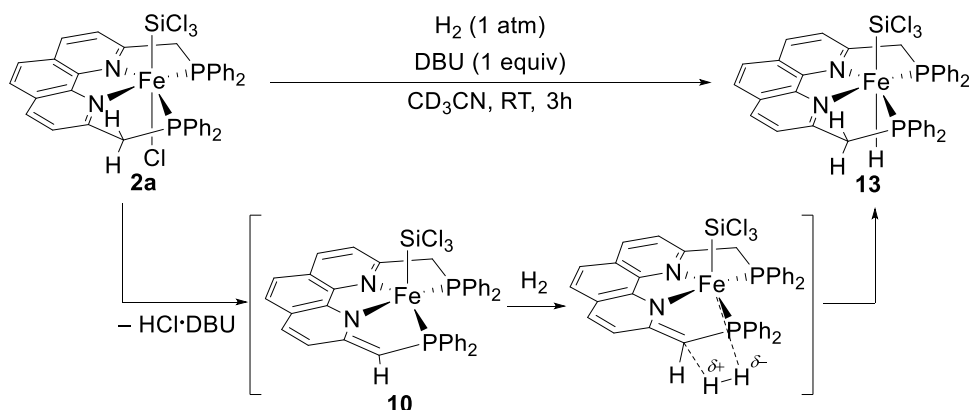
The single-crystal X-ray diffraction studies of **2a**, **10** and **12** were performed (Figure 4-3, Table 4-1). The bond lengths around the iron metal are suitable to diamagnetic iron(II) complex. The C1–C2 and C11–C14 bond lengths of **2a** and **12** are almost identical (**2a**: C1–C2 1.497(5) Å, C11–C14 1.496(5) Å, **13**: C1–C2 1.498(7) Å, C11–C14 1.510(8) Å). On the other hand, the C1–C2 and C11–C14 bond lengths of **9** are 1.491(14) Å and 1.368(15) Å. Thus, the dearomatization of **10** was confirmed.

Table 4-1. Selected bond lengths (Å) of the crystal structures for **2a**, **10**, **12**, and **13**.



Complex	2a	10	12	13
C1–C2	1.497(5)	1.491(14)	1.498(7)	1.504(3)
C2–N1	1.340(5)	1.363(13)	1.336(6)	1.339(3)
C11–C14	1.496(5)	1.368(15)	1.510(8)	1.505(3)
C11–N2	1.329(4)	1.378(14)	1.332(6)	1.338(3)
Fe1–N1	1.973(3)	1.952(9)	1.961(4)	1.9450(18)
Fe1–N2	1.960(3)	1.952(9)	1.964(4)	1.9473(17)
Fe1–P1	2.2338(10)	2.239(3)	2.2316(17)	2.1854(6)
Fe1–P2	2.2459(10)	2.264(3)	2.2599(17)	2.1875(6)
Fe1–Si1	2.2480(10)	2.254(4)	2.2719(18)	2.2582(7)
Fe1–X	2.3891(9)	1.943(10)	1.976(5)	1.43(3)
	(X = C11)	(X = N3)	(X = N3)	(X = H1)

Next, the examination of the rearomatization step corresponding to **iv** in Scheme 4-15 was performed (Scheme 4-19). Treatment of **2a** with DBU under hydrogen atmosphere in CD₃CN resulted in the formation of **13**. In the reaction, complex **10** was initially prepared and successively reacted with H₂, resulting in the rearomatization of PNNP-Ph via H–H bond cleavage. Complex **13** exhibited the hydride signals at δ –6.11 ppm (t , $^2J_P = 63.2$ Hz) in the ¹H NMR. In the ³¹P NMR spectrum, one singlet signal appeared at δ 85.9 ppm (Scheme 4-18). These results indicated the following reaction pathway; **10** was once generated *in-situ* by the reaction of **2a** with DBU in CD₃CN, then cleaved the H–H bond heterolytically associated with rearomatization of one pyridine ring to form **13**.



Scheme 4-19. Synthesis of **12** using **2a** with H_2 as hydride source.

Complex **13** could be alternatively synthesized as follows. The reaction of **2a** with LiBH_4 proceeded quickly to obtain **13** quantitatively as the deep blue crystals (Scheme 4-20). Based on the single crystal X-ray diffraction, the molecular structure of **13** exhibited an octahedral geometry in which tetradentate PNNP-Ph ligand coordinated to the iron center at the equatorial plane and the SiCl_3 and the hydride located to the axial position of the iron (Figure 4-4, Table 4-1). The hydride signal was detected by difference Fourier synthesis.

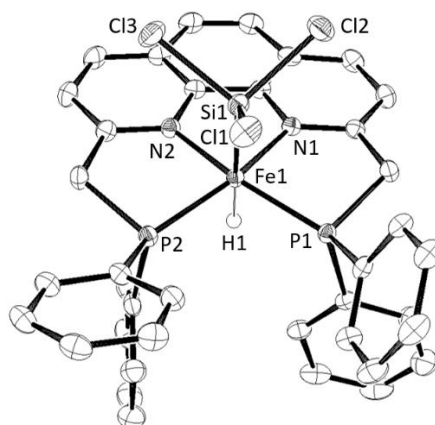
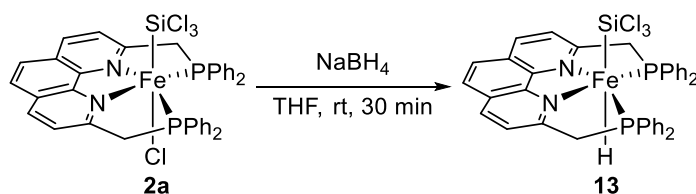


Figure 4-4. Molecular structure of **13** with 50% probability ellipsoids. Hydrogen atoms are omitted for clarity except H1. Selected bond lengths (Å) and bond angles (°): Fe1–N1 1.9450(18), Fe1–N2 1.9473(17), Fe1–P1 2.1854(6), Fe1–P2 2.1875(6), Fe1–Si1 2.2582(7), Fe1–H1 1.43(3), Si1–Cl1 2.1338(8), Si1–Cl2 2.1524(8), Si1–Cl3 2.1124(8), N1–Fe1–N2 81.22(7), P1–Fe1–P2 110.14(2), Si1–Fe1–N3 179.7(13).



Scheme 4-20. Synthesis of **13** using **2a** with NaBH_4 as hydride source.

Conclusion

The author succeeded in demonstrating the well-defined oxidative addition of chlorosilanes using $[\{\text{Fe}(\text{PNNP-Ph})\}_2(\mu\text{-N}_2)]$ **1**. The resulting oxidative addition complex, iron silyl(chloro) complexes were fully characterized and structurally determined by a single-crystal X-ray study. The reaction of **1** with SiCl_4 in presence of DHA resulted in the formation of hydrosilane complex **5**. The result strongly indicates that the oxidative addition of chlorosilanes proceed via the radical pathway. Complex **2a** easily underwent deprotonation by DBU in MeCN to form **10**. The reaction of **10** with hydrogen provided **13**. The author postulated that the MLC through aromatization/dearomatization from **2a** to **13** is the key reaction to convert from Si–Cl to Si–H.

Experimental section

General considerations

All experiments were performed under a nitrogen atmosphere using Schlenk techniques or a glove box unless otherwise noted. *n*-Hexane, tetrahydrofuran, toluene and dichloromethane were purified by a solvent purification system (MBraun SPS-800 or a Glass Contour Ultimate Solvent System). C_6D_6 was dried over sodium benzophenone ketyl and distilled. CD_2Cl_2 and CD_3CN was dried over CaH_2 and distilled. All other reagents were purchased from commercial suppliers and used without further purification unless otherwise noted. ^1H spectra of **7** was written in chapter 1. ^1H , $^{13}\text{C}\{^1\text{H}\}$, $^{29}\text{Si}\{^1\text{H}\}$, and $^{31}\text{P}\{^1\text{H}\}$ NMR spectra (^1H , 600 MHz; ^{13}C , 150 MHz; ^{29}Si , 119 MHz; ^{31}P , 243 MHz) were recorded on a Bruker AVANCE III HD 600 spectrometer. Chemical shifts are reported in δ (ppm) and referenced to the residual solvent signals for ^1H and ^{13}C , 1,4-bis(trimethylsilyl)benzene for ^{29}Si , and 85% H_3PO_4 as an external standard for ^{31}P . The high-resolution ESI mass spectra were obtained on a Bruker microTOF II. Column chromatography was performed with silica gel (Kanto Chemical CO., INC. Silica gel 60 N, 100–210 μm).

Synthesis of $[\text{Fe}(\text{SiCl}_3)(\text{Cl})(\text{PNNP-Ph})]$ (**2a**)

NaBEt₃H (1 M in THF, 74 μ l, 74 μ mol) was added to the suspension (0.2 mL) of [FeCl₂(PNNP-Ph)] (0.030 g, 37 μ mol) in 0.4 ml of C₆H₆ under N₂ atmosphere. After stirred at room temperature for 30 minutes, 5 ml of hexane was added. Removal of the solvent by filtration and the residual solid was washed by 0.5 ml of hexane for three times. The residual was resolved in C₆H₆ and added SiCl₄ 0.028 mg (0.14 mmol). After stirred overnight, removal of the solvent *in vacuo* and washed by hexane. After dryness, the purple solid mg (mmol, 81 %) was obtained. **2a** was crystallized from THF/*n*-hexane for 3 days to form purple block crystals. ¹H NMR (600 MHz, C₆D₆): δ 7.76 (br, 4H), 7.64 (br, 4H), 7.44 (d, J = 8.04, 2H), 7.18-7.11 (m, 6H) 7.79-7.01 (m, 10H), 4.82 (dt, J = 17.8, 4.10 Hz, 2H), 4.36 (dt, J = 17.6, 4.10 Hz, 2H) ppm. ¹³C{¹H} NMR (150 MHz, C₆D₆): δ 164.7, 149.9, 138.6-137.4 (multi), 135.2 (t, ² J_P = 4.42 Hz), 134.1 (t, ² J_P = 4.47 Hz), 130.1, 129.3 \times 2, 128.5, 117.5 (t, ² J_P = 4.42 Hz), 125.7, 125.5, 121.7 (d, ² J_P = 4.47 Hz), 49.7 (t, ¹ J_P = 17.2 Hz) ppm. ²⁹Si{¹H} NMR (243 MHz, C₆D₆): δ 46.9 (t, J = 67.8 Hz) ppm. ³¹P{¹H} NMR (243 MHz, C₆D₆): δ 67.9 ppm. ¹H NMR (600 MHz, C₆D₆) (**10**): δ 8.67 (d, J = 8.23, 4H), 8.25 (d, J = 8.34, 4H), 8.17 (s, 4H), 7.88 (tt, J = 12.2, 1.80, 4H), 7.59 (t, J = 7.50, 2H), 7.48 (t, J = 9.46 Hz, 4H), 7.32-7.25 (m, 6H), 5.05 (dd, J = 17.6, 5.17 Hz, 2H), 4.91 (dd, J = 18.4, 4.05 Hz, 2H) ppm. ³¹P{¹H} NMR (243 MHz, C₆D₆) (**10**): δ 67.4 ppm.

Synthesis of [Fe(SiBr₃)(Br)(PNNP-Ph)] (**2b**)

2b 0.033 g (35 μ mol, 86%) was prepared following the same procedure of **2a** using NaBEt₃H (1 M in THF, 74 μ l, 74 μ mol), [FeCl₂(PNNP-Ph)] (0.030 g, 37 μ mol) and SiBr₄ 0.044 mg (0.014 mmol). **2b** was crystallized from THF/*n*-hexane for 1 week to form purple block crystals ¹H NMR (600 MHz, C₆D₆): δ 7.98 (br, 4H), 7.65 (br, 4H), 7.43 (d, J = 8.04, 2H), 7.18-7.11 (m, 6H) 7.79-7.01 (m, 10H), 4.95 (dt, J = 16.9, 4.31 Hz, 2H), 4.44 (dt, J = 17.7, 4.06 Hz, 2H) ppm. ¹³C{¹H} NMR (150 MHz, C₆D₆): δ 164.7 (t, ³ J_P = 6.4 Hz), 149.5, 138.1-137.6 (multi), 134.9 (t, ² J_P = 4.5 Hz), 133.9 (t, ² J_P = 4.5 Hz), 129.8, 129.0, 128.2, 127.9, 126.8 (t, ² J_P = 4.2 Hz), 125.2, 121.8 (t, ² J_P = 5.4 Hz), 48.4 (d, ¹ J_P = 12.0 Hz), 48.3 (d, ¹ J_P = 12.0 Hz), 1.0 ppm. ²⁹Si{¹H} NMR (243 MHz, C₆D₆): δ 24.3 (t, J = 61.4 Hz) ppm. ³¹P{¹H} NMR (243 MHz, C₆D₆): δ 64.4 ppm.

Synthesis of [Fe(SiMeCl₂)(Cl)(PNNP-Ph)] (**3**)

3 0.028 (31 μ mol, 83%) was prepared following the same procedure of **2a** using NaBEt₃H (1 M in THF, 74 μ l, 74 μ mol), [FeCl₂(PNNP-Ph)] (0.030 g, 37 μ mol) and SiMeCl₃ 0.020 mg (0.13 mmol). ¹H NMR (600 MHz, C₆D₆): δ 7.72 (br, 4H), 7.56-7.54 (m, 4H), 7.51-7.48 (m, 4H), 7.74 (d, 2H, J = 8.26 Hz), 7.23 (d, 2H, J = 7.12), 7.07-7.04 (m, 6H), 6.99-6.98 (m, 4H), 4.26 (dt, 2H, J = 17.5, 4.79 Hz), 4.33 (dt, 2H, J = 16.7, 5.64 Hz), -0.49 ppm (s, 3H). ³¹P{¹H} NMR (243 MHz, C₆D₆): δ 69.4 ppm.

Synthesis of [Fe(SiPhCl₂)(Cl)(PNNP-Ph)] (**4**)

4 0.015 g (19 μ mol, 46%) was prepared following the same procedure of **2a** using NaBEt₃H (1 M in THF, 74 μ l, 74 μ mol), [FeCl₂(PNNP-Ph)] (0.030 g, 37 μ mol) and SiPhCl₃ 0.032 mg (0.14 mmol). ¹H NMR (600 MHz, C₆D₆): δ 7.84 (br, 4H), 7.56 (br, 4H), 7.39 (d, 2H, J = 8.22 Hz), 7.29 (br, 3H), 7.21-7.19 (m, 6H), 7.04-6.99 (m, 12H), 6.73 (t, 1H, J = 7.11 Hz), 6.47 (t, 2H, J = 7.62), 6.17 (d, 2H, J = 6.18 Hz), 4.28-4.26 (m, 4H) ppm. ³¹P{¹H} NMR (243 MHz, C₆D₆): δ 69.6 ppm.

Synthesis of [Fe(C₅H₁₀)(Br)(PNNP-Ph)] (**7**)

NaBEt₃H (1 M in THF, 74 μ l, 74 μ mol) was added to the suspension (0.2 mL) of [FeCl₂(PNNP-Ph)] (0.030 g, 37 μ mol) in 0.4 ml of C₆D₆ under N₂ atmosphere. After stirred at room temperature for 30 minutes, 5 ml of hexane was added. Removal of the solvent by filtration and the residual solid was washed by 0.5 ml of hexane for three times. The residual was resolved in C₆H₆ and added (bromomethyl)cyclobutane 0.1 mg (45 μ mol). After stirred overnight, removal of the solvent *in vacuo* and washed by hexane. After dryness, the purple solid was obtained. **7** was crystallized from THF/*n*-hexane for 3 days to form green block crystals. ¹H NMR (600 MHz, C₆D₆): δ 7.82-7.78 (m, 4H), 7.45 (br, 4H), 7.28 (br, 4H), 7.21-7.10 (m, 12H), 6.83 (t, J = 7.53, 2H), 4.56 (dm, J = 18.1 Hz, 2H), 4.45 (dm, J = 17.2 Hz, 2H), 1.31-1.22 (m, 2H), 0.99-0.93 (m, 2H), 0.94-0.86 (m, 2H), 0.35 (q, J = 8.54, 1H), 0.06 (quin, J = 9.81, 1H), -0.25 (q, J = 7.12, 1H) ppm. ¹³C{¹H} NMR (150 MHz, C₆D₆): δ 163.7, 151.3, 1.38-1.37 (multi), 135.4 (t, ²J_P = 6.7 Hz), 134.8 (t, ²J_P = 6.2 Hz), 133.4 (t, ²J_P = 6.2 Hz), 132.7 (t, ²J_P = 6.2 Hz), 129.2, 1291, 128.5,

127.5 (t, $^2J_P = 4.42$ Hz), 125.8, 119.5, 119.2, 48.1 (t, $^1J_P = 17.2$ Hz), 31.9, 22.8, 22.7, 17.9, 1.4 ppm. $^{31}\text{P}\{^1\text{H}\}$ NMR (243 MHz, C_6D_6): δ 67.9 ppm.

Synthesis of $[\text{Fe}(\text{SiCl}_3)(\text{PNNP-Ph}')] (\mathbf{10})$

2a 0.010 g (13 μmol) was dissolved in 0.4 ml of CD_3CN and added DBU 0.002 g (14 μmol). After 30 min, NMR measurement was carried out. Red needle crystals were obtained when proton sponge was added to the solution and stood at room temperature overnight. ^1H NMR (600 MHz, C_6D_6): δ 7.54 (br, 4H, PPh-*H*), 7.20 (s, 2H, Phen-*H*), 7.13-7.05 (m, 8H, Ar-*H*), 6.93 (d, 2H, $J = 7.26$ Hz, Phen-*H*), 6.83 (t, 1H, $J = 7.26$, SiPh), 6.71-6.69 (m, 6H, Ar-*H*), 6.61 (t, $J = 7.32$ Hz, 2H), 6.51-6.49 (m, 6H), 4.75 (s, 2H, SiH_2), 4.26 (d, 2H, $J = 15.84$ Hz, PCH_2), 3.81 (dt, 2H, $J = 16.5, 5.28$ Hz, PCH_2), -8.06 ppm (t, 1H, $J = 36.8$ Hz, agostic-*H*). $^{13}\text{C}\{^1\text{H}\}$ NMR (150 MHz, C_6D_6): δ 155.9, 140.8, 140.6, 133.1, 132.9, 132.8, 131.3, 131.2, 129.5, 128.3, 126.7, 126.0, 118.8, 114.6, 47.1 ppm. $^{31}\text{P}\{^1\text{H}\}$ NMR (243 MHz, C_6D_6): δ 106.22 ppm. $^{29}\text{Si}\{^1\text{H}\}$ NMR (119 MHz, C_6D_6): δ 12.2 ppm.

Synthesis of $[\text{Fe}(\text{SiCl}_3)(\text{H})(\text{PNNP-Ph})] (\mathbf{13})$

(Method A) **2a** 0.010 g (13 μmol) was dissolved in 0.4 ml of CD_3CN and added DBU 0.002 g (14 μmol). After substituted to hydrogen atmosphere, **13** was generated at room temperature for 3 hours tracked by NMR measurement.

(Method B) **2a** 0.030 g (37 μmol) was dissolved in 10 ml of THF and LiBH_4 50 μl (1M of THF, 50 μmol) was added to the solution. After stirred 30 min, the volatile was removed *in vacuo*. The resulting solids were washed by hexane. The blue solid of **13** 0.026 g (34 μmol , 91%) was obtained. **13** was crystallized from $\text{C}_6\text{D}_6/n$ -hexane for 1 day to form purple block crystals.

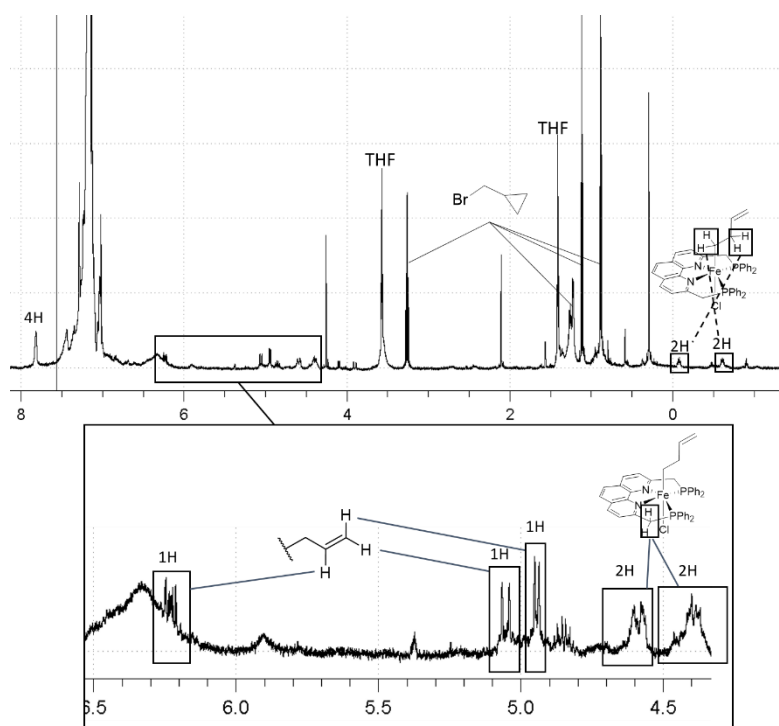
^1H NMR (600 MHz, C_6D_6): δ 7.76 (br, 4H), 7.38-7.32 (m, 6H), 7.17-7.14 (m, 4H), 7.10-7.09 (m, 4H), 7.02 (s, 2H), 6.90 (t, $J = 13.7$ Hz, 4H), 6.82 (t, $J = 14.2$ Hz, 2H), 4.94 (dd, $J = 16.0, 4.09$, 2H), 4.09 (dd, $J = 16.9, 6.41$, 2H), -6.08 ppm (t, 1H, $J = 63.2$ Hz, 1H). $^{31}\text{P}\{^1\text{H}\}$ NMR (243 MHz, C_6D_6): δ 67.9 ppm.

The reaction of **2a** with (bromomethyl)cyclopropane.

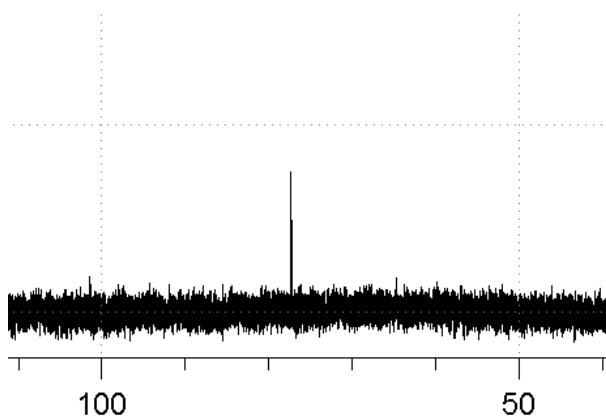
The crystal of **1** (0.005 g, 7.0 μmol), which was crystalized a –THF/hexane at $-40\text{ }^{\circ}\text{C}$,* in *J Young* NMR tube was dissolved in 0.4 ml of C_6D_6 and added (bromomethyl)cyclopropane 0.4 mg (0.003 mmol). As soon as, NMR measurement of the solution was carried out. See NMR caption. *The crystal of **1** was decomposed by dryness.

Therefore, the weight of **1** was include little amount of mother liquid.

^1H NMR (600 MHz, C_6D_6):



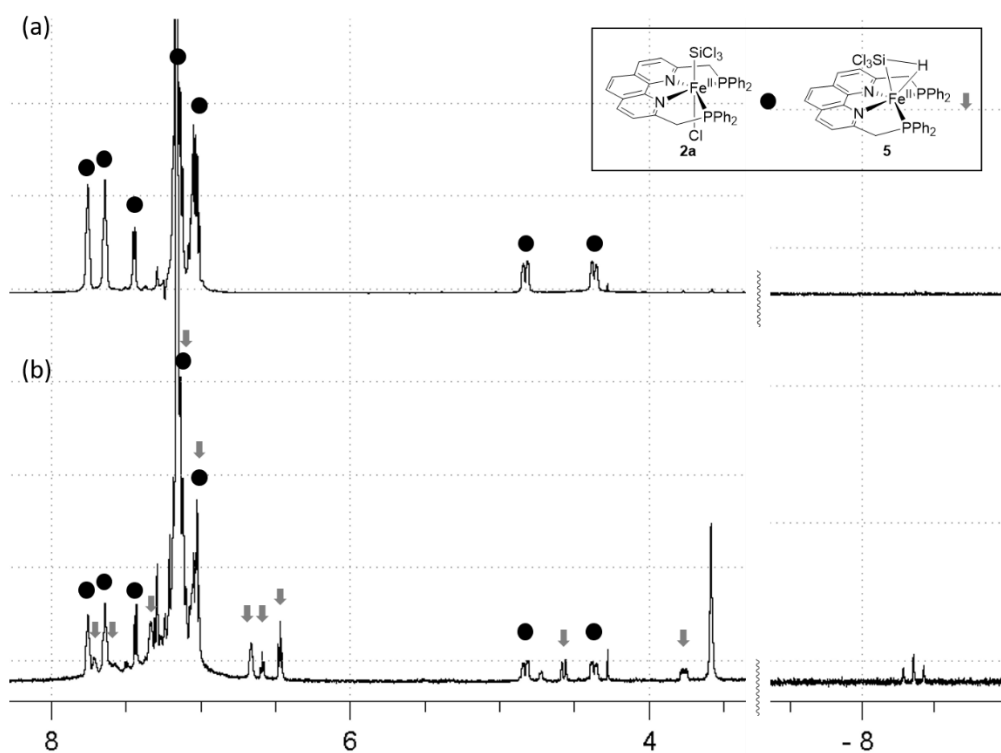
^{31}P NMR (600 MHz, C_6D_6):



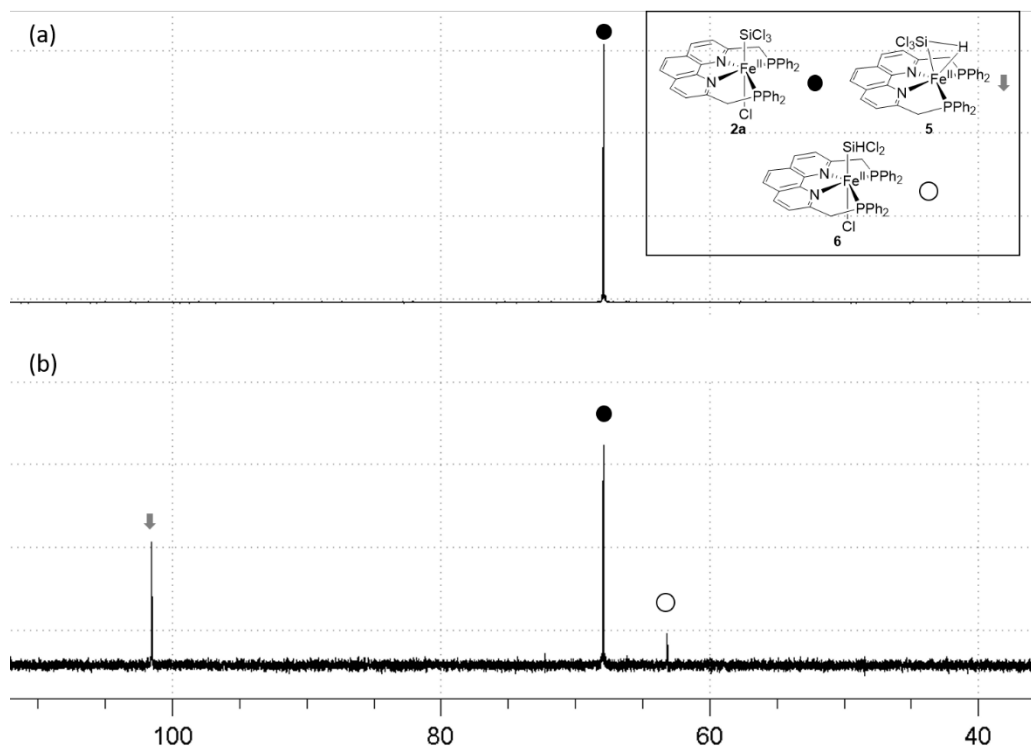
The reaction of **2a** with SiHCl_3

The crystal of **1** (0.005 g, 7.0 μmol), which was crystalized a –THF/hexane at $-40\text{ }^\circ\text{C}$,* in *J Young* NMR tube was dissolved in 0.4 ml of C_6D_6 and added SiHCl_3 (1 M in THF, 74 μl , 74 μmol). As soon as, NMR measurement of the solution was carried out. See NMR caption. * The crystal of **1** was decomposed by dryness. Therefore, the weight of **1** was include little amount of mother liquid.

^1H NMR (600 MHz, C_6D_6) (a) **2a**, (b) Reaction of **1** with SiHCl_3 :



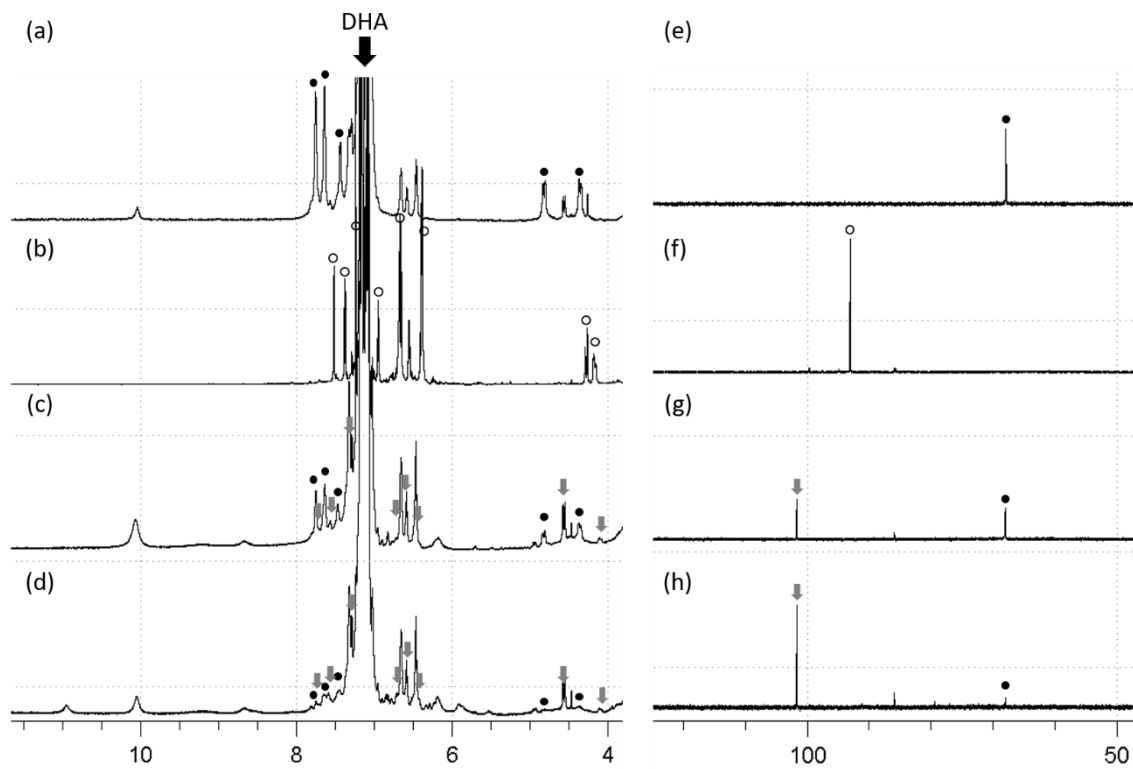
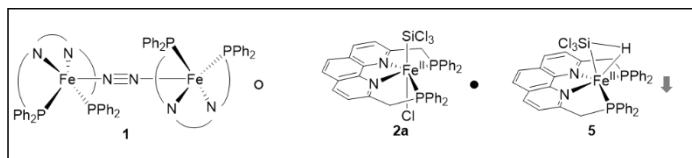
^{31}P NMR (243 MHz, C_6D_6) (a) **2a**, (b) Reaction of **1** with SiHCl_3 :



The reaction of **2a** with SiCl_4 in presence of DHA.

The crystal of **1** (0.005 g, 7.0 μmol), which was crystalized a $-\text{THF}/\text{hexane}$ at $-40\text{ }^\circ\text{C}$,* in *J Young* NMR tube was dissolved in 0.4 ml of C_6D_6 and added DHA 0.003 g (0.028 mmol) and SiCl_4 0.002 g (28 mmol). NMR measurement was carried out after 5 min (d, h) and 12 h (c, g). See NMR caption. * The crystal of **1** was decomposed by dryness. Therefore, the weight of **1** was include little amount of mother liquid.

^1H NMR (600 MHz, C_6D_6) of (a) **2a** with DHA, (b) **2a** with DHA, (c) **2a** with SiCl_4 presence of DHA (12 h), and (d) **2a** with SiCl_4 presence of DHA (5 min) and ^{31}P NMR (243 MHz, C_6D_6) of (e) **2a** with DHA, (f) **2a** with DHA, (g) **2a** with SiCl_4 presence of DHA (12 h), and (h) **2a** with SiCl_4 presence of DHA (5 min):



Single crystal X-ray diffraction studies.

The single crystal X-ray diffraction measurements of **2a**, **2b**, **6**, **9**, **11** and **12** was performed under a cold nitrogen stream on a Rigaku XtaLAB P200 diffractometer with a Pilatus 200K detector using multi-layer mirror monochromated Mo K α radiation. The determination of crystal systems and unit cell parameters and data processing were performed with the *CrystalClear* program package. The data sets were corrected for Lorentz and polarization effects and absorption. The structure was solved by direct methods using SIR2014 program,¹¹ and refined by full-matrix least squares calculations on F² for all reflections (SHELXL-2014/7),¹² using Yadokari-XG 2009.¹³

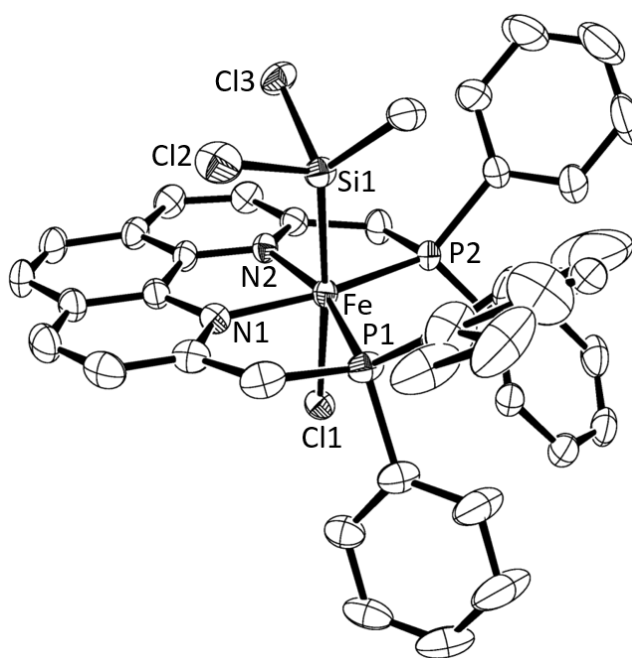


Figure 4-S1. Molecular structure of **3** with 50% probability ellipsoids. Hydrogen atoms are omitted for clarity. Selected bond lengths (Å) and bond angles (°): Fe1–N1 1.955(2), Fe1–N2 1.949(3), Fe1–P1 2.280(9), Fe1–P2 2.2114(9), Fe1–Si1 2.2851(9), Fe1–Cl1 2.3822(8), Si1–Cl2 2.1387(13), Si1–Cl3 2.1454(11), N1–Fe1–N2 81.71(11), P1–Fe1–P2 110.94(4).

Table S1 Crystallographic data of **2a**, **2b**, **3**, and **6**.

	2a	2b	3	6
Empirical formula	C ₃₈ H ₃₀ Cl ₄ FeN ₂ P ₂ Si·2C ₈ H ₄ O	2C ₃₈ H ₃₀ Br ₄ Fe ₁ N ₂ P ₂ Si ₁ ·C ₇ H ₈	C ₃₉ H ₃₃ Cl ₃ FeN ₂ P ₂ Si·C ₄ H ₈ O	C ₄₃ H ₃₉ BrFeN ₂ P ₂ ·C ₇ H ₈
Formula weight	946.53	2052.45	854.01	873.59
Temperature/K	93(2)	93(2)	93(2)	93(2)
Crystal system	monoclinic	triclinic	monoclinic	triclinic
Space group	<i>P</i> 2 ₁ / <i>c</i>	<i>P</i> -1	<i>P</i> 2 ₁ / <i>c</i>	<i>P</i> -1
<i>a</i> / Å	20.374(3)	14.313(2)	14.9907(13)	10.598(3)
<i>b</i> / Å	14.3897(14)	15.870(3)	15.2634(11)	13.112(4)
<i>c</i> / Å	16.074(2)	17.843(3)	19.0253(16)	15.439(4)
α / °	90	98.168(4)	90	96.098(4)
β / °	112.178(3)	92.892(4)	102.501(2)	99.571(5)
γ / °	90	99.592(5)	90	104.409(7)
Volume / Å ³	4363.9(9)	3944.3(11)	4250.0(6)	2024.4(9)
<i>Z</i>	4	2	4	2
<i>R</i> ₁ / %	0.0574	0.0562	0.0604	0.0513
<i>wR</i> ₂ / %	0.1417	0.0922	0.1887	0.1001
GOF	1.043	1.046	1.080	1.041

Table S2 Crystallographic data of **9**, **11**, and **12**.

	9	11	12
Empirical formula	C ₃₈ H ₂₉ Cl ₃ D ₃ FeN ₄ P ₂ Si·C ₂ D ₃ N	C ₆₄ H ₅₃ BCl ₃ FeN ₃ P ₂ Si·C ₄ H ₈ O	C ₃₈ H ₃₁ Cl ₃ FeN ₂ P ₂ Si·C ₆ H ₆
Formula weight	854.00	1199.23	845.98
Temperature/K	93(2)	93(2)	93(2)
Crystal system	monoclinic	monoclinic	triclinic
Space group	<i>P</i> 2 ₁ / <i>n</i>	<i>P</i> 2/ <i>n</i>	<i>P</i> -1
<i>a</i> / Å	10.707(5)	15.909(4)	10.4880(6)
<i>b</i> / Å	21.980(11)	18.043(4)	11.5601(7)
<i>c</i> / Å	18.362(8)	21.267(4)	18.1782(19)
α / °	90	90	93.5220(10)
β / °	91.645(12)	97.456(5)	103.7830(10)
γ / °	90	90	112.500(9)
Volume / Å ³	4320(4)	6053(2)	1948.8(3)
<i>Z</i>	4	4	2
<i>R</i> ₁ / %	0.1344	0.0924	0.0383
<i>wR</i> ₂ / %	0.3009	0.1238	0.0821
GOF	1.018	1.061	1.047

Reference

1. a) R. G. Jones, W. Ando and J. Chojnowski, *Silicon-Containing Polymers*, Kluwer Academic Publishers, Dordrecht, **2000**. b) M. A. Brook, *Silicon in Organic, Organometallic, and Polymer Chemistry*, Wiley-Interscience, New York, **2000**.
2. R. Walsh, *Acc. Chem. Res.* **1981**, *14*, 246.
3. a) J. R. McAtee, S. E. S. Martin, D. T. Ahneman, K. A. Johnson and D. A. Watson, *Angew. Chem. Int. Ed.* **2012**, *51*, 3663. b) I. Kownacki, B. Orwat and B. Marciniec, *Organometallics* **2014**, *33*, 3051.
4. K. Matsumoto, J. Huang, Y. Naganawa, H. Guo, T. Beppu, K. Sato, S. Shimada and Y. Nakajima, *Org. Lett.* **2018**, *20*, 2481.
5. a) A. A. Zlota, F. Frolow and D. Milstein, *J. Chem. Soc., Chem. Commun.* **1989**, 1826. b) H. Yamashita, A. M. Kawamoto, M. Tanaka and M. Goto, *Chem. Lett.* **1990**, *19*, 2107. c) H. Yamashita, M. Tanaka and M. Goto, *Organometallics* **1997**, *16*, 4696. d) S. Gatard, C.-H. Chen, B. M. Foxman and O. V. Ozerov, *Organometallics* **2008**, *27*, 6257.
6. H. Fleischer, *Eur. J. Inorg. Chem.* **2001**, 393.
7. a) J. P. Collman and W. R. Roper, *J. Am. Chem. Soc.* **1965**, *87*, 4008. b) C. E. Johnson and R. Eisenberg, *J. Am. Chem. Soc.* **1985**, *107*, 3148. c) J. A. Labinger and J. A. Osborn, *Inorg. Chem.* **1980**, *19*, 3230. d) J. K. Kochi, *Acc. Chem. Res.* **1974**, *7*, 351.
8. a) K. E. Liu, C. C. Johnson, M. Newcomb and S. J. Lippard, *J. Am. Chem. Soc.* **1993**, *115*, 939. b) I. D. Mackiea and G. A. DiLabio, *Org. Biomol. Chem.* **2011**, *9*, 3158.
9. a) H. Gilman and C. G. Brannen, *J. Am. Chem. Soc.* **1951**, *73*, 10, 4640. b) J. J. D'Errico and K. G. Sharp, *Inorg. Chem.* **1989**, *28*, 2886. c) M. Ito, M. Itazaki, T. Abe and H. Nakazawa, *Chem. Lett.* **2016**, *45*, 1434. d) T. Beppu, K. Sakamoto, Y. Nakajima, K. Matsumoto, K. Sato and S. Shimada, *J. Organomet. Chem.* **2018**, 869, 75. d) A. Glüer, J. I. Schweizer, U. S. Karaca, C. Würtele, M. Diefenbach, M. C. Holthausen and S. Schneider, *Inorg. Chem.* **2018**, *57*, 13822.
10. a) C. Gunanathan, D. Milstein, *Acc. Chem. Res.* **2011**, *44*, 588. b) C. Gunanathan, D. Milstein, *Science* **2013**, *341*, 1229712. c) C. Gunanathan, D. Milstein, *Chem. Rev.* **2014**, *114*, 12024. d) F. Ozawa, Y. Nakajima, *Chem. Rec.* **2016**, *16*, 2314.
11. M.C. Burla, R. Caliendo, B. Carrozzini, G. L. Cascarano, C. Cuocci, C. Giacovazzo, M. Mallamo, A. Mazzone and G. Polidori, *J. Appl. Cryst.* **2015**, *48*, 306.
12. G. M. Sheldrick, SHELXL-2014/7, University of Göttingen, Göttingen, Germany, 2014.
13. C. Kabuto, S. Akine, T. Nemoto, E. Kwon, Release of software (Yadokari-XG 2009) for crystal structure analyses. *Nippon Kessho Gakkaishi* **2009**, *51*, 218.

List of publications

Capter 1, 3

- 1) 「Selective hydrosiloxane synthesis via dehydrogenative coupling of silanols with hydrosilanes catalysed by Fe complexes bearing a tetradentate PNNP ligand」

Tomohiro Takeshita, Kazuhiko Sato, and Yumiko Nakajima, *Dalton Trans.*, **2018**, 47, 17004–17010.

Capter 2

- 2) 「Deprotonation of a PNNP-Iron Complex: Expanding the Concept of Metal-Ligand Cooperation to the PNNP-Fe System」

Tomohiro Takeshita, and Yumiko Nakajima, *Chem. Lett.* **2019** in press.

(DOI: 10.1039/C8SC04389B)

Acknowledgements

The study described in this thesis has been carried out under the direction of Associate Professor Yumiko Nakajima at Department of Chemistry, Graduate School of Pure and Applied Sciences, University of Tsukuba and Silicon team, Interdisciplinary Research Center for Catalytic Chemistry, National Institute of Advanced Industrial Science and Technology during the period of 3 years from April 2016 to March 2019.

The author sincerely thanks Associate Professor Yumiko Nakajima for her kind support, valuable suggestions and reviews of the presentations and manuscripts.

The author would like to express his thanks and appreciation to Prof. Sekiguchi Akira, Dr. Kazuhiro Matsumoto, Dr. Yuki Naganawa, and Dr. Shinji Tanaka for their helpful to discussions in the early phase of this research and reviews of the presentations and manuscripts. The author would like to express his thanks to Prof. Takahiko Kojima, Dr. Tomoya Ishizuka, Dr. Hiroaki Kotani, Dr. Dachao Hong, Dr. Tetsuo Yatabe, Dr. Toru Hashimoto, Dr. Teruo Beppu, Dr. Ohmori Yu, Dr. Koya Inomata, Mr. Keiya Aoyagi, and Mr. Yusuke Ishizaka for discussions in seminars.

The author would like to express his thanks and appreciation to Dr. Kazuhiko Sato (AIST) and Masumi Asakawa (AIST) for showing me the brand new visions regardless of science.

The author thanks all members of Interdisciplinary Research Center for Catalytic Chemistry and Prof. Kojima's group.

Finally, the author wishes to express his deep appreciation to his parents, Mr. Hiroyuki Takeshita and Chihiro Takeshita for constant assistance and affectionate encouragement.

March 2019

Tomohiro Takeshita